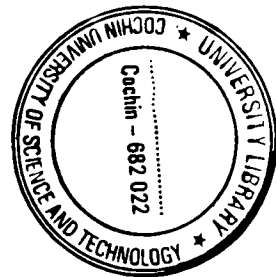


G9098

**ELASTIC CONSTANTS AND STRUCTURAL PARAMETERS
OF SELECTED POLYCRYSTALLINE CERAMICS
BY ULTRASONIC TECHNIQUE**

Thesis submitted to
COCHIN UNIVERSITY OF SCIENCE AND TECHNOLOGY
in partial fulfillment of the requirements for the award of the degree of
DOCTOR OF PHILOSOPHY

VIMALA GEORGE



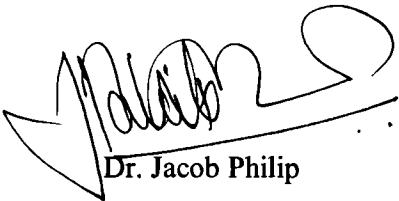
DEPARTMENT OF INSTRUMENTATION
COCHIN UNIVERSITY OF SCIENCE AND TECHNOLOGY
COCHIN - 682 022

OCTOBER 2005

CERTIFICATE

Certified that the work presented in this thesis is based on the bona fide work done by Ms.Vimala George under my guidance in the Department of Instrumentation, Cochin University of Science and Technology, and has not been included in any other thesis submitted previously for the award of any degree.

Kochi - 682 022
17th October 2005



Dr. Jacob Philip
Supervising Guide

CONTENTS

Preface *i*

Acknowledgements *v*

Chapter 1: Reviews of Elastic Properties of Solids and Ceramic Materials

A: Elastic Properties of Solids

1.1: Introduction	1
1.2: Elastic properties of crystalline solids	6
1.3: Elastic properties of non-crystalline solids	11
1.4: Experimental methods to determine elastic properties of solids	13

B: Ceramic Materials

1.5: The ceramic phase of solids	19
1.5.1: Composition	
1.5.2: Preparation methods	
1.6: Classification of ceramics	22
1.6.1: Oxide ceramics	
1.6.2: Mixed oxides	
1.6.3: Carbides	
1.6.4: Borides	
1.6.5: Nitrides	
1.6.6: Intermetallics and silicides	
1.6.7: Electronic Ceramics	
1.6.8: Dielectric resonators	
1.6.9: Glass ceramics	
1.7: Physical properties of ceramics	27
1.7.1: Mechanical properties	

1.7.2: Thermal properties	
1.7.3: Chemical properties	
1.7.4: Electrical properties	
1.8: Structure of Ceramics	29
1.9: Applications of Ceramics	34
1.9.1: Ceramics as substrate materials	
1.10: Outline of work presented in this thesis	37
References	39

Chapter 2: Experimental Method

2.1: Introduction	45
2.2: Ultrasonic Methods to determine elastic properties of solids	46
2.2.1: Pulse methods	46
(i) Pulse superposition method	
(ii) Phase comparison method	
(iii) Sing-around method	
(iv) Long pulse technique	
2.2.2: Continuous wave methods	49
(i) Resonant ultrasound spectroscopy (RUS)	
(ii) Composite oscillator method	
2.2.3. Low frequency methods	51
2.3: The pulse echo overlap method.	52
2.4: MATEC Model 7700 ultrasonic PEO setup	55
2.5: Measurement method	58
2.5.1: Bond correction and overlap identification	61
2.6: Structural properties by X-ray diffraction	67
2.7: Microscopic structure by scanning electron microscopy	69
References	71

Chapter 3: Influence of oxide glass addition on the elastic and structural properties of $\text{Ba}_{6-x}\text{R}_{8+2x}\text{Ti}_{18}\text{O}_{54}$ ceramics.

3.1: Introduction	74
3.2: Sample Preparation	79
3.3: Samples Studied	79
3.4: Structure by XRD and SEM	80
3.5: Elastic Properties by Ultrasonic technique	84
3.6: Results and Discussion	84
References	87

Chapter 4: Effect of adding Silica and similar glasses on the elastic properties of BST ceramics

4.1: Introduction	90
4.2: Sample Preparation	93
4.3: Samples Studied	93
4.4: Structure by XRD and SEM	94
4.5: Elastic Properties by Ultrasonic technique	97
4.6: Results and Discussion	97
References	111

Chapter 5: Elastic properties of Borosilicate added BST ceramics

5.1: Introduction	114
5.2: Sample Preparation	117
5.3: Samples Studied	118
5.4: Structure Characterization by XRD and SEM	118
5.5: Elastic properties by Ultrasonic Technique	121
5.6: Results and Discussion	122
References	137

**Chapter 6: Elastic and structural properties of $\text{Ca}_{5-x}\text{A}_x\text{Nb}_2\text{TiO}_{12}$
(A = Mg, Zn) ceramics**

6.1: Introduction	139
6.2: Sample Preparation	144
6.3: Samples Studied	145
6.4: Structure Characterization by XRD and SEM	145
6.5: Elastic properties by Ultrasonic Technique	149
6.6: Results and Discussion	149
References	159
Chapter 7: Summary and Conclusions	163

Preface

The search for new materials with interesting properties has a significant role in the development of science and technology. When a new material is discovered, one of the fundamental properties to be determined is the elastic property. The study of elastic properties gives information about the magnitude of the forces and nature of bonding between the atoms. Our aim has been to investigate systematically the effect of doping on the elastic properties of selected dielectric ceramic materials. These materials have got wide technological applications due to their interesting dielectric, thermal and elastic behaviour. Ultrasonic wave propagation measurements have been employed for the investigation of elastic properties of selected materials. Details of the work done and results obtained are presented in this thesis.

Ultrasonics is one of the most widely used and powerful techniques to measure elastic properties of solids. The ultrasonic technique is nondestructive in nature and the measurements are relatively straightforward to perform. One unique advantage of the ultrasonic technique is that both static and dynamic properties can be measured simultaneously. The velocity and attenuation coefficients of the ultrasonic waves propagating through a medium are related to the microscopic structure of the material and they provide valuable information about the structural changes in the system. Among the various ultrasonic techniques, the pulse echo overlap method is the most accurate and precise one.

In this thesis, we have investigated the influence of structure and chemical composition of a material on its elastic properties by measuring the ultrasonic

velocity as a function of composition. To study the structural details of the materials, the XRD and SEM of the samples are taken. The samples selected for the present investigations are dielectric ceramics belonging to the group $\text{Ca}_{5-x}\text{A}_x\text{Nb}_2\text{TiO}_{12}$ ($\text{A} = \text{Mg, Zn}$), $\text{Ba}_{6-2x}\text{Sm}_{8+2x}\text{Ti}_{18}\text{O}_{54}$ and its glass-added compositions. The glasses added include $\text{MgO-Al}_2\text{O}_3\text{-SiO}_2$, $\text{ZnO-B}_2\text{O}_3$ (77:23), $\text{ZnO-B}_2\text{O}_3$ (50:50), $\text{B}_2\text{O}_3\text{-SiO}_2$, $\text{ZnO-B}_2\text{O}_3\text{-SiO}_2$, $\text{PbO-B}_2\text{O}_3\text{-SiO}_2$, $\text{MgO-B}_2\text{O}_3\text{-SiO}_2$, $\text{Al}_2\text{O}_3\text{-SiO}_2$, $\text{Al}_2\text{O}_3\text{-B}_2\text{O}_3\text{-SiO}_2$, $\text{BaO-B}_2\text{O}_3\text{-SiO}_2$ (30:60:10), $\text{BaO-B}_2\text{O}_3\text{-SiO}_2$ (30:40:30) etc. This thesis is presented in 7 chapters, the contents of which are outlined below.

Chapter 1 provides a review of the elastic properties of solids, with particular reference to ceramic materials. Theory of elastic wave propagation in crystalline media is presented and the general theory and equations have been applied to the isotropic media. Starting from Christoffel's equations, the necessary relations connecting the elastic constants and sound velocities are derived. In the second section of the chapter, the general properties of the ceramics are briefly outlined. The relevance of dielectric resonator ceramics and their wide range of applications are also mentioned.

The second chapter explains the experimental method used for the measurements. The Matec model 7700 pulse modulator and receiver, along with necessary subsystems have been used for accurate measurement of ultrasonic velocity using pulse echo overlap technique. Details of the system and measurement technique are outlined in this chapter with the help of block diagrams. We have applied the bond corrections necessary to eliminate errors due to phase changes occurring in pulsed ultrasonic echoes due to reflections at various boundaries.

Details of the XRD and SEM measurements, used for the structural study are also briefly outlined.

Barium Samarium Titanate, $\text{Ba}_4\text{Sm}_{28/3}\text{Ti}_{18}\text{O}_{54}$ (BST) is a very important dielectric material used in microwave electronics and communications. A good amount of work has been conducted on the dielectric and structural properties of this material. We have measured the elastic properties of this material for the first time. As this is an important commercially used dielectric material, the search for methods to lower the sintering temperature is very important from the applications point of view. Glass addition is one such method. The experimental details and results of the measurements of the elastic properties of glass added BST is explained in Chapter 3. 0.5 wt % of a variety of glasses are added to the base material. The results of the XRD and SEM measurements are also given.

In Chapter 4, results of the detailed study of the effect of addition of Al_2O_3 - SiO_2 , B_2O_3 - SiO_2 , B_2O_3 , and La_2O_3 - B_2O_3 - TiO_2 glasses, on the elastic and structural properties of BST is given. The effects of addition of BaO - B_2O_3 - SiO_2 , $\text{Ba}_{30}\text{B}_{40}\text{Si}_{30}$, Al_2O_3 - B_2O_3 - SiO_2 and B_2O_3 - Bi_2O_3 - SiO_2 - ZnO glasses on the structural and elastic properties of BST are described in Chapter 5. The steady decrease of elastic strength of the material with increasing amount of glass can be seen in these results, which are explained with the help of XRD and SEM measurements.

Complex perovskites form important structural base for microwave dielectrics with important properties such as high dielectric permittivity ϵ_r , high quality factor Q (or low dielectric loss) and near-zero temperature coefficient of resonant frequency (τ_f). $\text{Ca}_5\text{Nb}_2\text{TiO}_{12}$ is an important microwave dielectric material

with a good combination of the aforementioned properties. Recently, this material is reported to be suited for the bandwidth enhancement of DR loaded microstrip patch antennas and for the fabrication of wideband dielectric resonator antennas. Also, $\text{Ca}_5\text{Nb}_2\text{TiO}_{12}$ exhibits an unusual double zero crossing of τ_f . Another set of novel low loss, temperature stable materials, belonging to this group is $\text{Ca}_{5-x}\text{A}_x\text{Nb}_2\text{TiO}_{12}$, with $\text{A} = \text{Mg}, \text{Zn}$. The dielectric properties of this set of materials are recently reported, but their elastic properties have not been probed. We have measured the ultrasonic velocity of these materials using the PEO method, from which their elastic properties are derived. The obtained results are presented in Chapter 6.

Chapter 7 is the concluding chapter in which the overall conclusions drawn from the work presented in the previous chapters are discussed. It also projects the future scope of these types of investigations.

The following papers have been communicated during the course of this work:

1. Elastic properties of $\text{Ca}_{5-x}\text{A}_x\text{Nb}_2\text{TiO}_{12}$ ($\text{A} = \text{Mg}, \text{Zn}$) microwave ceramics, Material Research Bulletin (in press)
2. Microwave dielectric and elastic properties of glass added $\text{Ba}_{6-3x}\text{Sm}_{8+2x}\text{Ti}_{18}\text{O}_{54}$ ($x=2/3$), Materials Chemistry and Physics (communicated)

Two more papers are under preparation

CHAPTER 1

Reviews of Elastic Properties of Solids and Ceramic Materials

A: Elastic Properties of Solids

1.1 : Introduction

The impact of solids on the world of science and technology has been enormous, covering such diverse applications as solar energy, image processing, energy storage, computer and telecommunication technology, thermoelectric energy conversion and new materials for numerous applications. The disordered phases of condensed matter are far more abundant, and of no less technological value than the idealized single crystals [1-2]. The technological importance of amorphous solids has mushroomed over the past few years due to the discovery of some surprising anomalies in the acoustic, electric and thermodynamic [3-4] behaviour of these materials. The study of these amorphous solids offers new frontiers of research and hopefully, promise for more technological developments.

In solid state physics, the structure determines the mechanical properties of the material, the phonon modes of solid determines the thermal properties of the material and electron structure controls the electrical and optical properties the material [5-8]. The crystalline solids possess a definite periodicity and long-range order, while amorphous materials exhibit only a short-range order [SRO] and atoms/molecules do not possess periodicity. Models of amorphous solids exhibiting

SRO and without any long-range crystalline periodicity are called random networks, which were first proposed by Zachariasen [9-13]. There are also several alternative models based on microcrystalline arrays. Like micro voids, much inhomogeneity may exist in particular materials, making the form of density fluctuations or compositional variations.

As in crystals, no crystalline constraints are present on coordination number (z), bond lengths (a) or bond angles (θ) in amorphous solids. However, the same chemical interactions that control the structure of crystals are present, and they provide strong driving forces for optimization of z , a and θ , i.e., the SRO. Furthermore, in multicomponent alloys a hierarchy of bond strengths can exist, favouring some local environment over others. In order to estimate the energies of the bonding and anti-bonding orbitals of a heteropolar bond, the difference in the electro negativities of the two atoms must be taken into account. In disordered systems, the SRO is maintained in the sense that the coordination number of each atom remains the same as in the case of corresponding ordered crystal, although the bond lengths and angles fluctuate.

It is important to bear in mind that amorphous solids are not ordinarily the lowest-energy structures for any large collection of atoms. Thus, under ideal preparation conditions, *e.g.* very slow cooling, crystalline solids will usually result. Thus most amorphous materials are metastable, and they must generally be processed using non-ideal techniques such as quenching from the liquid phase. The atomic mobility diminishes rapidly with decreasing temperature and long-range motions, which would normally induce crystallization, are retarded. A softening point or glass

transition temperature [14-15] T_g usually exists, below which the viscosity of the material increases by many orders of magnitude and the material becomes an amorphous solid. The ability to design and synthesize a great variety of amorphous materials depends on the fact that many do not have corresponding crystal structures [16].

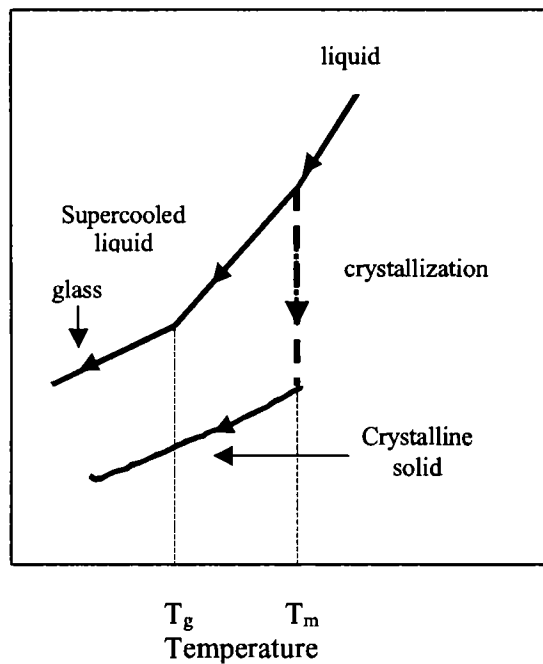


Fig.1.1: Behaviour of crystalline and noncrystalline materials on cooling. Crystalline materials solidify at the melting temperature T_m . T_g is the glass transition temperature of noncrystalline materials.

Many of the solid materials are preparation-dependent, because the same elements can combine with each other in a number of different and distinct configurations. The chosen local order actually depends on the nature of chemical bonding, which in turn is predicated by several factors, including dynamic

considerations. The possibility of steric isomerism results in the same elements in different configurations displaying very different chemical reactivities and electronic properties. The internal freedom for placement of atoms in three-dimensional space without long-range order allows for new design possibilities not found in crystals. Instead of lattice repetitive atoms, amorphous solids form a matrix, where bonding and non-bonding orbitals with different energies interact in three-dimensional space. The particular bonding option chosen by an atom as it seeks out equilibrium is dictated by the kinetics, the orbital directionality, the state of excitation of the relevant atoms, and the temperature distribution during the process of formation. In the same amorphous material, there can be a whole spectrum of bonds including metallic, covalent, ionic and coordinate.

Thermodynamically, slight differences in energy can have important influence on the various conformations and configurations that are inherent in amorphous materials and transformations available to them. There are not only energy barriers in amorphous materials inhibiting crystallization, but also many more subtle barriers involved with atomic and molecular changes, which are part of the relaxation process unique in amorphous materials. One internal structure can be converted into another without even breaking bonds. The closeness of energy of the various conformations and configurations can be masked by thermal vibrations (phonons) down to very low temperatures [17-20]. As in the case of crystalline materials, acoustic phonons represent sound propagation through the material and anharmonic forces lead to phonon-phonon coupling. Such anharmonicity has important consequences resulting in thermal expansion, temperature dependence for heat capacity, absorption of sound etc. The density of phonon modes per unit

volume per unit frequency in an amorphous solid can have strong resemblance to that of the corresponding crystalline solid. However, coupling between phonons and electrons is basically different in amorphous and crystalline materials. Amorphous solids are characterized by both localized and extended phonons, whereas crystalline solids exhibit only extended phonons. The relaxations that are inherent in amorphous materials are quite different from crystalline materials.

The elastic properties of a material are intimately connected with the coordination number. The controlling influence for the transition from a flexible to a rigid structure is the network connectivity which is characterized by a single parameter, the average coordination number. As one changes the average coordination by replacing the divalent materials in Group VI by tetrahedral materials in Group IV, the elasticity decreases. In order to attain necessary elasticity, atoms of lower valence are utilized. In contrast, if one starts with divalent materials, cross-links are to be added to assure and control rigidity and stability.

There are many bistable materials in which the amorphous-crystalline transition is likely to occur [21-22]. Solids with amorphous-crystalline transition are used as the basis of memory systems. In threshold switches, there is an irreversible transition between high impedance and low impedance states in less than 120 pico seconds at room temperature. The use of light to induce structural and phase changes has been very rewarding to technologists to produce new types of optical recording and photographic imaging with unique properties. Materials are developed, in which local structural changes can be induced and detected optically, and thus the associated properties can also be varied. Doping is another method to change the properties of materials.

1.2: Elastic Properties of Crystalline Solids

Interest in elastic properties dates back to studies of static equilibrium of bending beams by Galileo and other 17th century philosophers. With the basic physics introduced by Hooke in 1660, the development of the theory of elasticity followed the development of the necessary mathematics. The resulting theory was summarised in the treatise by Augustus Love in 1927 [23].

When a new material is discovered, one of the most fundamental properties to be determined is the atomic structure, defined by the minimum in the free energy with respect to the positions of atoms. Another fundamental characteristic of interest is the curvature of free energy within the vicinity of the minimum, and this would manifest in the elastic constants [24] of the material. As derivatives of free energy, elastic constants are closely connected to thermodynamic properties of the material. They can be related to the specific heat, the Debye temperature and the Gruneisen parameter (which relates the thermal expansion coefficient to the specific heat at constant volume), and they can be used to check theoretical models. Extensive quantitative connections among thermodynamic properties can be made if the elastic constants are known as functions of temperature and pressure. The damping of elastic waves provides information on anharmonicity and on coupling with electrons and other relaxation mechanisms involved. The elastic properties are perhaps the most valuable as probes of phase transitions, such as superconducting transitions as well as structural transitions. Clearly, precise and accurate measurements of elastic constants furnish significant information about the material under consideration.

Elastic waves are always generated by mechanical vibrations of various media. They can propagate through gases, liquids and solids and these waves are the result of collective vibrations of the atoms and molecules of the medium. The vibration characteristics of the atoms and molecules of the medium are determined by the interatomic forces. The nature of these forces is different in solids, liquids and gases and the wave propagation characteristics are also different. In solids, both transverse and longitudinal wave propagations are possible, while in liquids and gases only longitudinal type of wave propagation is possible. Liquids and gases have the same properties in all directions and hence the wave propagation characteristics are truly isotropic [25-26]. In general, amorphous solids like glasses have isotropic elastic properties, while others like single crystals have anisotropic elastic properties. Study of elastic wave propagation through solids enables one to determine their elastic properties. Wave propagation in a medium is characterized by its velocity and attenuation.

The elastic properties of a medium are better understood in terms of its response to an applied stress. Under the application of an external stress, the medium gets strained. The amount of strain developed for a given stress is characteristic of that medium. According to Hooke's law, within elastic limits, stress is proportional to strain, and the proportionality constant is known as elastic modulus. Stress can be of two types – compressive type and shear type. Liquids and gases can be elastically compressed but not elastically sheared. Hence, they have compressibility as their only elastic modulus. Isotropic solids can be compressed as well as sheared elastically and hence they have fundamentally two elastic moduli, identified as bulk and shear moduli. The elastic properties of a crystal are the most general case among

all solids and fluids. Here in any spatial direction there can be three types of stresses: one longitudinal and two shear types perpendicular to each other. On resolving the generalized stress and strain on an orthogonal axial reference frame, the stress and strain are second rank tensors and therefore require nine members to specify them. The stress tensor represents a force, which can be applied along any arbitrary direction of the system and is called a field tensor [26].

The components of the stress tensor are given by,

$$\sigma_{ij} = \begin{pmatrix} \sigma_{11} & \sigma_{12} & \sigma_{13} \\ \sigma_{21} & \sigma_{22} & \sigma_{23} \\ \sigma_{31} & \sigma_{32} & \sigma_{33} \end{pmatrix} \quad (1.1)$$

In a similar way, the strain tensor is represented as,

$$\varepsilon_{ij} = \begin{pmatrix} \varepsilon_{11} & \varepsilon_{12} & \varepsilon_{13} \\ \varepsilon_{21} & \varepsilon_{22} & \varepsilon_{23} \\ \varepsilon_{31} & \varepsilon_{32} & \varepsilon_{33} \end{pmatrix} \quad (1.2)$$

The generalized Hooke's law is represented as,

$$\sigma_{ij} \propto \varepsilon_{kl} \quad (1.3)$$

The constant of proportionality is a fourth rank matter tensor [26-27]. This tensor is the elastic stiffness C_{ijkl} and its inverse is the elastic compliance S_{ijkl} . The relations between these constants and stress and strain are,

$$\sigma_{ij} = \sum C_{ijkl} \varepsilon_{kl} \quad (1.4)$$

and
$$\varepsilon_{ij} = \sum S_{ijkl} \sigma_{kl} \quad (1.5)$$

The stiffness or elastic compliances are determined by undertaking elastic wave propagation measurements in solids. Further, there are the constants, which determine the velocity of elastic waves in any direction in a medium. C_{ijkl} and S_{ijkl}

have 81 elements relating 9 stress components and 9 strain components. In the absence of rotation in the material, the stress and strain tensors obey the symmetry,

$$\sigma_{ij} = \sigma_{ji} \quad (1.6)$$

and $\epsilon_{kl} = \epsilon_{lk} \quad (1.7)$

This reduces the number of independent stress and strain components from 9 to 6. The above symmetry leads to atmost 36 independent elastic constants. To avoid the difficulty in representing elastic constants with full subscript, Voigt notation can be used in which the tensor form of $C_{ijkl}(i, j, k, l = 1, 2, 3)$ is replaced by the matrix $C_{ij}(i, j = 1, 2, 3, 4, 5, 6)$ according to the following convention.

Tensor notation	11	22	33	23,32	31,13	12,21
Matrix notation	1	2	3	4	5	6
	$ij = m = i$			<i>if</i>	$i = j$	
	$ij = m = 9 - i - j$			<i>if</i>	$i \neq j$	

It may be noted that this two-suffix notation is used only for convenience and they do not transform like a second rank tensor. To transform the constants to other axes, it is necessary to go back to the original tensor notation.

Again, if the medium is elastic, one more symmetry condition is imposed giving, $C_{ij} = C_{ji}$ and $S_{ij} = S_{ji}$

This establishes another 15 equations in for elastic constants and reduces the maximum number of independent constants to 21.

Using all these concepts, the stress-strain relation can be expressed as

$$\sigma_i = \sum_{j=1}^6 C_{ij} \epsilon_j \quad (1.8)$$

$$\text{and } \varepsilon_i = \sum_{j=1}^6 S_{ij} \sigma_j \quad (1.9)$$

and in matrix form this can be written as,

$$\begin{pmatrix} \sigma_1 \\ \sigma_2 \\ \sigma_3 \\ \sigma_4 \\ \sigma_5 \\ \sigma_6 \end{pmatrix} = \begin{pmatrix} C_{11} & C_{12} & C_{13} & C_{14} & C_{15} & C_{16} \\ C_{12} & C_{22} & C_{23} & C_{24} & C_{25} & C_{26} \\ C_{13} & C_{23} & C_{33} & C_{34} & C_{35} & C_{36} \\ C_{14} & C_{24} & C_{34} & C_{44} & C_{45} & C_{46} \\ C_{15} & C_{25} & C_{35} & C_{45} & C_{55} & C_{56} \\ C_{16} & C_{26} & C_{36} & C_{46} & C_{56} & C_{66} \end{pmatrix} \begin{pmatrix} \varepsilon_1 \\ \varepsilon_2 \\ \varepsilon_3 \\ \varepsilon_4 \\ \varepsilon_5 \\ \varepsilon_6 \end{pmatrix} \quad (1.10)$$

Further reduction of the number of independent elastic constants is possible when the symmetry of the individual crystals are considered and this number is different for the different crystal classes, like cubic, hexagonal, tetragonal, trigonal, orthorhombic, monoclinic and triclinic. A set of 21 elastic constants exists only for crystals having triclinic symmetry. As the symmetry of the system increases, the number of independent elastic constants decreases. Also for an anisotropic medium, the equation of motion of an elastic wave with velocity V is expressed using the Christoffel's equation [26-29], given by

$$C_{ijkl} n_k n_j S_{0l} = \rho V^2 S_{0i} \quad (1.11)$$

It may be noted that the elastic constant tensor C_{ijkl} is equated to the second order differential of the crystal potential energy function and for this reason they are sometimes referred to as second-order elastic constants. The next term in Taylor series expansion of the crystal potential energy function gives rise to the third order elastic constants, which give a measure of the anharmonic form of the interatomic forces or their deviation from the harmonic form of ideal Hooke's law.

1.3: Elastic properties of Non-crystalline Solids.

In the case of a non-crystalline isotropic solid, the elastic stiffness coefficient must be independent of the particular set of rectangular coordinate axes chosen. This simplification leads to,

$$C_{12} = C_{13} = C_{23}; \quad C_{44} = C_{55} = C_{66}; \quad C_{11} = C_{22} = C_{33} \quad (1.12)$$

All other elastic coefficients are zero. Further, isotropic medium satisfies the Cauchy relation given by,

$$C_{44} = 1/2(C_{11} - C_{12}) \quad (1.13)$$

Therefore, the number of independent elastic constants is further reduced to two. They are C_{11} and C_{44} . Then the elastic constant matrix for an isotropic medium is reduced to,

$$\begin{pmatrix} C_{11} & C_{12} & C_{12} & 0 & 0 & 0 \\ 0 & C_{11} & C_{12} & 0 & 0 & 0 \\ 0 & 0 & C_{11} & 0 & 0 & 0 \\ 0 & 0 & 0 & 1/2(C_{11} - C_{12}) & 0 & 0 \\ 0 & 0 & 0 & 0 & 1/2(C_{11} - C_{12}) & 0 \\ 0 & 0 & 0 & 0 & 0 & 1/2(C_{11} - C_{12}) \end{pmatrix}$$

To define the elastic properties of an isotropic solid completely, two constants known as Lamé constants λ and μ are defined.

They can be expressed as,

$$\mu = 1/2(C_{11} - C_{12}); \quad \lambda = C_{12} \quad (1.14)$$

λ is the shear modulus and $\lambda + 2\mu$ is the longitudinal modulus. Then the elastic constant matrix in terms of λ and μ becomes,

$$\begin{pmatrix} \lambda + 2\mu & \lambda & \lambda & 0 & 0 & 0 \\ 0 & \lambda + 2\mu & \lambda & 0 & 0 & 0 \\ 0 & 0 & \lambda + 2\mu & 0 & 0 & 0 \\ 0 & 0 & 0 & \mu & 0 & 0 \\ 0 & 0 & 0 & 0 & \mu & 0 \\ 0 & 0 & 0 & 0 & 0 & \mu \end{pmatrix}$$

Considering plane wave propagation in isotropic media and considering the symmetry conditions, the Christoffel equation for the propagation of an elastic wave with velocity V becomes,

$$\begin{vmatrix} C_{11} - \rho V^2 & 0 & 0 \\ 0 & \frac{1}{2}(C_{11} - C_{12}) - \rho V^2 & 0 \\ 0 & 0 & \frac{1}{2}(C_{11} - C_{12}) - \rho V^2 \end{vmatrix} = 0 \quad (1.15)$$

where ρ is the density of the medium. From this three solutions can be obtained, in which one is for longitudinal and two are for transverse modes. But in the case of an isotropic sample, direction of polarization does not have any significance and so one gets the two elastic constants as,

$$\rho V_{long}^2 = C_{11} \quad (1.16)$$

$$\text{and } \rho V_{trans}^2 = \frac{1}{2}(C_{11} - C_{12}) = C_{44} \quad (1.17)$$

Using these expressions, C_{11} and C_{44} can be calculated. All the important elastic parameters of isotropic solids are expressed in terms of V_{long} and V_{trans} in the following manner.

$$\text{Young's modulus, } Y = \rho V_{long}^2 \frac{(3V_{long}^2 - 4V_{trans}^2)}{(V_{long}^2 - V_{trans}^2)} = \mu \frac{(3\lambda + 2\mu)}{(\lambda + \mu)} \quad (1.18)$$

$$\text{Bulk modulus, } B = (\rho/3)(3V_{long}^2 - 4V_{trans}^2) = \lambda + \frac{2\mu}{3} \quad (1.19)$$

$$\text{Poisson's ratio } \sigma = \frac{(V_{long}^2 - 2V_{trans}^2)}{2(V_{long}^2 - V_{trans}^2)} = \frac{\lambda}{2(\lambda + \mu)} \quad (1.20)$$

So by measuring the velocity of longitudinal and transverse elastic waves, one can determine the elastic constants of an isotropic medium.

1.4: Experimental methods to determine elastic properties of solids

The experimental measurement of elastic and related properties of solids is of importance to the theory of solids and for many practical applications. Several acoustic techniques have been developed to study these properties, like ultrasonic pulse-echo, the composite resonator, the torsion pendulum, capacitance drive and pick up etc [30-31]. In all these measurements, the basic parameters that are measured are sound velocity and absorption. There are a few other non-acoustic techniques developed to measure sound velocity and attenuation such as Brillouin scattering, X-ray based methods and others [32]. Each of these non-acoustic techniques has advantages and disadvantages. Among the disadvantages common to all of them is the lack of high precision. Only the acoustic technique can achieve 10^{-6} or better reproducibility.

Elastic constants of solids can also be determined by means of a static technique that measures a displacement, as a linear response to small applied force. There are several static techniques [33-34] to measure Young's modulus and rigidity modulus like Searle's apparatus, Cantilever, Koenig's method (for finding Young's

modulus), Barton apparatus (for Rigidity modulus), etc. Some of them are explained in the following section.

(i) Determination of Young's modulus

(a) Searle's method

The Searle's static torsion apparatus is used to determine the rigidity modulus of the material of a rod. It consists of a cylindrical rod AB arranged horizontally. The end A is firmly fixed to the frame. The end B is tightly held by a chuck at the center of a pulley. One end of a tape is attached to a point on the rim and it is wound round the pulley though the groove. The tape carries a weight hanger at its free end. The shift produced in the rod is measured using a scale and telescope arrangement.

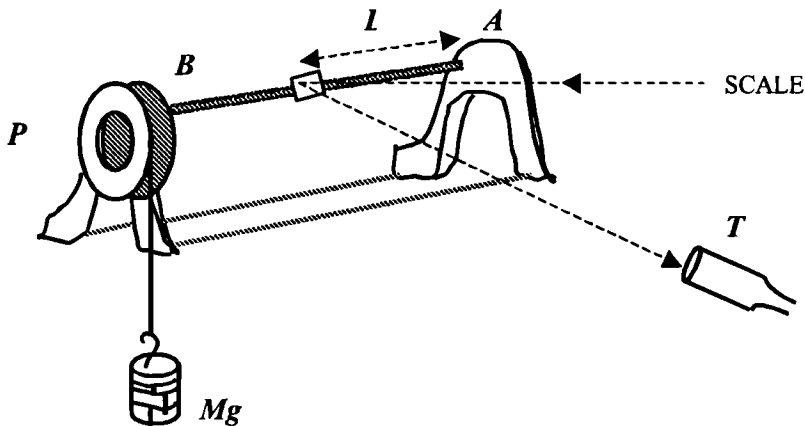


Fig. 1.2: Searle's Static Torsion apparatus

If the rod is twisted by applying a force Mg (load M kg), then the

$$\text{torsional couple} = \frac{\pi nr^4\theta}{2L}, \quad (1.21)$$

L and r being the length and radius of the wire and n is the rigidity modulus of the material of the rod.

$$\therefore \frac{\pi n r^4 \theta}{2L} = Mg.R \quad (1.22)$$

(moment of the twisting couple)

When a scale and telescope arrangement is used to measure twist, angle of twist $\theta = \frac{s}{2D}$, where s = shift in telescope reading due to load M and

D = distance between the mirror and scale.

Substituting, $n = \frac{4LDRg}{\pi r^4} \cdot \frac{M}{s}$ (1.23)

Repeating the experiment for different loads and plotting a load – shift graph, M/s is obtained.

(b) Ewing's extensometer Method

Extensometer is merely a device to magnify the small extension of the bar under test, and essentially consists of two clamp-pieces C_1 and C_2 , parallel to each other and fixed on to the test bar B by means of a pair of set screws S_1 and S_2 , with the distance between the two screw-points accurately known. This gives the initial length L of the bar before it is subjected to any tension.

A micrometer screw $M.S.$, attached to clamp C_1 near one end, has a conical hollow in its tip which engages with a ball-point $B.P.$ at the top of an upright clamp V carried by C_2 , the ball-point serving as a fulcrum about which clamp C_1 can turn when the bar is extended.

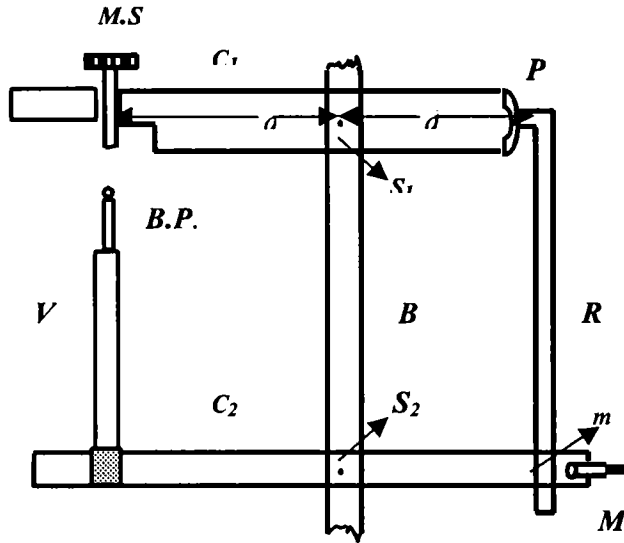


Fig. 1.3: Ewing's Extensometer

At the other, tapering end of P of C_1 , lying in a level with, and at the same distance d from, the axis of the test bar as the ball-point is pivoted a vertical rod R which passes through a slot in clamp C_2 . In its portion inside C_2 , the rod has a glass plate set into a rectangular notch in it, with a horizontal line of mark m engraved on the plate and kept illuminated by reflected light from a small mirror. The movement of m can thus be easily and accurately read with the help of a micrometer eye-piece of a microscope M , arranged inside, and co-axially with clamp C_2 , as shown.

The microscope is first focused on mark m on rod R and the micrometer screw $M.S.$ adjusted, if necessary, to make its image coincide with a convenient division on the micrometer scale of the eye-piece. The test bar is then stretched by means of a vertical testing machine and as it extends downwards, clamp C_1 turns about its fulcrum $B.P.$ resulting in a downward movement of R and a

consequent displacement of mark m . This displacement, read on the eye-piece scale, gives twice the extension l of the bar for the simple reason that the axis of the rod R lies twice as far away from the fulcrum as the axis of the bar. Half the displacement read thus gives the value of l .

Then from the length L of the bar between S_1 and S_2 , its area of cross-section and the stretching force applied to it, we can calculate the value of Young's modulus for its material in the usual manner.

(ii) Determination of the coefficient of Rigidity - Vertical Twisting apparatus for a wire.

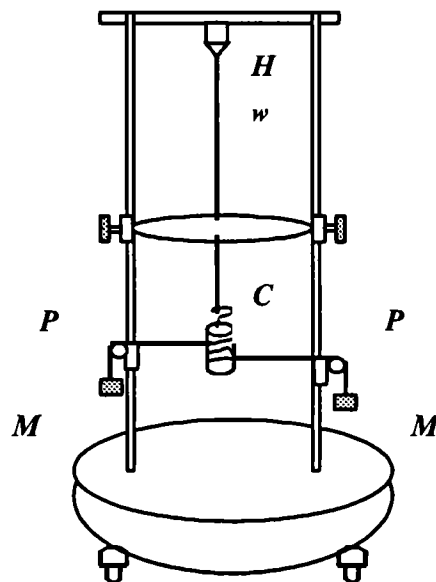


Fig.1.4: Barton's apparatus

This was designed by Barton, and here a couple, which is measured directly, is applied to the lower end of the vertically suspended wire, and the twist produced is noted. Then, equating this couple against the expression for twisting couple $\pi n r^4 \theta / 2l$ for it, the value of n for the wire can be easily calculated.

The wire W , whose coefficient of rigidity is to be determined, is clamped at its upper end H , and has a heavy cylinder C attached to it, at its lower end. Two pieces of cords are wound around the cylinder and, leaving it tangentially at either end, pass over two frictionless pulleys, as shown with equal masses M and M , suspended from their free ends.

The couple formed by the two masses, rotates the cylinder about the wire as axis, and thus twists the wire through an angle θ (radians), say, which is read directly on the horizontal circular scale by the movement of the pointer attached to the wire or by the more sensitive lamp and scale method, with the help of a telescope.

Due to loading and temperature-range limitations of static methods, it was learned long ago that a better method is to measure an elastic vibration, as found for example in a propagating sound wave [35]. Most existing complete sets of elastic constants for materials have been determined by measuring the time of flight of sound pulses. These dynamic methods are more accurate, more versatile and more convenient than static methods [36].

Recent sophisticated techniques of determining elastic constants mostly employ ultrasonic methods; Pulse Superposition Method, Pulse Echo Overlap, Resonant Ultrasound Spectroscopy, phase comparison or related techniques. It is evident from the theory of elasticity that the elastic constants of a material can be obtained by measuring sound velocities in that material. To determine these velocities, time-of-flight can be measured in methods like Pulse Echo Overlap (PEO) method. Measuring the different velocities and the density of the sample, the elastic moduli can be calculated.

In this thesis, results of the measurement of elastic properties of ceramic materials by ultrasonic pulse-echo overlap method are presented. So a detailed description of the ultrasonic methods is given in the thesis, which is in Chapter 2.

B: Ceramic Materials

1.5: The ceramic phase of solids

Ceramics are solid compounds, which are formed by the application of heat and pressure, comprising two or more elements, metals or non-metals. The ceramic family is large and varied including such materials as refractories, glasses, bricks, cements and plasters, abrasives, art wares, porcelain enamels, ferrites, ferroelectrics and dielectric insulators etc.

The main features of ceramic are [37-39] the following.

- (i) The presence of strong covalent character of chemical bonding. The high strength of the covalent bond is responsible for the general high melting point of ceramics, their brittleness, good corrosion resistance, low thermal conductivity and high compressive strength. The enormous range of electronic and diamagnetic properties of ceramics is the manifestation of slight variation in the chemical bonding.
- (ii) Microstructure comprising inorganic crystalline compounds and/or amorphous glass in varying proportions.
- (iii) Processed at high temperatures. High temperature processing in ceramics is important as chemical reactions are accelerated and many raw material constituents of ceramic bodies decompose at high temperature and form

more stable compounds. High temperatures are also necessary to produce new crystal compounds and form homogenous solid solutions. Thermal processing also increases the density of ceramic objects as porosity is gradually eliminated and inter-granular bonds are strengthened.

1.5.1: Composition

Broad ranges of metallic and non-metallic elements are the primary ingredients of ceramic materials. Some of the common metals are Aluminium, Silicon, Magnesium, Beryllium, Titanium and Boron. Non-metallic elements with which they are commonly combined are oxygen, carbon or nitrogen. Ceramics can be either simple one-phase material composed of one compound or multiphase consisting of a combination of two or more compounds.

The structure of ceramics is quite complex. In a ceramic material, the electrons of adjacent atoms are either shared to produce covalent bonds or transferred from one atom to another to produce ionic bonds. These strong bonding mechanisms are what account for many of the ceramic properties, such as high hardness, stiffness and good high-temperature and chemical resistance.

At the micro structural level, ceramic materials can have one, two or three major constituents or components. The component termed the 'body' is an aggregate of the crystalline constituents. The other component is a vitreous or glassy matrix or phase that cements the crystalline particles together. It is often referred to as the ceramic bond. This glassy phase is the weaker of the two components. In most technical ceramics, it is eliminated and replaced by what is termed as crystalline bonding, in which the individual particles of the powder raw material are sintered together in the solid state. During sintering, the temperature is hot enough to cause

the particles to fuse together. A third component, often but not always present, is a surface glaze, which is a thin glassy ceramic coating, fired onto a ceramic body to make it impervious to moisture or to provide special surface properties. Macrostructurally, there are essentially three types of ceramics: (i) crystalline bodies with glassy matrix (ii) crystalline bodies sometimes referred to as holocrystalline and (iii) glasses. Microstructure of ceramics can be entirely glassy, entirely crystalline or a combination of crystalline and glassy.

1.5.2: Preparation methods

The basic steps involved in producing ceramic materials are (i) preparation of the ingredients for forming (ii) shaping or forming the part (iii) drying and (iv) sintering.

(i) Preparation of raw materials

The raw materials are weighed, mixed and blended either wet or dry. In dry processing, the mixture is sometimes heated in order to cause preliminary chemical reactions. In wet processing, the required plasticity for shaping is obtained by grinding and blending plastics with finely pulverized non-plastic ingredients and adding alkalies, acids, and salts.

(ii) Forming methods

Ceramics can be formed by a large number of methods, either in a dry semi liquid or liquid state and in either a cold or hot condition. The different methods include slip casting, jiggering, pressing, extrusion, molding etc.

The dielectric ceramics for the present measurements are formed by pressing. This method can be done with dry, plastic or wet raw materials. In dry processing, ceramic mixtures with liquid level up to 5% by weight are pressed into shape under high pressure in a metal die. This method is widely used for manufacturing

ceramics like electric insulators, electronic ceramic parts etc, since it produces small uniform parts to close to tolerances. Powder pressing produces bodies with the lowest porosity and highest strength because of the high pressure and the small amount of binder required.

(iii) Drying and sintering

The purpose of drying is to remove any water if present. The function of sintering is to convert the shaped dry ceramic part into a permanent product. The sintering process and temperatures used depend on the ceramic composition and desired properties. The top temperature to which a ceramic is sintered is called the maturing temperature. In the first stage of firing, any moisture still present after drying is removed. In the next stage, chemical reactions cause the material to lose its plasticity. In the last stage, vitrification of the ceramic begins and continues up to the maturing temperature. During vitrification, a liquid glassy phase forms and fills the pore spaces. Upon cooling, the liquid solidifies to form a vitreous or glass matrix that bonds the inert unmelted particles together. Electronic ceramics are often fired at high temperatures, sometimes above 3000°C, to obtain the desired vitrification or ceramic bond.

1.6: Classification of ceramics

A wide variety of ceramic materials have been developed over the years for various industrial and technical applications. Many of the commercial types are complex bodies composed of high-melting oxides or a combination of oxides of elements like silicon, aluminium, magnesium, calcium and zirconium. Other technical ceramics are relatively simple crystalline borides, carbides, nitrides,

sulfides and silicides. The major difference between the common and high-grade technical ceramics is that high-grade types do not have a glassy matrix. Instead, in the sintering process, the fine particles of the ceramic material are bonded together by solid surface reactions that produce a crystalline bond between the individual particles.

1.6.1: Oxide ceramics

The oxide ceramics can be divided into two groups, single oxides that contain one metallic element and mixed or complex oxides that contain two or more metallic elements. They differ widely among themselves. Each of them can be produced in a variety of compositions, porosities and microstructure to meet specific property requirements. Alumina, beryllia, zirconia, thoria etc are examples for some oxide ceramics. Beryllia has good dielectric properties and high thermal conductivity. Because of high thermal conductivity they are widely used as transistor heat sinks, resistors and substrates for cooling in electronic equipment.

1.6.2: Mixed oxides

Most of the mixed oxides are composed of various combinations of oxides of different elements. By changing the percentage of different oxides, ceramics with required characteristics can be made

1.6.3: Carbides

There are different classes of carbide ceramics. The carbide family contains materials with highest melting points of all engineering materials. Silicon carbide is an important carbide ceramics. Works dealing with the processing, solidification, influence of sintering atmosphere etc of SiC as well as other biomorphic carbide ceramics like (Si, Ti, Zr)-carbide has been reported in several papers [40-47]

1.6.4: Borides

The major materials in this group of refractory ceramics are borides of Hafnium, Tantalum, Titanium, Uranium, Thorium, Zirconium and Nickel. As a class, they feature a combination of high strength-to-stiffness ratio, high hardness and good high temperature strength retention. Magnesium boride is a superconducting ceramics having a transition temperature of 38K [48]. Boride ceramics having enhanced mechanical characteristics such as high fracture toughness and hardness can be produced by adding a specific amount of Ni–Zr powder to powder Titanium boride, Zirconium boride or Hafnium boride, compacting and firing them [49]. Preparation of other borides like Aluminium boride [50] and Vanadium boride [51] has also been reported.

1.6.5: Nitrides

Boron and silicon nitrides [52-56] are the major commercial materials in this group of refractory ceramics. Boron nitride has a high hardness, equal to that of diamonds, and can withstand high temperatures up to 3600°C without appreciable oxidation. Also, it has high thermal conductivity; five times that of copper at room temperature, which makes it potentially useful for tiny heat-sink devices. Like commercial graphite, hot-pressed boron nitride is anisotropic. Also it has high resistivity and dielectric strength at elevated temperatures. The interface structure and atomic bonding characteristics in silicon nitride ceramics have been studied by A. Ziegler *et al.* [57]. Y. Lin *et al.* [58] found that the thermal conductivity of Silicon nitride ceramics can be improved with magnesia and yttria as sintering additives. Porous Silicon nitride can be fabricated using Yb_2O_3 as sintering additive [59].

1.6.6: Intermetallics and silicides

They are hard and brittle in their polycrystalline form at room temperature, but they can be deformed plastically at elevated temperatures. They are generally considered as having the greatest potential among ceramic materials for achieving low-temperature ductility. Preparation and properties of nitrogen doped Cobalt silicide film is reported by J. H. Ting *et al.* [60]. The thermal expansion anisotropy in binary Molybdenum vanadium silicide has been investigated by C. J. Rawn *et al.* [61]. Other commercially available silicides are Nickel silicide, Iron silicide and Tungsten silicide.

1.6.7: Electronic Ceramics

A number of ceramics are widely used in the electrical field applications, including porcelains, steatites, zircons and cordierites [62]. They are materials like ferrites and ferroelectric ceramics with unusual properties that are of specific use in electronic circuits. Ferrites are mixed-metal oxide ceramics, almost completely crystalline with high electrical resistivity and strong magnetic properties. Ferrites have high volume resistivity and high permeability. They can be divided into soft and hard or permanent-magnet types. Soft ferrites having cubic or spinel crystal structure, can be varied over a wide range for specific uses such as memory cores for computers and cores for radio and television loop antennas. Permanent ceramic magnets have hexagonal crystal structure.

Ferroelectric ceramics have the unusual ability to convert electrical signals to mechanical energy such as sound. They also can change sound pressure or motion into electric signals. Thus they function effectively as transducers. Barium titanate is the most common of ferroelectrics. Others are niobates, tantalates and zirconates.

Lead niobate is widely used as piezoelectric transducer. The new directions in ferroelectric random access memories (FRAMs) and ferroelectric capacitors for dynamic random access memories (DRAMs) have been studied and reported by J. F. Scott [63].

1.6.8: Dielectric resonators

A dielectric resonator [64-65] (DR) is a piece of unmetallised ceramic, which can confine microwave energy at selected discrete frequencies. They are commonly used in devices like filters, oscillators and duplexers used in modern microwave communication systems such as mobile phones. Dielectric resonators are ceramics having high dielectric constant (ϵ_r), high quality factor (Q), and very small temperature coefficient of resonant frequency (τ_f). Generally complex perovskite oxides have proved to be excellent DR materials.

1.6.9: Glass ceramics

Glass ceramics are a family of fine-ground crystalline materials made from special glass compositions. They are sometimes referred to as devitrified ceramics or vitro ceramics. Since they are mixed oxides, different degrees of crystallinity can be produced by varying composition and heat treatment. Glass ceramics are nonporous and generally are either opaque white or transparent. Although not ductile, they have much greater impact strength than commercial glasses and ceramics. Thermal expansion varies from negative to positive values depending on composition. Excellent thermal-shock resistance is obtained for them, if desired. Like chemical glasses, these materials have excellent corrosion and oxidation resistance. They are

electrical insulators and are suitable for high temperature applications in electric field.

1.7: Physical properties of ceramics

1.7.1: Mechanical properties

As a class, ceramics are low tensile strength, relatively brittle materials. Ceramics are notable for the wide difference between their tensile and compressive strengths. They are normally much stronger under compressive loading than in tension. Tensile strength varies considerably depending on composition and porosity. The stress condition of the outer layers also greatly influences the strength. One of the major distinguishing characteristics of ceramics, as compared to metals, is the total absence of ductility. Being strictly elastic, ceramics exhibit very little yield or plastic flow under applied loads.

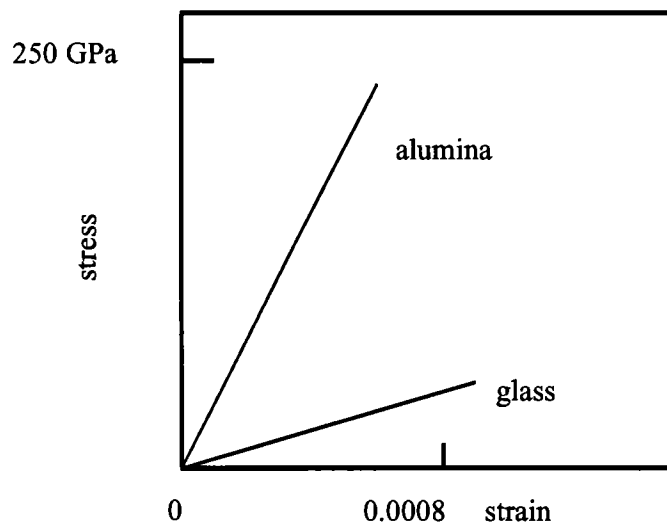


Fig. 1.5: Typical stress - strain behaviour for aluminium oxide and glass.

Ceramics are the most rigid of all materials. For ceramic materials, a linear stress-strain relationship exists. Fig. 1.5 compares the stress-strain behaviour of alumina with that of glass. The slope in the elastic region is the modulus of elasticity; the range of moduli of elasticity for ceramic materials is between 70 and 500GPa, being slightly higher than that for metals. Also they are considerably harder than most other materials.

1.7.2: Thermal properties

Ceramics have the highest melting points of known materials. Hafnium and Tantalum carbide for *e.g.*, have melting points slightly above 7000°C. In general, thermal conductivities of ceramic materials fall between those of metals and polymers. However, thermal conductivity varies widely among ceramics. Thermal conductivity depends on their composition, crystal structure and texture. Simple crystalline structures usually have higher thermal conductivities. Thermal conductivity versus temperature depends on whether the amorphous or crystalline phase predominates in the material.

Compared to metals and plastics, the thermal expansion of ceramics is relatively low, but it varies widely between different types and grades. In brittle materials such as ceramics, the thermal shock resistance is closely related to thermal conductivity and thermal expansion. High thermal conductivity and low thermal expansion favour good shock resistance. Also, small differences between tensile and compressive strength lead to good shock resistance. Since the compressive strengths of ceramic materials are greater than their tensile strength, and because of relatively low heat conductivity, majority of the ceramics have fairly low thermal shock resistance.

1.7.3: Chemical properties

Practically all ceramic materials have excellent chemical resistance. Organic solvents do not normally affect them. All technical ceramics can withstand prolonged heating at minimum of 1900°C. Therefore atmosphere, gases and chemicals cannot penetrate the material surface and produce internal reactions, which normally are accelerated by heat.

1.7.4: Electrical properties

Unlike metals, ceramics have relatively few free electrons and therefore are essentially nonconductive and considered to be dielectric. Most porcelains, aluminas, quartz, mica and glass have large electrical resistivity values and dielectric constants. Electrical resistivity of many ceramics decreases rather than increases with an increase in impurities and is markedly affected by temperature. Ceramics used as dielectric resonators have high dielectric constants, ($20 < \epsilon_r < 100$), high quality factor ($Q > 2000$) and very small temperature coefficient of resonant frequency.

1.8: Structure of Ceramics

Because ceramics are composed of at least two elements, and often more, their crystal structures are generally more complex than most of the metals. The atomic bonding in these materials ranges from purely ionic to totally covalent. Many ceramics exhibit a combination of these two binding types, the degree of ionic character being dependent on the electro negativities of the atoms. For the ceramic materials, for which the atomic bonding is predominantly ionic, the crystal structures

may be thought of as being composed of electrically charged ions instead of atoms. The metallic ions form the cations and the nonmetallic ions form the anions [66]. The magnitude of the electrical charge on each of the compound ions and the relative sizes of the cations and anions influences the crystal structure in crystalline ceramic materials. Since the metallic elements (cations) give up electrons, they are ordinarily smaller than anions, and, consequently, the ratio r_C/r_A is less than unity (r_C – ionic radius of cation and r_A – ionic radius of anion). Each cation/anion prefers to have as many nearest- neighbour anions/cations as possible. Stable ceramic crystal structures form when those anions surrounding a cation are all in contact with that cation, as illustrated in Fig. 1.6.

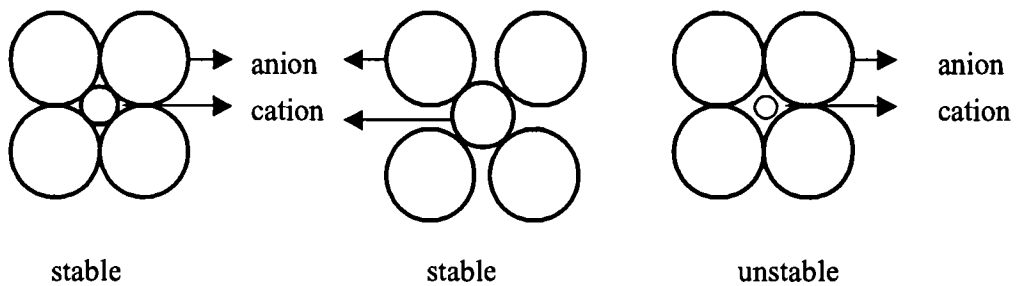




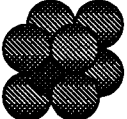


Fig. 1.6: Stable and unstable anion - cation coordination configuration.

The coordination number is related to the cation-anion radius ratio. For a specific coordination number, there is a critical or minimum r_C/r_A ratio. The coordination numbers and nearest-neighbour geometries for various r_C/r_A are presented in Table 1.1.

Table 1.1: Coordination Numbers and Geometries for various Cation–Anion ratios

Coordination Number	Cation – Anion Radius Ratio	Coordination Geometry	
2	<0.155	linear	
3	0.155-0.225	equilateral triangle	
4	0.225-0.414	tetrahedron	
6	0.414-0.732	octahedron	
8	0.732-1.0	cube	

As FCC and HCP crystal structures are formed in metals by stacking the close-packed planes of atoms on one another, a number of ceramic crystal structures also may be considered in terms of close-packed planes of ions, as well as unit cells [66-67]. Ordinarily, the close packed planes are composed of the large anions. As these

planes are stacked atop each other, small interstitial sites are created between them in which the cations may reside. The interstitial positions exist in two different types: tetrahedral and octahedral positions. The coordination numbers for cations filling tetrahedral and octahedral positions are 4 and 6 respectively. For each of the anion, one octahedral and two tetrahedral positions exist as shown in Fig. 1.7. Ceramic crystal structures of this type depend on two factors: (1) the stacking of the close packed anion layers, both FCC and HCP arrangements are possible which correspond to ABCABC.... and ABAB... sequences respectively and (2) the manner in which the interstitial sites are filled with cations. Some of the common ceramic structures are summarised in Table 1.2.

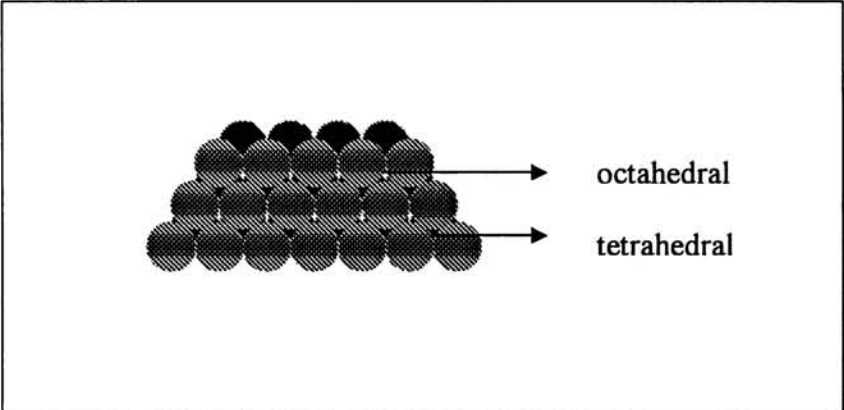


Fig. 1.7: The stacking of one plane of close - packed anions on the top of another, forming tetrahedral and octahedral interstitial sites

Table 1.2: Summary of some common ceramic structures

<i>Structure Name</i>	<i>Structure Type</i>	<i>Anion Packing</i>	<i>Coordination Numbers</i>		<i>Examples</i>
			<i>Cation</i>	<i>Anion</i>	
Rock Salt (Sodium Chloride)	AX	FCC	6	6	NaCl, MgO, FeO
Cesium Chloride	AX	Simple Cubic	8	8	CsCl
Zinc blende (sphalerite)	AX	FCC	4	4	ZnS, SiC
Flourite	AX ₂	Simple Cubic	8	4	CaF ₂ , UO ₂ , ThO ₂
Perovskite	ABX ₃	FCC	12(A) 6(B)	6	BaTiO ₃ , SrZrO ₃ , SrSnO ₃
Spinel	AB ₂ X ₄	FCC	4(A) 6(B)	4	MgAl ₂ O ₄ , FeAl ₂ O ₄

1.9: Applications of Ceramics

Ceramics are vital for a whole spectrum of applications in areas such as electronics, communication, medical electronics, environmental engineering research etc. There are ceramics used as capacitor dielectrics, piezoelectric and ferroelectric ceramics, ceramic substrate materials, ferroelectric films, superconductors, NTC and varistors, microwave dielectrics, ferrites and pyroelectric ceramics. They form the basis of thermal imaging systems, gas sensors, circuit protection devices for computers, precision control devices in cameras and automobile suspension systems.

With the technological advances in using dielectric ceramics as microwave resonators, the progress in microwave telecommunication and satellite broadcasting has risen rapidly [68-75]. In microwave applications, dielectric resonators are used to manufacture microwave integrated circuits, pass-band filters, oscillators etc. High quality dielectric ceramics with high dielectric constant, low dielectric loss and low temperature coefficient of resonant frequency are extensively used in mobile communications for the purpose of miniaturization of dimensions of resonator. By the use of the new generation of ceramic resonators, the filter/combiner units of cellular base stations processes the messages and send them out again. Today, the ceramic resonators look a bit like a do-nut in shape, about 5-10 cm in diameter, depending on the working frequency. Much smaller filters are used in handsets [76]. Resonant frequency of a band-pass filter may be adjusted by using a tuning metallic element. Dielectric ceramic monoblock microwave band pass filters are compact, high Q , surface mountable filters with excellent temperature and time stability.

Dielectric ceramic resonators are also used for impedance converters, discriminators and matching circuits. Combiners are used to transmit multiple frequencies on a single antenna [77].

Coaxial resonators made with modern, high performance ceramic dielectric materials are very useful as compact frequency standards and distributed inductive or capacitive circuit elements. The high Q obtained in the UHF and microwave frequency range makes resonators ideal for many applications. When cost, size and stability are important, these resonators are the best choice. High dielectric ceramic materials assure antennas with compact – small size, wide band and high gain. Low loss and high gain antenna switch modules suitable for SMD mounting in portable wireless designs can be constructed using ceramic materials. Ceramic components help to reduce the near field of the antenna, which in turn reduces the specific absorption rate (SAR) [78]. The main applications [77] of microwave dielectric resonators are,

- (i) Low Noise Block Converters (LNB) for Digital Broadcasting Systems.
- (ii) Microwave sources
- (iii) Microwave filters and multiplexers
- (iv) Security systems, detectors
- (v) Auto Cruise Control (ACC) radar systems
- (vi) Wireless communication equipments, cellular base stations
- (vii) Satellite multiplexing filter devices
- (viii) High stability DROs (Dielectric Resonator Oscillators)
- (ix) Microwave duplexers
- (x) Radio links

- (xi) Wideband networks LMDS, MVDS
- (xii) GSM
- (xiii) PCN/PCS
- (xiv) GPS (Global Positioning Systems) antennas

Several industrial components like high vibration high power ultrasonic transducers and sensors with excellent electro-acoustic efficiency, electronic igniter having high energy output and voltage with low power consumption. Such growing importance of ceramic dielectrics has led to great advances in material research and development also.

1.9.1: Ceramics as substrate materials

Dielectric ceramics are electrical insulators with dielectric strength, dielectric constant and loss tangent values tailored for specific device or circuit applications [79]. In capacitor applications, ceramics with a high dielectric constant are used to increase the charge that can be stored. In microelectronic circuits, low dielectric constant materials are sought to reduce inductive cross talk and noise generation in the circuit. In high voltage insulator applications, high electrical resistivity (ohm-cm) and high dielectric strength (kV per meter) are required.

Ceramic compositions in the system BaO-TiO₂-REO₂ (RE - rare earth elements) are extensively used in the manufacture of electronic components. These compositions have high relative permittivity or dielectric constant, which are useful at high frequencies. Compositions based on BaTiO₃ are used in the preparation of PTC resistors and high dielectric contact capacitors. On the other hand, TiO₂-rich compositions may be used for the preparation of dielectrics with low temperature coefficient of capacitance over a wide range of temperatures and with low dielectric

loss. Such materials are regarded particularly suitable for manufacture of multilayer monolithic capacitors.

The recent advance of novel materials and fabrication technologies, including monolithic microwave integrated circuit (MMIC), micro electro mechanical systems (MEMs), micromatching, high temperature superconductor (HTS) and low temperature co-fired ceramics (LTCC) have stimulated the rapid development of new microstrip and other filters. LTCC stands for a ceramic substrate system, which is applied in electronic circuits as cost-effective and competitive substrate technology with nearly arbitrary number of layers [80]. Printed gold and silver conductors or alloys with platinum or palladium will be used in general. Copper conductors are available too. In today's mobile phones, the power amplifier and also more often the duplexers are made of LTCC. The power amplifier exhibits the advantages that LTCC has a better thermal conductivity and that LTCC is suitable for high integration of passive components. Additionally, the high volume production costs for such small modules are very low. Each layer can be manufactured and inspected in parallel before the substrate stack is laminated.

1.10: Outline of work presented in this thesis

In this thesis, the results of our work on the structural and elastic properties of some selected dielectric ceramics are reported. The experimental techniques we have used are described in detail in Chapter 2. The subsequent chapters describe the work done on various materials, results obtained and discussion of results in each case. The samples selected for investigation are $\text{Ca}_{5-x}\text{Zn}_x\text{Nb}_2\text{TiO}_{12}$, $\text{Ca}_{5-x}\text{Mg}_x\text{Nb}_2\text{TiO}_{12}$ of, and Barium Samarium Titanate (BST) added with different

glasses. The variation of the properties of BST added with different glasses is studied. Also the variation of properties with increasing wt % of glass is studied and reported. The different glasses selected for addition are MgO-Al₂O₃ -SiO₂, ZnO-B₂O₃, B₂O₃ - SiO₂, PbO- B₂O₃ - SiO₂, ZnO- B₂O₃ - SiO₂, MgO-B₂O₃ - SiO₂, ZnO-B₂O₃, Al₂O₃ -SiO₂, Al₂O₃ -B₂O₃ -SiO₂, BaO-B₂O₃ -SiO₂ (30:60:10) and BaO-B₂O₃ - SiO₂ (30:40:30).

The samples are prepared using the standard solid-state ceramic preparation method. To study the elastic properties, we have measured the longitudinal as well as the transverse velocities of ultrasonic waves propagating through the sample. The well-established ultrasonic pulse echo overlap technique has been used to measure ultrasonic velocities accurately. Details of the measurement technique used are given in Chapter 2.

References

1. S. R. Ovshinsky and H. Fritzsche, *IEEE Trans. Electron Devices* Ed. 20 (1973) 91
2. J. M. Ziman, *Models of Disorder*, Cambridge University Press, ix(1979)
3. R. C. Zeller, R. O. Pohl, *Phy. Rev.* **B4**, (1971) 2029
4. W. Heinicke, G. Winterling and K. Dransfeld, *J. Acoust. Soc. Am.* **49** (1971) 954
5. S. R. Ovshinsky and D. Adler, *Contemp. Phys.* **19** (1978) 109
6. P. W. Anderson, *Phys. Rev. Lett.* **34** (1973) 953
7. A. Bienenstock, F. Betts and S. R. Ovshinsky, *J. Noncryst. Solids.* **2** (1970) 347
8. R. A. Flasck, M. Izu, K. Sapru, T. Anderson, *Proc. 7th Intl. Conf. on Amorph. and Liquid Semiconductors*, Edinburgh, Scotland, (1977) 524
9. S. R. Ovshinsky, *J. Noncryst. Solids* **32** (1979) 179
10. W. H. Zachariasen, *J. Am. Chem. Soc.* **54** (1932) 3841
11. See, H. Koizumi and T. Ninomiya, *J. Phys. Soc. Japan* **44** (1978) 898
12. S. R. Herd and P. Chaudhuri, *Phys. Status Solidi A* **26** (1974) 627
13. D. E. Sayer, E. A. Stern and F. W. Lytle, *Phy. Rev. Lett.* **35** (1974) 584
14. N. H. Ritland, *J. Am. Ceram. Soc.* **37** (1954) 370
15. C. Kittel, *Introduction to Solid State Physics*, 4th ed. Wiley, New York (1971)
16. R. J. Bell, P. Dean, *Phil. Mag.* **25** (1972) 1381
17. S. R. Ovshinsky, *Phys. Rev. Lett.* **36** (1976) 1469

18. P. W. Anderson, B. I. Halperin and C. M. Varma, *Philos. Mag.* **25** (1972) 1
19. W. A. Phillips, *J. Low Temp. Phys.* **7** (1972) 351
20. H. P. Baltes, *Solid State Commun.* **13** (1973) 225
21. S. R. Ovshinsky, Proc. *4th Intl. Congress for Reprography and Information*, Hanover, Germany (1975) 109
22. P. H. Klose and S. R. Ovshinsky, *J. Noncryst. Solids*, **8-10** (1972) 892
23. A. E. H. Love, *Treatise on Mathematical Theory of Elasticity*, Cambridge U. K. (1927)
24. Julian Maynard, *Physics Today*, Jan (1996) 26
25. B. A. Auld, *Acoustic Fields and Waves in Solids*, Vol 1, John Wiley and Sons, New York (1973)
26. R. Truell, C. Elbaum, B. B. Chick, *Ultrasonic Methods in Solid State Physics*, Academic Press, New York (1973)
27. E. Schreiber, O. L. Anderson, N. Soga, *Elastic constants and thier measurements*, Mc. Graw Hill, New York (1973)
28. H. J. McSkimin, *Physical Acoustics*, Vol.I, Part a, ed. W. P. Mason, Academic Press, New York (1964)
29. F. I. Fedorov, *Theory of Elastic Waves in Crystals*, Plenum Press, New York (1968)
30. W. P. Mason, *Physical Acoustics and the Properties of Solids*, D. Van Nostrand Company, Inc. Princeton, New Jersey (1958)
31. B. Golding, W. H. Haemmerk, L.F. Schneemeyer and J. V. Waszczak, *IEEE 1988 Ultrasonic Symposium* (IEEE, Piscataway, 1988) 1079

32. A. Migliori, J. L. Sarrao, William, M.\ Visscher, T. M. Bell, *Physica B* **1-24** (1993) 183
33. D. S. Mathur, *Elements of Properties of Matter*, Shyamlal Charitable Trust, Ram Nagar, New Delhi (1978)
34. Brijlal and N. Subrahmanyam, *Properties of Matter*, Eurasia Publishing House Pvt. Ltd., New Delhi (1987)
35. H. J. Stokes, *J. Sci. Instrum.* **37** (1960) 255
36. G. S. Radley and P. J. Banks, *J. Phys. E: Sci. Instrum.* **14** (1981) 546
37. Henry R. Clauser, *Industrial and Engineering Materials*, McGraw Hill, Inc. Japan (1975)
38. The American Ceramic Society *About Ceramics*. Htm 11/18/89.
39. Sheela K. Ramasesha, Science and Technology of Ceramics, *Resonance*, Aug (1999) 16
40. P. Griel, E. Vogli, T. Fey, A. Bezold, N. Popovska, H. Gerhard and H. Sieber, *J. Euro. Ceram. Soc.* **22** (2002) 2697
41. K. Suzuki and M. Sasaki, *J. Euro. Ceram. Soc.* **25** (2005) 1611
42. J. Ihle, M. Herrmann and J. Adler, *J. Euro. Ceram. Soc.* **25** (2005) 987
43. P. Gonzalez, J. Serra, S. Liste, S. Chiussi, B. Leon, M. Perez – Amor, J. Martinez – Fernandez and F. M. Varela – Feria, *Biomaterials*, **24** (2003) 4827
44. M. Singh and J. A. Salem, *J. Euro. Ceram. Soc.* **22** (2002) 2709
45. W. Li, Z. Liu, M. Gu and Y. Jin, *Ceram. Internat.* **31** (2005) 159
46. H. J. Choi and Y. W. Kim, *J. Euro. Ceram. Soc.* **24** (2004) 3795
47. C. R. Rambo, J. Cao. O. Rusina and Sieber, *Carbon*, **43** (2005) 1174
48. http://www.issp.ac.ru/lpcbc/DANDP/MgB2_adv.html

49. http://industrial-ceramics.globalspec.com/Industrial-Directory/zirconium_boride
50. J. M. Mota, M. A. Martinez, F. Velasco and A. J. Criado, *Ceram. Internat.* **30** (2004) 301
51. S. Sen, *Surface Coatings Technology*, **190** (2005) 1
52. Y. Iwamoto, H. Nomura and K. Uematsua, *J. Mater. Res.* **9** No. 5 (1996) 1208
53. M. Amaral, F. Mohasseb, F. J. Oliveira, F. Benedic, R. F. Silva and A. Gicquel, *Thin Solid Films*, **482** (2005) 232
54. F. Zhou, J. Pan and K. Chen, *Mat. Lett.* **58** (2004) 1383
55. M. Hirota, M. C Valecillos, M. E. Brito, K. Hirao and M. Toriyama, *J. Euro. Ceram. Soc.* **24** (2004) 3337
56. A. Neumann, T. Reske, M. Held, K. Jahnke, C. Ragoss and H. R. Maier, *J Mater Sci Mater Med.* **15(10)** (2004) 1135
57. A. Ziegler, J. C. Idrobo, M. K. Cinibulk, C. Kisielowski, N. D. Browning and R. O. Ritchie, *Sci.*, **306** (2004) 1768
58. Y. Lin, X. S. Ning, H. Zhou, K. Chen, R. Peng and W. Xu, *Mat. Lett.* **57** (2002) 15
59. J. F. Yang, Z. Y. Deng and T. Ohji, *J. Euro. Ceram. Soc.* **23** (2003) 371
60. J. H. Ting, S. H. Shiau, Y. J. Chen, F. M. Pan, H. Wong, G. M. Pu and C. Y. Kung, *Thin Solid Films*, **468** (2004) 1
61. C. J. Rawn, J. H. Schneibel and C. L Fu, *Acta Materialia*, **52** (2005) 3843
62. G. S. Brady, *Materials Handbook*, 10th ed., McGraw Hill, Inc., New York
63. J. F. Scott, *Mat. Sci. and Eng. B* **120**, issues 1-3, July (2005) 6

64. R. D. Richtmyer, *J. Appl. Phys.* **10** (1939) 389
65. D. Kajfez and P. Guillon, *Dielectric Resonators*, Artech House, Massachussettes (1986)
66. William D. Callister, Jr, *Materials Science and Engineering: An Introduction*, John Wiley & Sons, Inc. Sixth Edition, (2003)
67. M. W. Barsoum, *Fundamentals of Ceramics*, McGraw- Hill, New York, (1997)
68. D. Kolar, Z. Stadler, S. Gaberseek and D. Suvorov, *Ber. dl. Keram. Ges.* **55** (1978) 346
69. H. M. O. Bryan, J. Thomson and J. K. Plourde, *Ber. dt. Keram. Ges.* **55** (1978) 348
70. H. Oshato, T. Ohhashi, S. Nishigaki, *J. Appl. Phys.* **32**. (1993) 4323
71. I. Laffez, G. Desgardin, B. Raveau, *J. Mat. Sci.* **30** (1992) 267
72. Zhai Jiwei, Yao xi, Cheng Xiaogang, *J. Mat. Sci.* **37** (2002) 3739
73. S. Solomon, N. Santha, N. Jawahar, H. Sreemoolanadhan, M. T. Sebastian and P. Mohanan, *J. Mat. Sci: Materials in Electronics* **11** (2000) 595
74. X. M. Chen, N. Qui and Y. Li, *J. Electroceram.* **9** (2002) 31
75. Chang Chung Lee, *Jpn. J. Appl. Phys.* **37** (1998) 6048
76. <http://www2.umist.ac.uk/material/research/microwave/tutorial.htm>
77. <http://www.soquelec.com/filters.asp>
78. http://www.morganadvancedceramics.com/case_studies/sarantel2.htm
79. http://materials.globalspec.com/LearnMore/Materials_Chemicals_Adhesives/Ceramics_Glass_Materials/Electroceramics/Dielectric_Ceramics_Substrates

80. R. Kulke, *LTCC – Multilayer Ceramic for Wireless and Sensor Applications*,
<http://www.ltcc.de>

CHAPTER 2

Experimental Method

2.1: Introduction

Elastic waves can be propagated through solids, resulting in the collective vibrations of the atoms and molecules in the medium. The vibration characteristics of the atoms and molecules in the medium are determined by the interatomic forces. The nature of these forces is different in different solids and thus the wave propagation characteristics are also different. The wave propagation in a medium is characterized by its velocity and attenuation. The study of interaction of elastic waves with matter provides a great deal of information about their elastic properties. Accurate values of the elastic constants are necessary to determine characteristic model parameters as lists of various atomic models of solids. The quantitative study of elastic constants and their variation with temperature and pressure give information about the interactions of lattice vibrations and other elementary excitations in solids. They also provide a sensitive probe of structural phase transitions in solids.

Ultrasonics is the most established technique to determine the elastic moduli of solids. It is one of the most widely used techniques to investigate phase transitions in solids. One unique advantage of the ultrasonic technique is that both static and dynamic properties can be measured simultaneously. Ultrasonic velocity

measurements provide information about the equilibrium adiabatic properties of the system and the effects of temperature, pressure and external fields can be readily studied. Dynamic aspects of the theories of phase transitions also require information gathered from ultrasonic work.

2.2 Ultrasonic Methods to determine elastic properties of solids

Many advanced and sophisticated methods have been developed to give the precise information about the elastic properties of the materials. Of these, the ultrasonic techniques are widely accepted because of their accuracy and nondestructive nature. The techniques for the measurement of ultrasonic velocity and attenuation are broadly classified into,

- (a) Pulse methods
- (b) Continuous wave methods
- and (c) Low frequency methods.

2.2.1: Pulse methods

In pulse methods [1] short pulses of sound waves are generated with a piezoelectric transducer (usually quartz or materials like LiNbO_3 , BaTiO_3 , SrTiO_3 , PZT etc) which is bonded to the sample under investigation. The sample should be cut and polished to have a pair of perfectly plane and parallel end faces. The propagating waves will get multiply reflected from the end faces and will produce an electric signal each time it hits the transducer. These electric echo pulses are amplified and displayed on an oscilloscope or processed otherwise. From the length of the sample and the transit-time of the pulse in the sample, the velocity, and from

the decay rate of the pulse amplitude, the attenuation can be determined. The absolute accuracy of such methods is generally better than 1%.

Using phase sensitive methods in pulse techniques, the accuracy can be increased and a very high precision of 10^{-6} can be obtained in the measurement of velocity. Such modified pulse methods include (i) pulse superposition method, (ii) phase comparison method, (iii) sing-around method, (iv) long pulse technique, (v) pulse echo overlap method etc., which are briefly explained below.

(i) Pulse superposition method

The pulse superposition method, first proposed by Mc Skimin [2-4], is highly accurate for measuring the ultrasonic wave velocity in materials. In this method, a single transducer is used on the specimen and multiple echoes are obtained. Generally, pulse sequences are produced every T sec, with T approximately equal to some multiple (p) of the round trip delay of ultrasonic wave in the specimen. When the pulse repetition frequency (PRF) is critically adjusted, the applied pulse is superimposed on the echo and the continuous wave in the applied pulse will be phase added with the continuous wave in the echo. The measured delay time is then given by [4]

$$T = p\delta - \frac{p\gamma}{2\pi f} + \frac{n}{f} \quad (2.1)$$

where T is the measured period of the PRF in the interference condition, δ is the true time delay in the specimen, γ is the phase shift introduced by the bond, f is the frequency of the CW oscillator and n is an integer associated with the phase difference between continuous wave within the applied pulse and within the return

echo. From the time of travel of the wave, the velocity of the ultrasonic wave in the sample can be determined.

Errors may occur in the measurement due to diffraction effects [5], distortion of the leading edge of the pulse on reflection, lack of resolution, unknown bond thickness etc. The pulse superposition method has been discussed in detail in several papers and reviews [2-5].

(ii) Phase comparison method

In this method [6-8], coherent wave packets are generated by gating an oscillator. A comparison signal is superimposed on one of the echo signals. The oscillator frequency is adjusted till the comparison signal and the echo are in phase. The frequency then will correspond to an integral number of half wavelengths within the sample. The adjustment of the phase and amplitude of the comparison signal can lead to cancellation of two pulses. This method gives rise to accuracies of the order of 1 part in 10^4 . Errors due to bonding can be minimized by reducing the thickness of bond as nearly as possible to an odd number of quarter wavelengths, at the frequency of measurement. Hydemann [9] designed a fringe counting pulse interferometer, which is capable of measuring large changes in transit time of the order of 1 to 20 microseconds with an accuracy of 2.5×10^{-4} sec.

(iii) Sing-around method

This method [10] is highly sensitive to ultrasonic velocity changes. Two transducers are used for the measurement in the sing around system. A triggered transmitter sends an electrical pulse to the transmitting transducer, which generates a mechanical wave in the specimen. The second transducer receives these waves and amplifies the signal. The leading edge of the received and amplified signals is used

to generate a trigger signal that produces a new pulse from the transmitter. This process repeats continuously. The travel time through the loop is the reciprocal of the trigger signal frequency, which can be measured using a frequency counter.

This method is very useful for relative measurements such as measurement of changes in velocity with change in temperature or pressure; but it is not very good for making absolute velocity measurements, because travel time through the loop is often greater than the travel time through the specimen.

(iv) Long pulse technique

Here, the pulse [11] applied to the transducer is lengthened until echoes from the sample overlap. Such a pattern can be obtained at several frequencies nearby the center transducer frequency. If the successive frequencies in which ‘in phase’ is observed are obtained, then the velocity is given by [12],

$$V = \frac{2l(v_{n+1} - v_n)}{1 + (\phi_n - \phi_{n+1})} \quad (2.2)$$

where l is the sample thickness and ϕ is the phase change on reflection.

Among the several techniques developed for the measurement of ultrasonic velocity and attenuation, the pulse echo overlap (PEO) method is found to be the most used one. To study the elastic properties of the selected ceramics we used this PEO technique. Details of PEO method along with the McSkimin Δt criterion for selecting properly overlapped echoes and method for making bond correction are explained in detail in sections 2.3 and 2.5.1.

2.2.2: Continuous wave methods

Standing waves or continuous waves (CW) have also been successfully applied in various problems in physical acoustics. In this method, one excites

standing wave resonances with quartz transducers. For a sample length l , the number of excited resonances of frequency f is

$$n = \frac{2lf}{v}, \quad (2.3)$$

whereby sound velocity v can be determined. For 10 MHz, n is of the order of 10^2 . Using frequency modulation techniques, one can measure changes in velocity and attenuation with high precision [13-15]. Different CW methods are briefly described below.

(i) Resonant ultrasound spectroscopy (RUS)

Resonant ultrasound spectroscopy is based on the measurement of the vibrational eigen modes of samples of well-defined shapes, usually parallelepipeds or spheres [17-20]. A sample, often a parallelepiped, is held lightly between two piezoelectric transducers. The sample is excited at one point by one of the transducers. The frequency of this driving transducer is swept through a range corresponding to a large number of vibrational eigen modes of the sample. The resonant response of the sample is detected by the opposite transducer. A large response is observed when the frequency of the driving transducer corresponds to one of the sample eigen frequencies. The eigen frequencies depend on the elastic constants, the sample shape, the orientation of the crystallographic axis with respect to the sample, and the density. By measuring a large number of resonant frequencies on one sample, it is possible to obtain information about all these quantities. Usually the sample shape, crystallographic orientation, and density are known and one determines the complete elastic constant matrix from such a spectrum. There is no

need to prepare different samples with different crystalline orientations to carry out the experiment.

(ii) Composite oscillator method

In the continuous composite wave oscillator method [13], the specimen and the transducer act as two terminal electrical network whose characteristics depend on the rapid variation of impedance at each acoustic resonance of the system. The impedance is measured by balancing a bridge [14-15]. If there is a small change in the velocity of the sound in the sample, there is change in resonant frequency or bridge capacity adjustment. The accuracy of the measurement using this technique is ± 0.1 ppm.

2.2.3. Low frequency methods

These methods are particularly suitable for piezoelectric materials, which can be excited into mechanical resonances by an electric field, directly without transducers [22]. The lower limit of frequency is given by the sample dimensions. Here the number n in eqn. (2.3) is of order unity. In this case the elastic compliances (Young's modulus Y and Shear modulus G) are determined by a CW resonance method or by measuring flexural and torsional oscillations. These techniques are described by Read *et.al.* [23].

Other non-piezoelectric crystals can be studied in a similar way with an additional dc bias field using the electrostrictive effect [24]. The low frequency dynamic resonance methods are described by Schreiber *et. al* [25].

2.3: The pulse echo overlap method.

The Pulse Echo Overlap (PEO) method is a highly accurate technique [25-29] for measuring ultrasonic velocity through solids. This method was developed by John E. May [26] in 1958 and modified to its present form by E.P.Papadakis in 1964 [28], with the McSkimin calculation for correct cycle-to-cycle superposition incorporated into this technique. The correct overlap of the rf cycles in echoes, obtained by McSkimin's calculation, permits travel time measurement with high accuracy of the order of 0.001%. The pulse echo overlap method is able to handle diffraction phase corrections properly.

The PEO method has several advantages compared to the other methods. This method can operate with transducer bonded directly to the specimen or with a buffer rod introduced between the specimen and the transducer. The PEO method may be operated with broadband pulses or rf bursts [30]. Simultaneous measurement of attenuation and velocity of ultrasonic wave is another advantage of the PEO method. The group velocity as well as phase velocity can be measured [31] with PEO method by using envelope of moderately narrow band rf pulses.

The fundamentals of PEO measurement can be understood by examining the block diagram in Fig. 2.1.

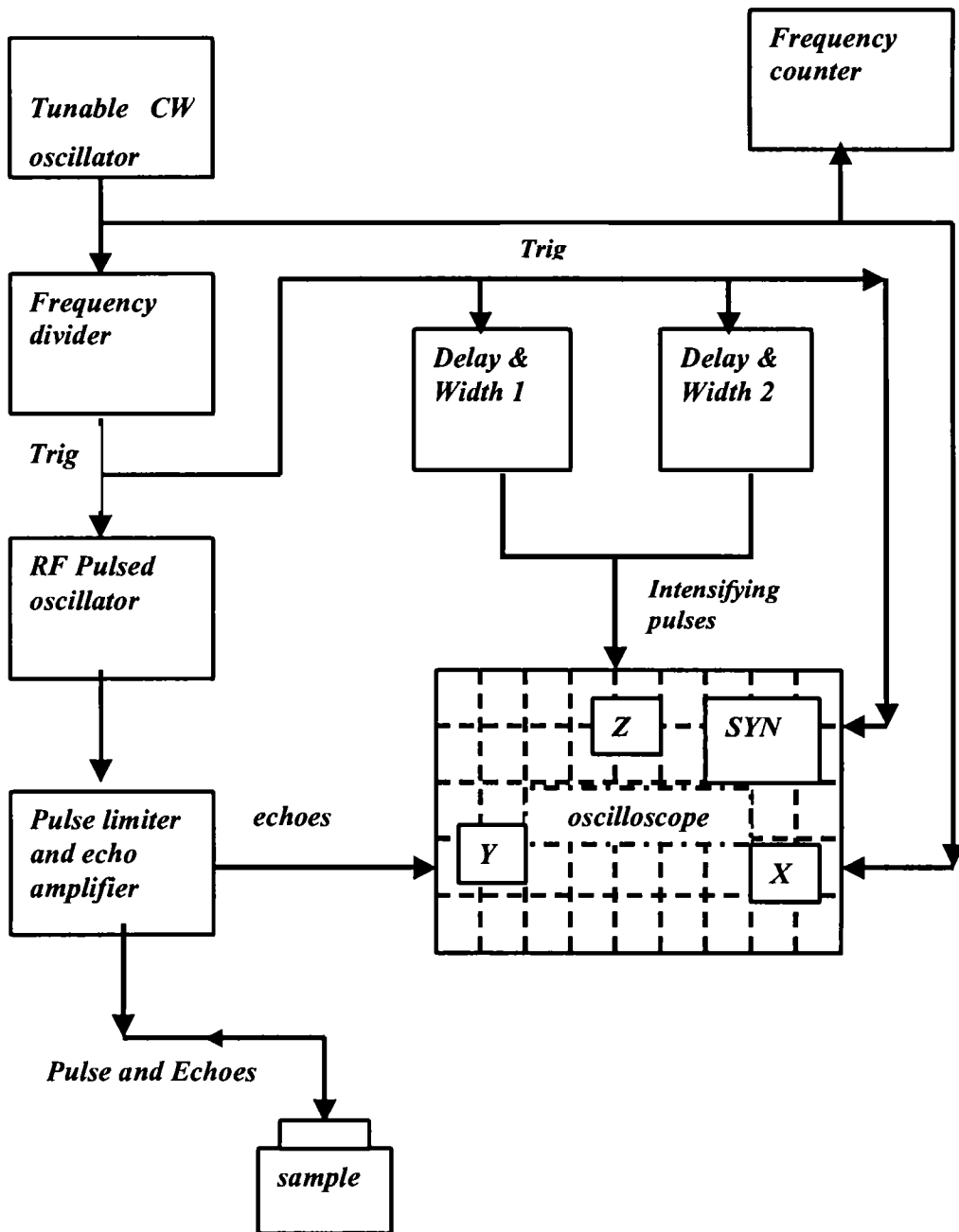


Fig.2.1: The block diagram of the Pulse Echo Overlap method

The CW oscillator is the basic unit and which supplies the frequency, which is to be set as the reciprocal of the delay time between the echoes of interest. The CW signal is given to the x-input of the CRO to display the overlapped echoes, when the CRO is in the x-y mode. A frequency counter measures the exact frequency of the CW oscillator. The frequency divider provides synchronous triggers for the pulsed rf oscillator and the delay circuits. The delay generators provide the two synchronised intensifying pulses of adjustable width and delay to permit the observation of two selected echoes by intensifying the CRO display at the two echoes of interest. The rf pulse energizes the piezoelectric transducer, which sends the ultrasonic signal and receives its echoes. The echoes are sent to the y-input of the CRO after amplification. The diode pulse limiter protects the amplifier input from the high power rf pulses.

When the CRO is in the linear sweep mode, if the time base is properly set, then all the echoes, with exponentially decaying amplitudes, along with the first rf pulse can be seen on the screen. In the frequency divider, division by a large integer of the order of 100 or 1000 allows all echoes from the pulse to be attenuated before the next pulse is supplied. The two echoes of interest between which the time delay is going to be measured, can now be selected by positioning the intensifying pulses on them by adjusting the delay and width of the intensifying pulses. The approximate time interval between the echoes can be noted from the CRO to enable an initial frequency setting for the CW oscillator. When the CRO is switched to the x-y mode, the x-axis sweep is produced by the CW oscillator and a sweep is there corresponding to every echo. The echoes appear on the screen one after the other on successive sweeps. Due to the persistence of vision, the echoes appear as if one is

overlapped on the other. The overlap is exact, if the CW frequency is exactly equal to the reciprocal of the time interval between the echoes. The echoes can be viewed on the screen in an expanded form, with the individual rf cycles in the echo visibly resolved. By fine-tuning the CW oscillator, the cycle-to-cycle overlap of the echoes can be achieved.

The frequency of the CW signal can be obtained from the frequency counter, the reciprocal of which gives the round trip travel time of the echoes in the sample. By knowing the length of the sample, the velocity can be calculated. Due to the attenuation and other pulse distortion effects, the number of rf cycles in the two selected echoes will be different and so it is difficult to find which cycle of the first echo should be overlapped with which cycle of the second. To get correct cycle-to-cycle overlapping, a technique called McSkimin Δt criterion [3-4] is used. This technique is described in detail in section 2.5.1.

2.4: MATEC Model 7700 ultrasonic PEO setup

The experimental set up used for the measurement of ultrasonic velocity consists of equipments from MATEC Inc. (USA). These equipments include Matec Model 7700 pulse modulator and receiver together with Model 760 V rf plug in, Model 110 high resolution frequency source, Model 122B decade divider and dual delay generator, Model 2470B attenuation recorder, Model 70 impedance matching network, HIL Model 2722 frequency counter and a HIL Model 5022 100 MHz dual trace oscilloscope. The block diagram of the experimental setup used is shown in Fig 2.2.

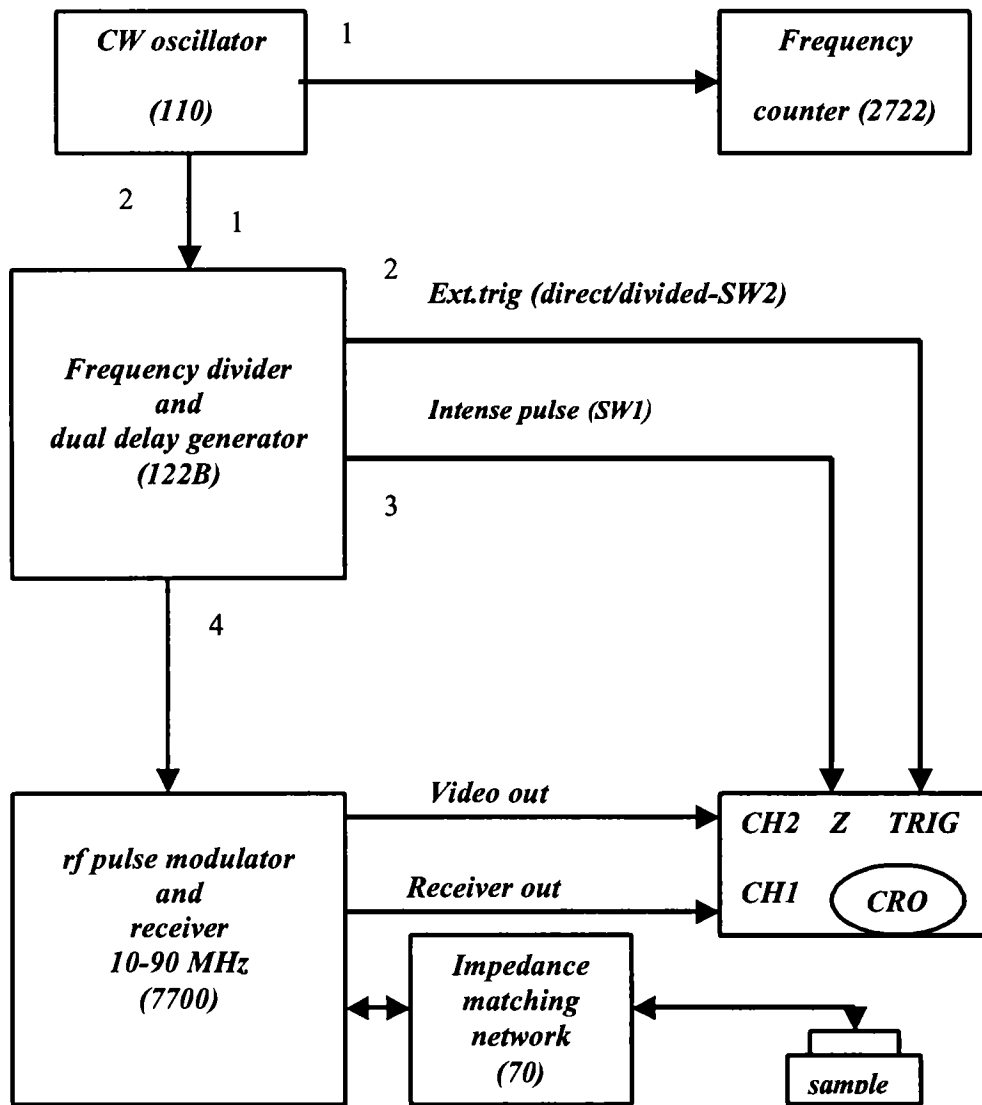


Fig.2.2: Block diagram of the PEO setup used in the present experiments

The tunable CW source has a highly stable internal high frequency oscillator and its output can be varied from 5 Hz to 50 MHz. This oscillator supplies the required low frequency CW signal for PEO, by selectable frequency division, with dual delay and divider unit, which has dividers selectable as 10, 100 or 1000. The division factor 100 is quite acceptable for most measurements. The terminal 2 of this unit gives trigger pulses for the CRO, which is operated in the external sweep trigger mode. By using the switch SW2 in 122B, the trigger at terminal 2 can be made direct trigger or divided trigger for observing the overlapped echoes or the full echo pattern respectively. The dual delay generators in 122B can be adjusted for delay and width of the intensifying pulses for selecting the two echoes of interest for overlap. These pulses are available at terminal 3 and are connected to the z-input of the CRO through selector switch SW1.

The divided trigger from terminal 4 of 122B goes to the most important unit in the setup, the pulse modulator and receiver system (Model 7700 with rf plug-in model 760 V). An rf pulse packet of peak power 1kW is obtained from the output when the unit is triggered at the input. The rf frequency of the triggered power oscillator can be adjusted in the range 10 to 90 MHz. The width and amplitude of the pulse are also adjustable. For good pulse shape, the unit is usually operated at full amplitude and the amplitude reduction is achieved by using an rf attenuator (Allan attenuators) at the output. The unit has a sensitive tunable superheterodyne receiver with a maximum gain of 110 db for amplifying the echoes. The amplified echoes are available at the video out terminal, which is connected to the CRO channel 1 input. The detected output (envelope of the echoes) is available at the video out terminal,

which is connected to channel 2 input of the CRO. The transducer is connected to the pulse output of the modulator and receiver system through an impedance matching network (Model 70) in order to match the impedances of the cable and transducer for optimum power transfer.

The transducer is bonded to the sample using a proper bonding medium. Paraffin oil, motor oil SAE40, nonaq stop cock grease, silicon grease etc are found to be very good bonding media. Silicon grease is found to be suitable for transverse measurements while nonaq stopcock grease gives better response for longitudinal measurements. Their acoustic impedance are accurately determined by measuring ultrasonic velocity at 2 MHz in them and the density. Selection of bonding material is very much dependent on the sample. A photograph of the PEO system in the present measurements is shown in Fig. 2.3.

2.5: Measurement method

By using SW2 in 122B the trigger 2 can be made a divided trigger to observe the echo pattern on the oscilloscope screen. The dual delay generator in 122B can be adjusted for delay and width of intensifying pulses for selecting two desired echoes of interest for overlap.

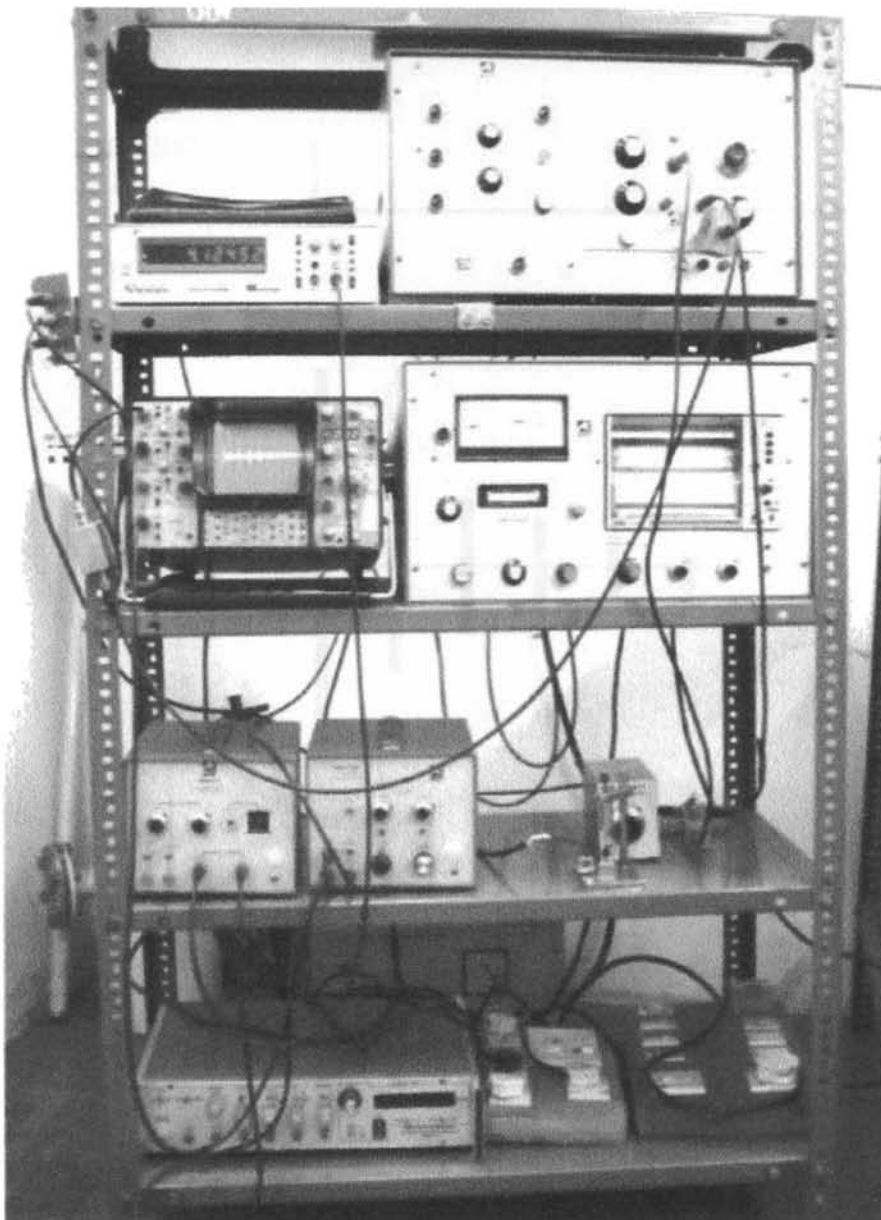


Fig. 2.3: Photograph of the MATEC Model 7700 ultrasonic PEO setup used for the measurements

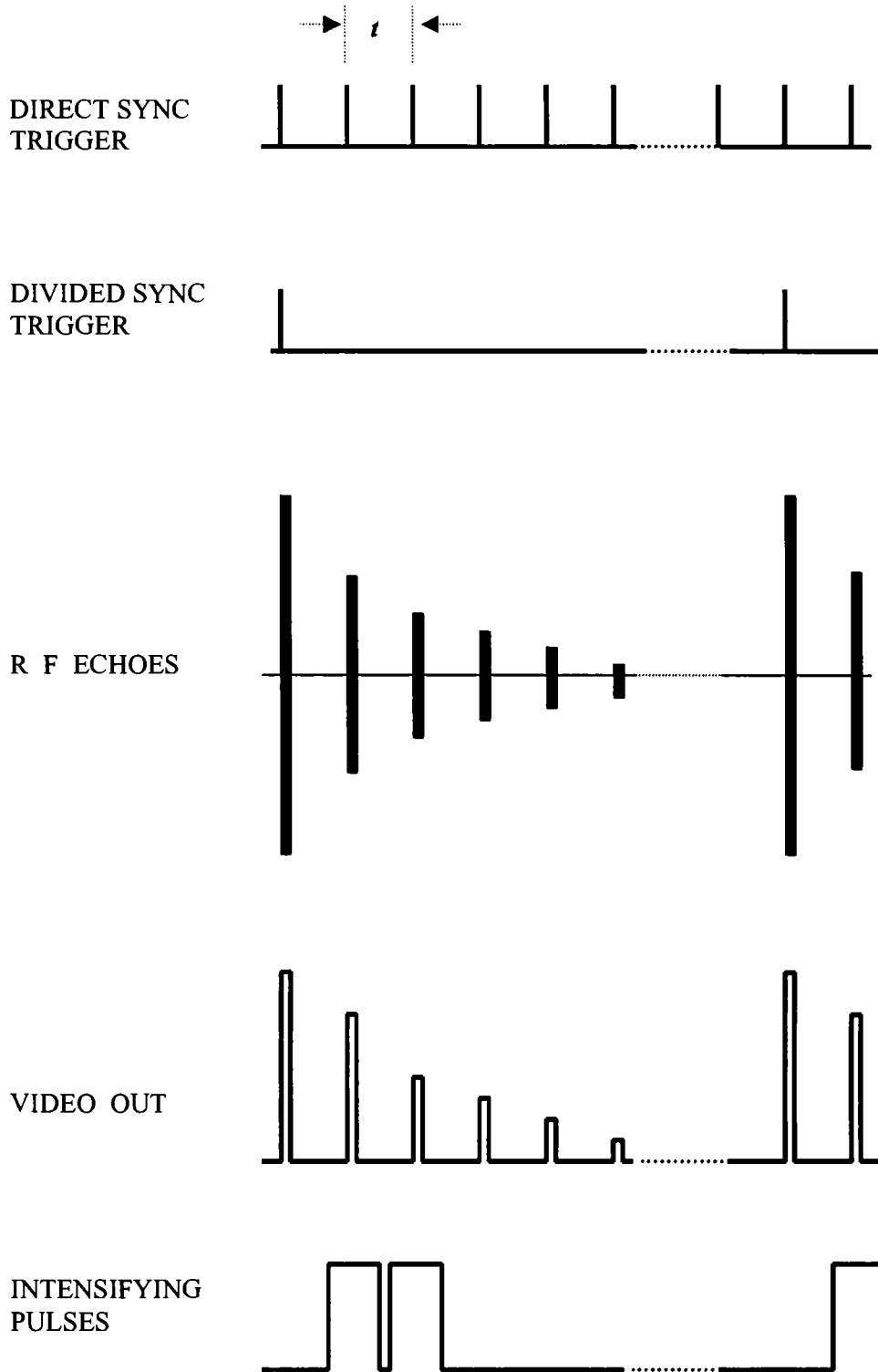


Fig. 2.4: A timing diagram of various system signals. The interval t is the travel time in an overlapped situation.

The switch SW2 in 122B is changed to direct position to overlap the selected echoes. By adjusting the frequency of the CW source, proper overlapping can be made. Now the frequency can be measured from the frequency counter from which the travel time can be determined. By taking the reading for six or seven overlapped conditions and repeating the same for a lower frequency (say, $0.9f_r$), Mc Skimin Δt criterion is applied for getting the corrected velocity as is explained in section (2.5.1).

A timing diagram of the various signals in measurement system is shown in Fig.2.4. The first and second echoes are shown as selected. In a typical setting one divided sync pulse will be produced for every 100 direct sync pulses. The diagram shown is for the overlapped situation.

2.5.1: Bond correction and overlap identification (McSkimin Criterion)

Consider the propagation of ultrasonic waves of single frequency echoing back and forth within the specimen. The specimen is bare on one end but has transducer bonded to the other end. The transducer is half a wavelength thick at its resonant frequency and the bond has finite thickness. The transducer is unbacked. To select the correct cycle-to-cycle matching of one echo with any subsequent echo, the effect of the bond and transducer upon the phase of the reflected wave at the bonded end of the specimen is studied.

Fig. 2.5 shows the sketch of the specimen, bond and the transducer. The phase angle γ relating the reflected wave phase to the incident wave phase is defined in the figure. The specific acoustic impedances are Z_s for the specimen, Z_1 for the bond and Z_2 for the transducer.

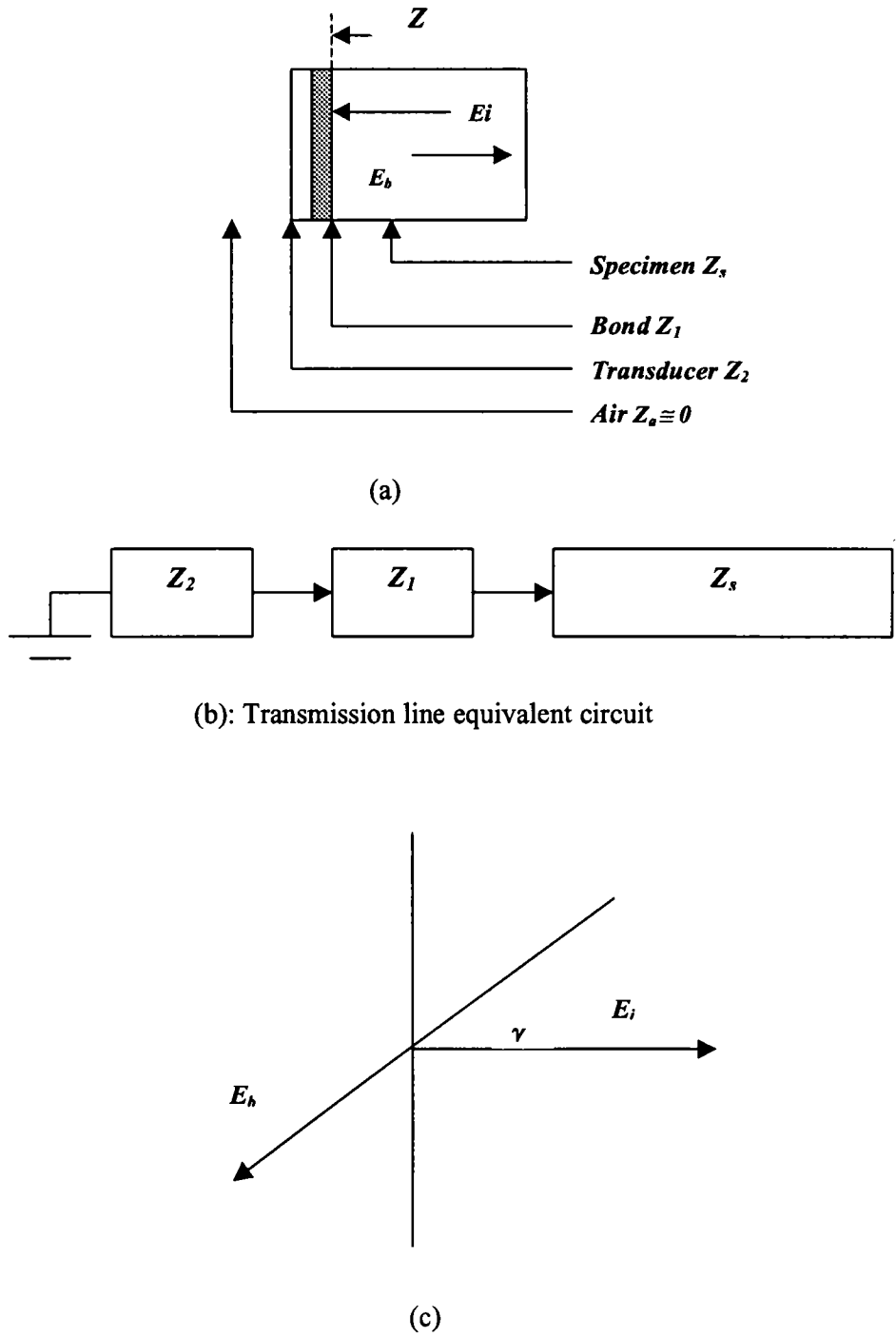


Fig. 2.5: The phase angle γ generated at each reflection of the echoes from the specimen/ bond / transducer interface is shown here diagrammatically

The impedance looking into the termination (bond and transducer) from the specimen is Z_d . Since the transducer is unbacked, the impedance Z_a seen by it at its back is that of air, which is approximately zero.

Assuming negligible attenuation in bond and transducer, the theory of lossless transmission line [32] can be used to obtain an expression for Z_d . as,

$$Z_d \equiv jZ_e = jZ_1 \left(\frac{(Z_1/Z_2)\tan\beta_1 l_1 + \tan\beta_2 l_2}{(Z_1/Z_2) - \tan\beta_1 l_1 \tan\beta_2 l_2} \right) \quad (2.4)$$

where β_1 and β_2 are the propagation constants and l_1 and l_2 are the thicknesses of the bond and transducer respectively. The propagation constants β_1 and β_2 are related to the ultrasonic frequency f impressed upon the transducer by the RF pulse generator and also velocities V_1 and V_2 of the wave in bond and transducer respectively. The relations are,

$$\beta_1 = \frac{2\pi f}{V_1} \text{ and } \beta_2 = \frac{2\pi f}{V_2} \quad (2.5)$$

Z_d can now be used to define the ratio of reflected to incident pressure as,

$$\frac{E_b}{E_i} = \frac{Z_d - Z_s}{Z_d + Z_s} \quad (2.6)$$

with Z_d imaginary ($Z_d \equiv jZ_e$), the real and imaginary parts of eqn.(2.6) can be separated as,

$$\frac{E_b}{E_i} = \frac{Z_e^2 - Z_s^2}{Z_e^2 + Z_s^2} + j \frac{2Z_e Z_s}{Z_e^2 + Z_s^2} \quad (2.7)$$

from which the phase angle γ on reflection is given by,

$$\tan \gamma = \frac{2Z_e Z_s}{Z_e^2 - Z_s^2} \quad (2.8)$$

In the above expression, there is one unknown parameter, the bond thickness l_1 and one running variable, the ultrasonic frequency f . By varying f , one can change β_1 and β_2 using the relations (2.5). The phase angle γ is the relevant measure of the effect of the transducer and bond upon the reflected wave.

McSkimin has shown that the measured travel time t_M is made up of the true round-trip travel time t plus some increments:

$$t_M = pt - \left(\frac{p\gamma}{2\pi f} \right) + \left(\frac{n}{f} \right) \quad (2.9)$$

Here p is the number of round trips in the measurement. The phase angle γ per reflection yields a fraction $\gamma/2\pi$ of a period of the rf, so that a time increment $\gamma/2\pi f$ is generated per round trip. n is the number of cycles of mismatch in the overlap measurement. The aim of the mathematical analysis is to develop a method to make $n=0$ and to estimate the minimum of the residual γ value. The situation corresponding to correct overlap of echoes, with $n=0$, is illustrated in Fig. 2.6.

From the above equations, it is clear that both γ and t_M are functions of the frequency f . It is possible to utilize this dependence of t_M on f to eliminate n , the mismatch. For this consider the possibility of making the measurement of t_M at a high frequency f_H and at a low frequency f_L (for e.g., at the resonant frequency $f_H = f_r$ and $f_L = 0.9f_r$).

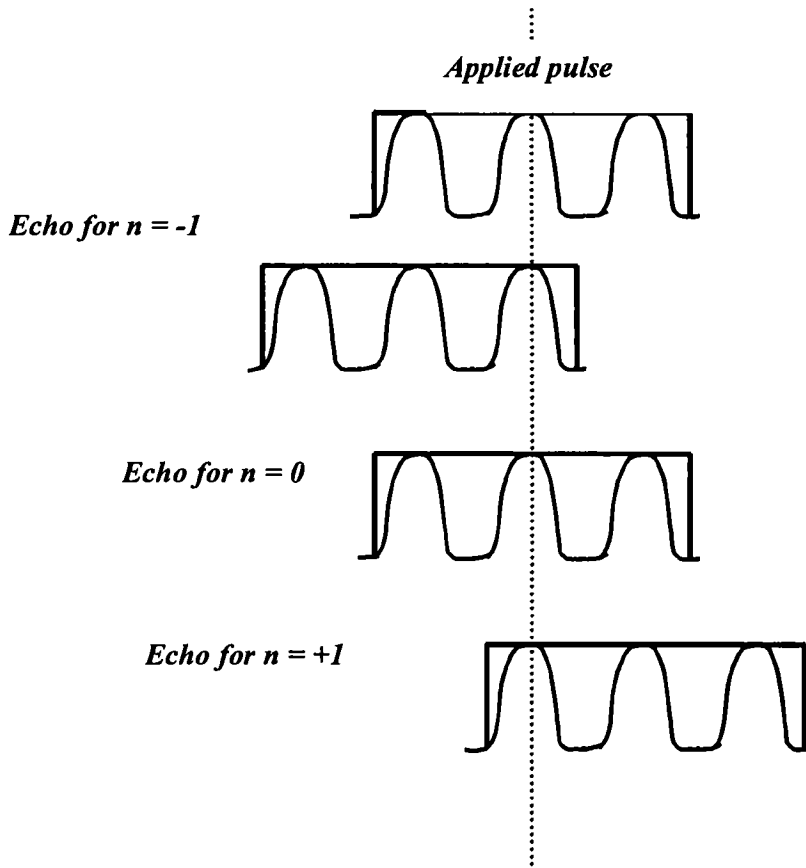


Fig. 2.6: Meaning of $n = 0$

If t_H and t_L are the measured times at f_H and f_L respectively then,

$$t_H = pt - \left(\frac{p\gamma_H}{2\pi f_H} \right) + \left(\frac{n}{f_H} \right) \quad (2.10)$$

and
$$t_L = pt - \left(\frac{p\gamma_L}{2\pi f_L} \right) + \left(\frac{n}{f_L} \right) \quad (2.11)$$

where the same overlap condition (same n) has been maintained by shifting the repetition frequency slightly as the rf frequency is changed. Subtraction eliminates t , the true travel time as,

$$\Delta t_M = t_L - t_H = \frac{1}{f_L} \left(n - \frac{p\gamma_L}{2\pi} \right) - \frac{1}{f_H} \left(n - \frac{p\gamma_H}{2\pi} \right) \quad (2.12)$$

Equation (2.12) expresses Mc Skimin's Δt criterion for finding $n=0$ case. If f_H , f_L , t_H and t_L are measured and if γ_H and γ_L are computed from l_1 , l_2 , V_1 , V_2 , Z_1 , Z_2 and Z_s using equations (2.8), (2.10) and (2.11), then there is only one possible value for Δt_M when $n=0$. Conversely if $n=0$ is set in the measurement, the measured value for Δt_M will agree with the value calculated theoretically.

To apply the McSkimin criterion to PEO technique, one has to follow the following procedure. (i) With the oscilloscope in the triggered sweep, find the approximate time between the echoes of interest from the graticule of the CRO and set the CW oscillator frequency to have that time as its period. (ii) Switch to the direct sync sweep trigger mode and against the CW oscillator frequency to bring about a plausible overlap with the leading edges of the echoes nearly aligned and every cycle of the later echo smaller than the corresponding cycle of the earlier echo because of attenuation. (iii) Measure t_L and t_H of equations (2.10) and (2.11) at the frequencies f_L and f_H usually $0.9f_r$ and f_r . (iv) Repeat step 3 for several possible adjacent overlaps, *e.g.*, three toward lower CW repetition frequencies and as many towards higher. (v) Compute Δt_M found experimentally with theory and choose the correct cycle-to-cycle match. Then the measured time at $f_H = f_r$ will be t_M in eqn (2.9) with $n=0$. Here t_M is the correct expression for the measured time before correction for phase shift due to bond.

Due to the unknown bond thickness, calculation of theoretical value of Δt_M is difficult and hence the comparison of experimental values of Δt_M with the theoretical value is not so simple as explained in step (v). To overcome this difficulty a graphical technique is often used. For this, it is assumed that the bond is very thin, that is less than a quarter of the acoustical wavelength, which is usually satisfied in the experimental situation. This means that the bond phase $\beta_1 l_1$ expressed in degree can be in the range 0 to 90 degrees. A plot of Δt vs bond angle is then made. This gives a range of possible Δt values for the given transducer, bond and sample combination for $n = 0$ case. Then it can be examined in which overlap-case in the measured values falls in this range and that overlap-case can be taken as the $n = 0$ case. Thus the correct overlap can be identified.

To find the correction factor we need the value of the unknown phase angle γ . All parameters except the bond thickness (or bond angle) are known for the computation of γ . The bond angle can now be found out from the plot as the angle corresponding to the measured value of Δt which has fallen in the possible range. Thus the correction factor in equation (2.12) can now be estimated and the true round-trip time t in the sample can be obtained. It may be noted that a graph has to be plotted for every measurement.

The Mc Skimin Δt criterion has been used to identify the correct overlap in all the measurements reported in this thesis. This ensures accuracy better than 1% in all the velocity measurements.

2.6: Structural properties by X-ray diffraction

The X-ray diffraction (XRD) pattern is a fingerprint of a crystalline compound. Using XRD pattern the structure of the crystalline components of a mixture can be identified [33].

A crystal contains a very large number of periodic array of atoms. Diffraction would occur if a radiation having a wavelength comparable to the interatomic distance is incident on a crystal. X-rays meet this wavelength requirement. The condition for diffraction of an X-ray beam from a crystal of interatomic spacing d is given by the Bragg equation as,

$$n\lambda = 2d \sin \theta_n \quad (2.13)$$

where $n \rightarrow$ order of diffraction

$\lambda \rightarrow$ wavelength of the wave used and

$\theta_n \rightarrow$ angle of diffraction

Atoms located exactly on the crystal planes contribute maximally to the intensity of the diffracted beam. Atoms exactly halfway between the planes exert maximum destructive interference and those at some intermediate location interfere constructively or destructively depending on their exact location but with less than the maximum effect. Furthermore, the scattering power of an atom for X-rays depends on the number of electron it posses. Thus the position of the diffraction beams from a crystal depend only on the size and shape of the repetitive unit of a crystal and the wavelength of the incident X-ray beam. The intensities of diffracted beams depend on the type of the atoms in a crystal and the location of the atoms in

the unit cell. No two substances therefore have identical diffraction patterns, when both direction and intensity of all diffracted beams are considered.

The XRD patterns of the various samples are recorded with a Bruker D8 Advance X-Ray Diffractometer with the following specifications.

Configuration	: vertical, Theta / 2 Theta geometry
Measuring circle diameter	: 435, 500, 600 mm predefined
Angle range	: 360°
Max. Usable angular range	: 3° to 135°
Smallest addressable increment	: 0.001°
Max. angular speed	: 30°/s
X- ray source	: Cu

2.7: Microscopic structure by scanning electron microscopy

The scanning electron microscope (SEM) is widely used for studying sample surfaces [34]. The scanning electron microscope has an electron gun producing an electron beam, usually, consisting of thermionically emitted electrons from a hot metal filament. This electron beam is focused to a point in the plane of the specimen, by electromagnetic coils (magnetic lenses). The position of the point can be varied by deflecting the electron beam and the entire surface of the specimen can be scanned using the beam. When the electron beam impinges upon a point on the surface, it gets scattered and the scattering depends on the surface geometry. The scattered beam is collected at a detector and sent to a cathode ray tube for display. The cathode ray tube is synchronized with the beam in the microscope and each

point on the screen of the tube corresponds to a point on the specimen. The detector signal modifies the light intensity appearing on the screen. For example, those points on the specimen which cause a large number of electrons to strike the detector will appear as light regions on the screen and vice versa. In this way contrast is provided and the cathode ray tube provides a picture of the surface. The resolution of this microscope is determined by the size of the beam when it impinges upon the specimen.

Microstructural analysis of ceramic samples was held using scanning electron microscopic (SEM, Model S – 2400, Hitachi, Japan) techniques. SEM of most of the samples investigated in this work has been recorded. SEM pictures were recorded from carefully finished surfaces of the samples.

References

1. F. Birch, *J. Geophys. Res.* **65** (1960) 1083
2. H.J. McSkimin, *J. Acoust. Soc. Am.* **33** (1961) 12
3. H.J. McSkimin and P. Andreatch, *J. Acoust. Soc. Am.* **34** (1962) 609
4. H.J. McSkimin and P. Andreatch, *J. Acoust. Soc. Am.* **41** (1967) 1052
5. E.P.Papadakis, *Physical Acoustics* Vol. XII A, Ed: W.P. Mason, Academic Press, New York (1976)
6. E.P.Papadakis, *J. Acoust. Soc. Am.* **40** (1966) 863
7. H.J. McSkimin and P. Andreatch, *J. Acoust. Soc. Am.* **22** (1950) 413
8. J.J. Moran, B.Leithi, *Phys. Rev.* **187** (1969) 710
9. P.L.M. Heydemann, *Rev. Sci. Instr.* **42** (1971) 983
10. N.P. Cedrone, D.R. Curram, *J. Acoust. Soc. Am.* **26** (1954) 963
11. R.D. Holbrook, *J. Acoust. Soc. Am.* **20** (1948) 590
12. R. Truell, C. Elbaum and Chick, *Ultrasonic Methods in Solid State Physics*, Academic Press, New York and London (1969)
13. D.I. Bolef, *Physical Acoustics*, Vol. IV PT A, Ed: W. P. Mason and R. N. Thurston, Academic Press, New York (1966)
14. D.I. Bolef and J. G. Miller, *Physical Acoustics*, Vol.VIII, Ed: W.P. Mason and R. N. Thurston, Academic Press, New York (1971)
15. B.Luthi and W. Rehwald, *Structtural Phase Transitions I*, Ed: K.A. Muller and H. Thomas, Springer Verlag Berlin (1981)
16. A. Migliori, J.L.Sarrao, William M. Visscher, *Physica B* **183** (1993) 1
17. J. Maynard, *Phy. Today*, Jan. (1996) 26

18. I. Ohno, *J. Phys. Earth*, **24** (1976) 355
19. R. G. Leisure and F.A. Wiliis, *J.Phys: Condens. Matt.* **9** (1997) 6001
20. A. G. Beathe, H.B.Silsbee and E.A. Uchling, *Bull. Am. Phys. Soc.* **7** (1962) 475
21. G.A. Alers, *Physical Acoustics* Vol. IV A, Ed: W.P. Mason, Academic Press, New York (1976)
22. W.P. Mason, *Piezoelectric crystals and their application to Ultrasonics*, Van Nostrand, Princeton (1950)
23. T.A. Read, C.A. Wert, M.Metzger, *Methods of Experimental Physics*, Vol.6 A, Ed: K. Lark-Horovitz, V.A. Johnson, Academic Press, New York (1974)
24. G. Rupprecht, W.H. Winter, *Phys. Rev.* **155** (1967) 1019
25. E. Schreiber, O.L. Anderson, N.Soga, *Elastic Constant and their measurement*, McGraw-Hill, New York (1973)
26. J.E. May, Jr. IRE Nat. Conv. Rec. **134** (1958) 6
27. E.P.Papadakis, *J. Acoust. Soc. Am.* **42** (1967) 1045
28. E.P.Papadakis, *J. Appl. Phys.* **35** (1964) 1474
29. E.P.Papadakis, *Physical Acoustics Vol. XI*, Ed: W.P. Mason, Academic Press, New York (1975)
30. E.P.Papadakis, *J. Acoust. Soc. Am.* **45**, (1979) 1547
31. E.P.Papadakis, *J. Acoust. Soc. Am.* **52** (1972) 843
32. W.C. Johnson, *Transmission lines and Networks*, McGraw Hill, Singapore (1963).
33. Willard, Merritt, Dean and Settle, *Instrumental Methods of Analysis*, 7th Edition, CBS Publishers and Distributors, New Delhi (1986)

34. Melvin M. Eesenstadt, *Introduction to Mechanical Properties of Materials*,
The Mac Millian Company, New York

CHAPTER 3

Influence of oxide glass addition on the elastic and structural properties of $\text{Ba}_{6-x}\text{R}_{8+2x}\text{Ti}_{18}\text{O}_{54}$ ceramics

3.1. Introduction

The revolution in wireless communication and information access is one of the most dramatic changes in technology during the past decade. This revolution is apparent on a daily basis in the ever-increasing number of cellular phone users. As in all technological systems, the basis of these revolutionary changes is advances in materials, which have their own specialized requirements and functions [1]. High quality microwave dielectric ceramics have been extensively used in mobile communication as well as satellite broadcasting systems, for the purpose of miniaturization of dimensions of circuit components such as filters and resonators [2]. The materials for microwave resonators are required to excel in the following three dielectric characteristics. The first one is high dielectric constant (ϵ_r), because microwave wavelength (λ) is inversely proportional to $\sqrt{\epsilon_r}$ of the dielectric materials ($\lambda = \lambda_0 / \sqrt{\epsilon_r}$, λ_0 is the initial wavelength). The second characteristics is the quality factor Q , which is the inverse of dielectric loss tangent ($Q = 1/\tan \delta$), is required to be high for achieving prominent frequency selectivity and stability in microwave transmitter and receiver components. As the third characteristic, the temperature coefficient of resonant frequency (τ_f) is required to be as close to

0 ppm/°C for the system to be stable [3] as temperature changes. Presently, high ϵ_r dielectric systems replaced SiO₂ for use as the basis of advanced capacitance components in microelectronic memory and other applications in thin film rather than in bulk form [1].

One of the first materials utilized for this application was TiO₂, which was inexpensive, displayed excellent Q ($\approx 15,000$ at 3 GHz) and high ϵ_r (≈ 100), but it possesses a large τ_f of about 400 ppm /°C [4]. The binary barium titanates were the first dielectric materials described as having practical application in modern microwave resonators [5-6] and remain in commercial use. Since 1970s, microwave dielectric ceramics with dielectric constant in the range 20 – 40, such as Ba(Mg, Ta)O₃, Ba(Zn,Ta)O₃, BaTi₄O₉ and Ba₂Ti₉O₂₀ systems, have been developed and applied successfully to many commercial units [7-8]. O'Bryan and coworkers developed Ba₂Ti₉O₂₀ based ceramics as filters for the base stations of the infant cellular industry and for conventional telephone microwave relays. The dielectric behaviour of Ba₂Ti₉O₂₀ and BaTi₄O₉ can be improved by forming composites with additives like ZnO, SnO₂, Ta₂O₅ etc [9-10]. An excellent description of many considerations involved in developing new materials for commercialization can be found in reference 9. This family of materials is quite sensitive to firing conditions and defect chemistry. This is due to the reduction of Ti⁴⁺ to Ti³⁺, which can be reduced by substituting Mn for Ti in small proportions. The detailed study of the factors affecting the formation of Ba₂Ti₉O₂₀ is done by J. Wu and Wang [11].

Other important members of barium titanate family are complex ternary materials in BaO-R₂O₃-kTiO₂ chemical systems with a bronze structure, where R =

Sm, Nd, Pr, La, are rare earth elements, with $k = 3 - 5$ [12-14]. The main phases of $\text{BaO-R}_2\text{O}_3\text{-kTiO}_2$ were reported as $\text{BaO-R}_2\text{O}_3\text{-4TiO}_2$ with a conventional formula $\text{Ba}_{6-x}\text{R}_{8+2x}\text{Ti}_{18}\text{O}_{54}$ and $\text{BaO-R}_2\text{O}_3\text{-5TiO}_2$ having conventional formula $\text{Ba}_{1-3x}\text{R}_{2+x}\text{Ti}_5\text{O}_{14}$ in different studies [2, 4, 15-17]. The possible existence of solid solutions on the tie line of $\text{BaO-R}_2\text{O}_3\text{-3TiO}_2$ and $\text{BaO-R}_2\text{O}_3\text{-5TiO}_2$ were also suggested [18]. Nishigaki *et al.* [19] had studied the microwave dielectric properties of $\text{BaO-Sm}_2\text{O}_3\text{-4.7TiO}_2$ and $\text{BaO-Sm}_2\text{O}_3\text{-4.8TiO}_2$ systems. Y. C. Chen *et al.* [18] reported the zero temperature coefficient (τ_f) compounds $\text{Ba}_{2-x}\text{R}_{4+2x/3}\text{Ti}_9\text{O}_{26}$ belonging to the $\text{BaO-Sm}_2\text{O}_3\text{-4.5TiO}_2$ system. The phase development and microwave dielectric properties of $\text{BaO-xSm}_2\text{O}_3\text{-4.5TiO}_2$ ($x = 0 - 1.25$) were described by S. W. Jung *et al.* [20]. C. L. Huang *et al.* [21] investigated the microstructure and dielectric properties of $\text{Ba}_{2-x}\text{Sm}_{4+2x/3}\text{Ti}_{8+y}\text{O}_{24+y}$ ceramics, belonging to the $(1-x/2) \text{BaO} : (1+x/3x) \text{Sm}_2\text{O}_3 : k\text{TiO}_2$, with $x = 0.1$ and $y = 0 - 2$.

$\text{BaR}_2\text{Ti}_4\text{O}_{12}$ and $\text{BaR}_2\text{Ti}_5\text{O}_{14}$ are important members belonging to the $\text{BaO-R}_2\text{O}_3\text{-4TiO}_2$ family. The reaction sequence and dielectric properties of $\text{BaSm}_2\text{Ti}_4\text{O}_{12}$ in different calcining temperatures were studied by P. S. Cheng *et al.* [22]. Different intermediate phases like BaTiO_3 , BaTi_4O_9 , $\text{Sm}_2\text{Ti}_2\text{O}_7$ were revealed in the X-ray diffraction patterns, as the calcining temperature was increased from 850°C to 1250°C . Tailoring of microwave properties of $\text{BaR}_2\text{Ti}_4\text{O}_{12}$ and $\text{BaR}_2\text{Ti}_5\text{O}_{14}$ ($\text{R} = \text{Nd, Sm}$) ceramics, by the addition of Bi_2O_3 was reported by S. Solomon *et al.* [23]. The effect of B_2O_3 doping on the dielectric properties of $\text{BaNd}_2\text{Ti}_5\text{O}_{14}$ is explained by C. H. Lee *et al.* [24]. They found that when the amount of B_2O_3 was greater than 5 wt %, $\text{BaNd}_2\text{Ti}_5\text{O}_{14}$ get decomposed to $\text{Ba}_2\text{Ti}_9\text{O}_{20}$ causing to decrease ϵ_r , whereas Y.

Song *et al.* [25] reported as the dielectric properties of $\text{BaEu}_2\text{Ti}_4\text{O}_{12}$ were improved by mixing it with BaTi_4O_9 . Addition of 5 –10% $\text{Bi}_2\text{Ti}_2\text{O}_7$ was found to improve the τ_f of $\text{BaNd}_2\text{Ti}_5\text{O}_{14}$. It has been reported that the variation of dielectric properties of $\text{BaNd}_2\text{Ti}_5\text{O}_{14}$ and $\text{BaSm}_2\text{Ti}_5\text{O}_{14}$ is due to the presence of secondary phases such as $\text{Ba}_2\text{Ti}_9\text{O}_{20}$, BaTi_4O_9 , TiO_2 , $\text{Nd}_2\text{Ti}_2\text{O}_7$, $\text{Sm}_2\text{Ti}_2\text{O}_7$ etc. The temperature coefficient of resonance frequency in the above systems can be improved by substituting Ba partially by Sr or Pb [26].

$\text{Ba}_{6-x}\text{Sm}_{8+2x}\text{Ti}_{18}\text{O}_{54}$ (BST) is an important microwave dielectric ceramic in the $\text{Ba}_{6-x}\text{R}_{8+2x}\text{Ti}_{18}\text{O}_{54}$ solid solution family, which received much scientific and commercial interest as the key material for microwave dielectric resonators and filters [27 – 31]. The relation of microwave dielectric properties of $\text{Ba}_{6-x}\text{Sm}_{8+2x}\text{Ti}_{18}\text{O}_{54}$ solid solutions with crystal structure in the range $0.3 \leq x \leq 0.7$ was reported by H. Ohsato *et al.* [2]. The dielectric properties as a function of composition x for the Sm and Nd systems and for the Pr system were reported by Fukuda *et al.* [33]. Matveeva *et al.* [34] determined first the crystal structure of $\text{Ba}_{3.75}\text{Pr}_{9.5}\text{Ti}_{18}\text{O}_{54}$ (for $x = 3/4$) based on the fundamental unit cell by single crystal X-ray diffraction. BST has the typical microwave dielectric properties for the composition of $x = 2/3$, reported as $\epsilon_r = 81$, $Q.f = 9600$ GHz and $\tau_f = -14\text{ppm}/^\circ\text{C}$ [32, 35]. The end members of the solid solution family are $3\text{BaO} \cdot 2\text{R}_2\text{O}_3 \cdot 9\text{TiO}_2$ for $x = 0$ and $3\text{BaO} \cdot 5\text{R}_2\text{O}_3 \cdot 18\text{TiO}_2$ for $x = 1$ [16]. The tungsten – bronze structure was confirmed by Roth *et al.*, Ohsato *et al.* [35], Kolar *et al.* [37] and so on. A superlattice with two times the fundamental lattice spacing along the c -axis has been found in $\text{Ba}_{3.75}\text{R}_{9.5}\text{Ti}_{18}$ ($\text{R} = \text{La}, \text{Nd}, \text{Sm}$) crystals.

To get dense ceramics with homogenous microstructure, BST ceramics has to be sintered at temperature of about 1300-1400 °C. When materials are sintered at such high temperatures, the bottom electrode (for thick film or thin film technology) or inner electrode (for MLC structure) must be of a noble metal, such as Pt, and which increases manufacturing costs. Therefore, studies of dielectric ceramics have focused on decreasing the sintering temperature and improving the dielectric properties by controlling the sintering conditions and microstructure and by adding sintering aids [38-40]. One method of decreasing the sintering temperature is to add sintering aids like glasses that have low melting points and make liquid phases below the sintering temperature. The relationship between the sintering temperature and dielectric properties are discussed in several papers [41-44] by earlier workers. However, not much effort has been made to understand the effects of adding such sintering aids on the elastic and mechanical properties of these materials.

The purpose of this study is to investigate how glass addition affects the elastic properties of BST ceramics. Since the dielectric constant, quality factor, dielectric loss and structural stability of ceramics are interconnected parameters and these are influenced by the mechanical strength and stability of the system, it is necessary to know the elastic stability of the system, which is closely related to structural stability. Elastic constants C_{11} and C_{44} are measured on BST samples added with different mixed oxide glasses and the results are presented in this chapter.

3.2. Sample Preparation

The pure BST ceramics were prepared by accurately weighing high purity (99.9 %) BaCO₃, Sm₂O₃ and TiO₂ in the stoichiometric proportions and wet mixed with distilled water and ball-milled with ZrO₂ balls for 24 hrs. The dried powders were calcined in platinum crucibles at 1150°C for 4 hrs. The calcined powder was again ground well in agate mortar and PVA (5%) was added and mixed well. After drying, the mixture was again ground well for half an hour. This fine powder was pressed into cylindrical compacts of 12 mm or 14 mm diameter and 6 mm length under a pressure in the range of 100 to 150 MPa. The pellets so obtained were then sintered at a temperature of 1350°C for about 4 hours.

For the glass added samples, the chemicals BaCO₃, Sm₂O₃ and TiO₂ were weighed in stoichiometric ratios. The powders were mixed well and calcined as described above. The calcined powder was then divided into five or six parts and fixed wt % of the different glasses were added to different parts. Dielectric ceramics were prepared from the powders by the conventional method as described above and the samples were then sintered at appropriate optimized temperatures.

3.3. Samples Studied

The samples selected for study are pure Ba_{6-x}Sm_{8+2x}Ti₁₈O₅₄ with $x = 2/3$ (BST) and BST with 0.5 wt% of different glasses added to it. The glasses added include MgO-Al₂O₃-SiO₂, ZnO-B₂O₃ (77:23), ZnO-B₂O₃ (50:50), B₂O₃ - SiO₂, ZnO-B₂O₃ - SiO₂, PbO- B₂O₃ - SiO₂, MgO-B₂O₃ - SiO₂, Al₂O₃ -SiO₂, Al₂O₃ -B₂O₃ -SiO₂, BaO-B₂O₃ -SiO₂ (30:60:10) and BaO-B₂O₃ -SiO₂ (30:40:30).

3.4. Structure by XRD

The $\text{Ba}_{6-x}\text{Sm}_{8+2x}\text{Ti}_{18}\text{O}_{54}$ solid solutions were reported as ternary compounds existing on the tie line between BaTiO_3 and R_2TiO_9 composition in the $\text{BaO-R}_2\text{O}_3\text{-TiO}_2$ ternary system [2, 16, 45-46] as illustrated in Fig. 3.1.

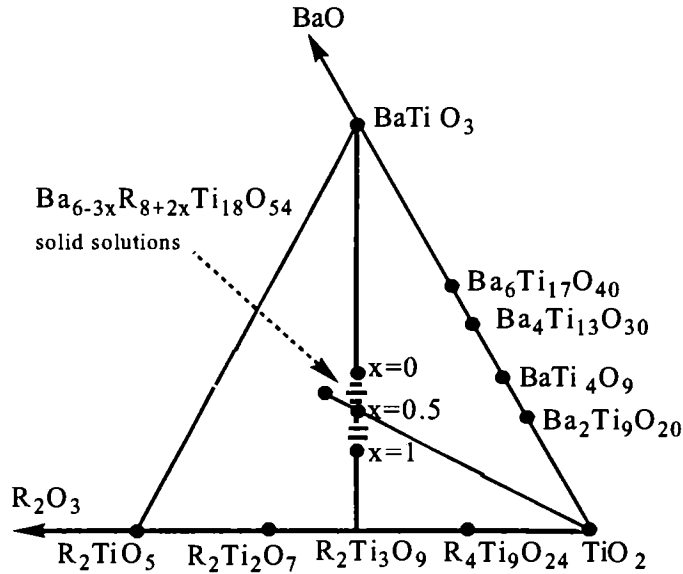


Fig.3.1: A part of the $\text{BaO-R}_2\text{O}_3\text{-TiO}_2$ ternary system.

The solid solution has a new tungsten bronze-type structure [4, 34-35] with perovskite columns, which have 2×2 unit cells of perovskite blocks and have pentagonal sites occupied by the large cation (Ba^{2+} , Sm^{3+}), which have been shown by Matveeva *et.al.* [34] and Ohsato *et al.* [35]. The formation region of the solid solutions is revealed as $0.3 \leq x \leq 0.7$ in the $\text{Ba}_{6-x}\text{R}_{8+2x}\text{Ti}_{18}\text{O}_{54}$ equation in the case of $\text{R} = \text{Sm}$ [12, 45].

The crystal structure of $\text{Ba}_{6-x}\text{Sm}_{8+2x}\text{Ti}_{18}\text{O}_{54}$ has been reported by several authors [34-37]. The superlattice with twice fundamental lattice spacing along c -axis was pointed out by Matveeva *et. al* [34] and Kolar *et. al* [37]. The basic structural

formula for the $Ba_{6-x}Sm_{8+2x}Ti_{18}O_{54}$ tungsten bronze type structure is $[S_{10}]_{A1}[S_4]_{A2}B_{18}X_{54}$. This structure has three types of large cation sites: the largest ones are the four pentagonal sites (A2), the medium ones are the ten rhombic sites (A1) and finally the trigonal sites (C). The trigonal C-sites are empty in our case. Again, B is a cation (Ti) in an octahedron and X is an anion (O^{2-}). The basic crystal structure of these samples is given in Fig.3.2.

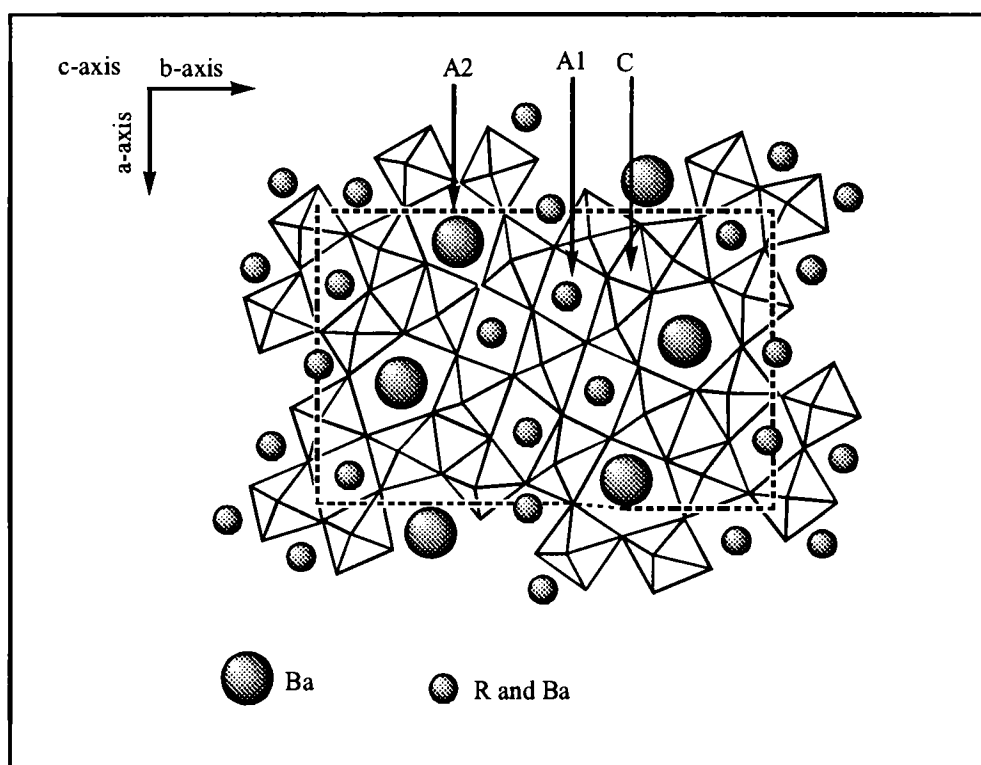


Fig.3.2: Tungsten-bronze crystal structure of $Ba_{6-x}Sm_{8+2x}Ti_{18}O_{54}$ solid solutions

Here the A2-sites are occupied by Ba ions, A1-sites are occupied by Sm and partly by Ba according to the value of x in the structural formula $[Sm_{8+2x}Ba_{2-3x}V_x]_{A1}[Ba_4]_{A2}Ti_{18}O_{54}$ (for $0 \leq x \leq 2/3$). Here V means vacancy. Only when $x = 2/3$, the A1-

sites and A2-sites are separately occupied by Sm and Ba respectively. This ordering results in the lowest internal strain. As the x value decreases Ba ions with larger ionic radii start to occupy a part of the rhombic sites (A1) with their smaller size and this leads to internal strain. On the other hand, as the x -value increases, vacancies are produced in the pentagonal sites (A2), which might lead to unstable crystal structures. For $2/3 \leq x \leq 1$, the structural formula can be written as, $[R_{9+1/3+2(x-2/3)}V_{2/3-2(x-2/3)}]_{A1}[Ba_{4-3(x-2/3)}V_{3(x-2/3)}]_{A2}Ti_{18}O_{54}$. Also it has been revealed that the crystal structure with the largest size difference between Ba and R has low internal strain, i.e., when $R = Sm$. H. Ohsato [46] reported that the tilt of TiO_6 octahedron along the c -axis is the main factor for the superlattice formation.

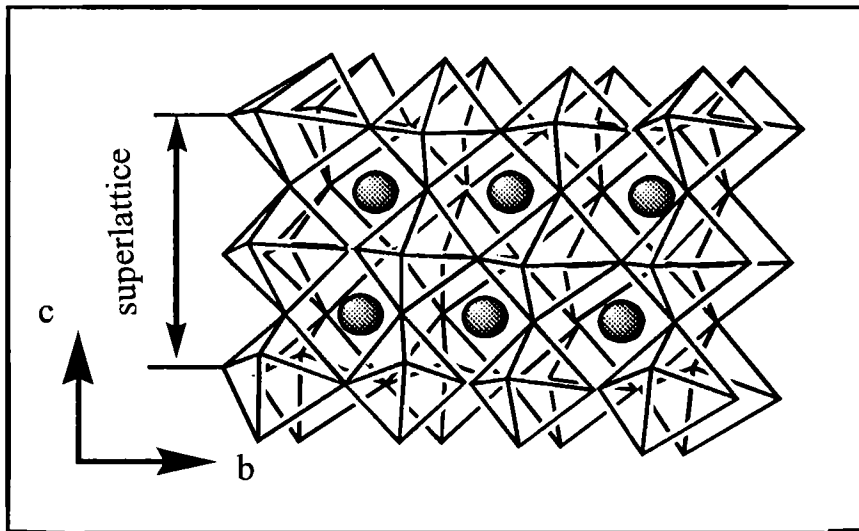


Fig.3.3: Tilting of the TiO_6 octahedron

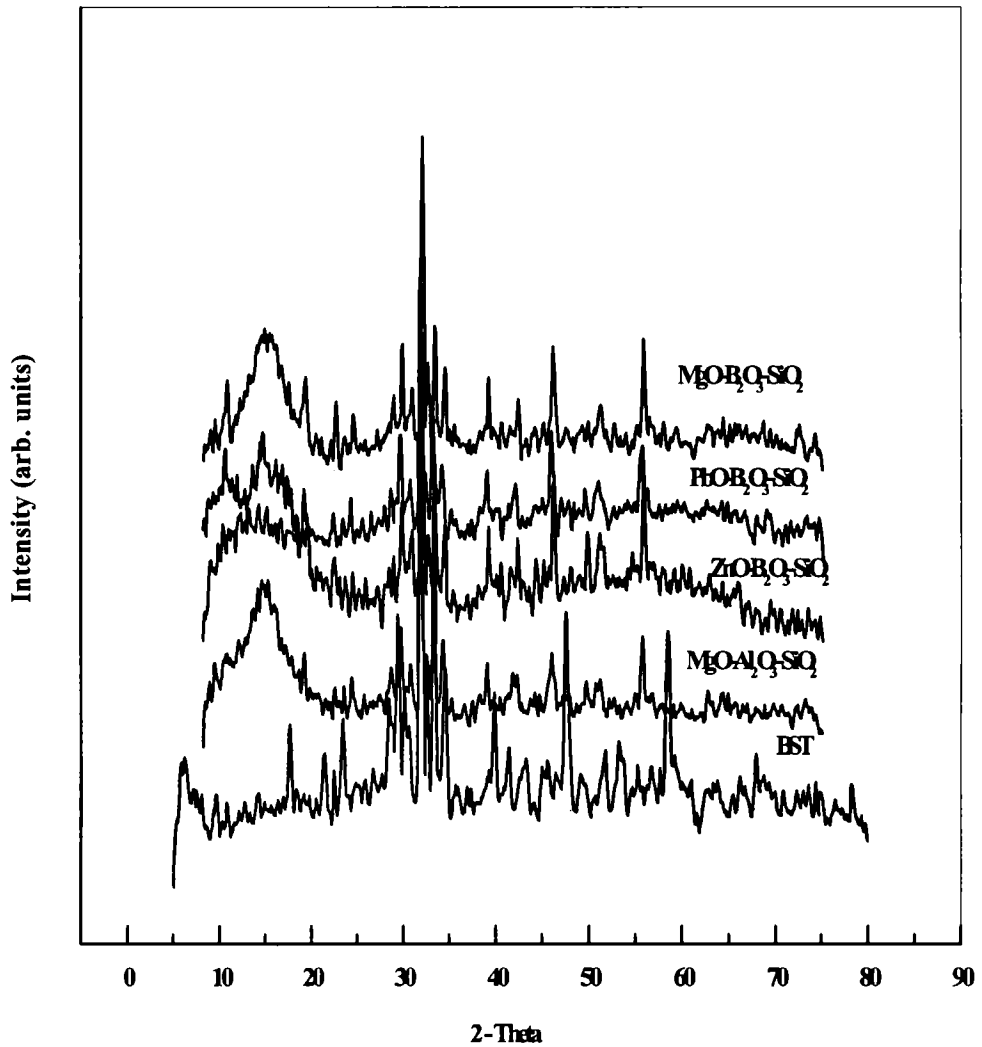


Fig.3.4: XRD pattern of BST added with 0.5 wt% of different glasses

The X-ray powder diffraction patterns of the samples were recorded with a Bruker D8 Advance X-ray powder diffractometer. The patterns for the pure sample and the same added with different glass are shown in Fig.3.4. As can be expected, the XRD patterns shown in Fig. 3.4 are similar, indicating that the addend is an amorphous solid such as glass.

3.5. Elastic Properties by Ultrasonic technique

Ultrasonic wave velocities in the ceramic samples have been measured by the Pulse Echo Overlap technique using Matec 7700 pulse modulator and receiver system [47] as described in Chapter 2. Pelletized samples of thickness 5-6 mm have been used for the measurements. The faces of the samples are well polished after making their faces parallel to each other. X-cut quartz transducer of frequency 10 MHz is mounted on the sample using nonaqueous stop-cock grease as the bond, which acts as the transmitter of the ultrasonic wave to the medium as well as receiver of echoes from the medium. The time gap between two selected echoes is measured following the pulse echo overlap method. Knowing the sample thickness and density (ρ), the longitudinal velocity (V_l) and elastic modulus (C_{11}) can be calculated using relation $C_{11} = \rho V_l^2$. To get the transverse velocity (V_t) and modulus (C_{44}), Y-cut quartz transducer is used for excitation and detection of ultrasonic waves. The transducer is bonded to the sample with silicon grease.

While measuring the time interval between selected echoes, the McSkimin Δt criterion [48] is applied to correct the phase lag due to bonding medium on RF echoes. This technique helps to measure ultrasound transit time in the sample to an accuracy of the order of few ppm. The overall accuracy of the elastic constant value is of the order of 0.1%.

3.6. Results and Discussion

The measured elastic properties of pure BST and BST added with 0.5 wt % of different glasses are presented in Table 3.1.

Table 3.1 shows that the ultrasonic velocities and hence the elastic moduli decreases when glass is added to BST. Also the elastic properties are almost independent of the type of glass, which is added.

Generally, ceramics are inhomogeneous materials because they consist of matrix grains, grain boundaries, pores, inclusions, incomplete densification, second phases etc. If a glassy phase is formed, it decreases the density and the mechanical strength. The elastic properties are definitely affected by intragranular (crystallinity) and intergranular (grain boundary) properties. Therefore elastic properties are the result of combined contribution of degree of crystal structure imperfections and microstructural inhomogeneity. The random distribution are considered to be kind of imperfection in the atomic ordering. So the lowering of elastic constants due to glass addition may be due to the disorder in ion distribution or the formation of second phase.

It is evident from Table 3.1 that addition of glass does not drastically reduce the values of elastic constants. Moreover, the Poisson's ratio remains more or less the same. This means that the hardness of the specimen is not affected significantly due to the addition of glass. So one can say that if the addition of glass leads to significant advantages during sintering, one can truly accommodate a minor reduction in mechanical strength and hardness. The results presented in this chapter show that the mechanical strength of these materials decrease due to glass addition, but is not very significant. So one can take advantage of glass addition while using these materials for application.

Table.3.1. Elastic properties of Barium Samarium Titanate ($\text{Ba}_4\text{Sm}_{28/3}\text{Ti}_{18}\text{O}_{54}$)

BST with 0.5 wt % of	V_l (m/s)	C_{11} (GPa)	V_t (m/s)	C_{44} (GPa)	Young's Modulus Y (GPa)	Bulk Modulus B (GPa)	Poiss- on's ratio
BST (pure)	6607 ± 33	244 ± 6	3729 ± 18	77 ± 2	196 ± 5	140 ± 3	0.266
MgO- Al_2O_3 - SiO_2	6439 ± 32	228 ± 6	3657 ± 18	73 ± 2	185 ± 5	130 ± 3	0.262
ZnO- B_2O_3 (77:23)	6480 ± 32	233 ± 6	3673 ± 18	75 ± 2	189 ± 5	133 ± 3	0.263
B_2O_3 - SiO_2	6504 ± 33	234 ± 6	3680 ± 18	75 ± 2	189 ± 5	134 ± 3	0.265
ZnO- B_2O_3 - SiO_2	6541 ± 33	235 ± 6	3699 ± 18	75 ± 2	190 ± 5	135 ± 3	0.265
PbO- B_2O_3 - SiO_2	6505 ± 33	236 ± 6	3680 ± 18	75 ± 2	191 ± 5	135 ± 3	0.265
MgO- B_2O_3 - SiO_2	6512 ± 33	235 ± 6	3677 ± 18	75 ± 2	189 ± 5	135 ± 3	0.266
ZnO- B_2O_3 (50:50)	6587 ± 33	242 ± 6	3718 ± 18	77 ± 2	196 ± 5	140 ± 3	0.266
Al_2O_3 - SiO_2	6419 ± 32	225 ± 6	3649 ± 18	73 ± 2	184 ± 5	130 ± 3	0.261
Al_2O_3 - B_2O_3 - SiO_2	6445 ± 32	228 ± 6	3666 ± 18	74 ± 2	186 ± 5	130 ± 3	0.261
BaO- B_2O_3 - SiO_2 (30:60:10)	6603 ± 33	241 ± 6	3723 ± 18	77 ± 2	194 ± 5	139 ± 3	0.267
BaO- B_2O_3 - SiO_2 (30:40:30)	6643 ± 33	245 ± 6	3725 ± 18	77 ± 2	195 ± 5	142 ± 3	0.271

References

1. R. J. Cava, *J. Mater. Chem.* **11** (2001) 54
2. H. Ohsato, T. Ohhashi, H. Kato, S. Nishigaki and T. Okuda, *Jpn. J. Appl. Phys.* **34** (1995)187
3. N. Ichinose, H. Amada, *J. Europ. Ceram. Soc.* **21** (2001) 2751
4. C. J. Rawn, D. P. Birnie, M. A. Bruck, J. H. Enemark, R. S. Roth, *J. Mater.Res.* **3** (1998) 187
5. M. O'Bryan, J. Thomson, J. K. Plourde, *J. Am. Ceram. Soc.* **57** (1974) 450
6. J. K. Plourde, D. F. Linn, H. M. O'Bryan, J. Thomson, *J. Am. Ceram. Soc.* **58** (1975) 418
7. K. Wakino, D. Sagala, H. Taura, *Jpn. J. Appl. Phys.* **24** (1985) 1042
8. J. H. Jonker, W. Kwestroo, *J. Am. Ceram. Soc.* **41** (1958) 1390
9. T. Negas, G. Yeager, S. Bell, N. Coats, I. Minis, *Am. Ceram. Soc. Bull.* **72** (1993) 80
10. W. Y. Lin, R. F. Speyer, *J. Am. Ceram. Soc.* **82** (1999) 1207
11. Wu, H. W. Wang, *J. Am. Ceram. Soc.* **82** (1999) 1207
12. H. Ohsato, T. Ohhashi, S. Nishigaki T. Okuda, K. Sumiya and S. Suzuki, *Jpn. J. Appl. Phys.* **32** (1993) 4323
13. H. Ohsato, H. Kato, M. Mizuta, S. Nishigaki, T. Okuda, *Jpn. J. Appl. Phys.* **32** (1995) 5413
14. T. R. N. Kutty, P. Murugaraj, *J. Mater. Sci.* **22** (1987) 3652
15. M. Imaeda, K. Ito, M. Mizuta, H. Ohsato, S. Nishigaki, T. Okuda, *Jpn. J. Appl. Phys.* **36** (1997) 6012

16. H. Ohsato, T. Ohhashi and T. Okuda, *Jpn. J. Appl. Phys.* **31** (1992) 3136
17. R. Ubie, I. M. Reancy, W. E. Lee, *J. Am. Ceram. Soc.* **82(5)** (1999) 1336
18. Y. C. Chen, C. L. Huang, *Mat. Sci. Eng.* **A334** (2002) 250
19. S. Nishigaki, H. Kato, S. Yang, R. Kamimura, *Am. Ceram. Soc. Bull.* **66** (1987) 1405
20. S. W. Jung, J. H. Lee, J. J Kim, H. Y. Lee and S. H Cho, *Mat. Chem. Phys.* **79** (2003) 282
21. C-L Huang and Y-C Chen, *Mat. Sci. Eng.* **A345** (2003) 106
22. P. S Cheng, C. F Yang, Y. C Chen and W. C Tzou, *Ceram. Internat.* **26** (2000) 877
23. S. Solomon, N. Santha, I. N. Jawahar, H. Sreemoolanadhan, M. T. Sebastian and P. Mohanan, *J. Mat. Sci: Mat. in Electron.* **11** (2000) 595
24. C. H Lee and Y-H Huang, *Mat. Sci. Eng.* **B98** (2003) 33
25. Y. Song, F. Wang, Z. Jiang, *Microelectron. Eng.* **66** (2003) 615
26. H. Sreemoolanadhan, M. T. Sebastian, P. Mohanan, *British. Cerm. Transac.* **95** No. 2 (1996) 79
27. R. Kudesia, A. E. McHale, R. L. Snyder, *J. Am. Ceram. Soc.* **77** (1994) 3215
28. Y. Zhang, P. K. Davies, *J. Am. Ceram. Soc.* **77** (1994) 1743
29. S. B. Desu, H. M. O'Bryan, *J. Am. Ceram. Soc.* **68** (1985) 546
30. P. K. Davies, J. Tong, T. Negas, *J. Am. Ceram. Soc.* **80** (1997) 1727
31. M. A. Akbar, P. K. Davies, *J. Am. Ceram. Soc.* **81** (1998) 670
32. T. Negas and P. K. Davies, Materials and Processes for Wireless Communications, *Ceram.Trans.* **53** (1995) 196
33. K. Fukuda, R. Kitoh and I. Awai, *J. Mater. Res.* **10** (1995) 312

34. R. G. Matveeva, M. B. Varforomeev and L. S. Hyuschenko, *Russ. J. Inorg. Chem.* **29** (1984) 17
35. H. Ohsato, T. Ohhashi and T. Okuda, Ext. Abstr. AsCA '93 Conf. Singapore, November, 14U-50.
36. X. M. Chen, N. Qin and Y. Li, *J. Electroceram.* **9** (2002) 31
37. D. Kolar, S. Gabrseek and D. Suvorov, *Third Euroceramics 2* (1993) 229
38. S. M. Rhim, S. K. Honu, H. J. Hak and O. K. Kim, *J. Amer. Ceram. Soc.* **83** (2000) 1145
39. I. C. Ho, *ibid*, **77** (1994) 829
40. H. I. Chinu, T. T. Lim, C. I. Hu and I. M. Lin, *ibid*, **76** (1993) 827
41. Zhai Jiwei, Yao Xi, Cheng Xiaogang, Zhang Liang Ying, Haydn Chen, *J. Mater. Sci.*, **37** (2002) 3739
42. S. Solomon, N. Santha, I. N. Jawahar, H. Sreemoolanadhan, M. T. Sebastian and P. Mohanan, *J. Mat. Electron.* **11** (2000) 595
43. P. Laffez, G. Desgardin and B. Raveau, *J. Mat. Sci.* **27** (1992) 5229
44. C. C. Lee and P. Lin, *Jpn. J. Appl. Phys.* **37** (1998) 6048
45. H. Ohsato and M. Imaeda, *Mater. Chem. Phys.* **79** (2003) 208
46. H. Ohsato, *J. Europ. Cera. Soc.* **21** (2001) 2703
47. E. P. Papadakis, *Physical Acoustics* (Eds: M. P. Mason, R. N. Thurston, Academic Press, New York) **12** (1976) 277
48. H. J. McSkimin, *J. Acoust. Soc. Am.* **33** (1961) 12

CHAPTER 4

Effect of adding Silica and similar glasses on the elastic properties of BST ceramics

4.1. Introduction

Dielectric ceramic materials have been studied for decades owing to their applications in important technologies and fundamentally interesting relationships among the crystal chemistry, crystal structures and the physical properties [1]. Recently, microwave dielectric resonators (DRs) have made dramatic changes in microelectronics, in particular in wireless communication technologies. Some of the major advantages of using DRs are [2], (i) small circuit sizes (ii) greater degree of circuit and subsystem integration due to simpler coupling schemes from microwave integrated circuits (MICs) to DRs (iii) better circuit performance and (iv) reduction of overall circuit cost. The important material properties for DR applications [2] are the following,

- (a) High dielectric constant (ϵ_r) that enables the miniaturization of devices by a factor of $\sqrt{\epsilon_r}$.
- (b) Low temperature coefficient of resonant frequency (τ_f). Resonant frequency shifts due to intrinsic material parameters are given as; $\tau_f = -(1/2)\tau_\epsilon - \alpha_L$, where τ_ϵ is the temperature coefficient of dielectric constant and α_L is the linear expansion coefficient of the material.

(c) The unloaded Q factor, which depends strongly on the dielectric losses

$(Q = 1/\tan \delta)$. Q is defined as the ratio between stored energy and the dissipated energy per cycle.

There are a number of research works for developing new ceramics and also for improving the properties through substitution and addition of additives. Several series of microwave dielectric ceramics have been developed like (a) Ba-R₂O₃-TiO₂ (R = La, Nd, Sm) system, (b) (Zr, Sn)TiO₄ system, (c) BaO-TiO₄ titanium rich system, (d) Ba (B_{1/3}Ta_{2/3})O₃ (B= Mg, Zn) [3-6] etc. There was significant research on the (1-x) BaO – (1+2/3)R₂O₃-kTiO₂ ternary compounds [7-14]. Most of the reports have investigated the microwave properties of BaO- R₂O₃-kTiO₂ ceramics. Dielectric ceramics in the TiO₂- rich region of the BaO – Nd₂O₃ – TiO₂ ternary system were reported to have excellent dielectric constants, low dielectric losses and low temperature coefficients of capacitance [9]. The BaTiO₃ – Nd₂O₃ – TiO₂ system was first studied [15] in the 1970s. Matveeva *et al.* conducted studies on the fundamental structure and composition of Ba_{8-2x}Pr_{8+2x}Ti₁₈O₅₄ [16] for $x = 3/4$. They also reported the much better dielectric characteristics of BaO – Sm₂O₃ – 4.7TiO₂ system. The microwave dielectric properties of BaO – xSm₂O₃ – 4.5TiO₂ are described by some other researchers [17-18]. Ba_{6-3x}Sm_{8+2x}Ti₁₈O₅₄ with $0.3 \leq x \leq 0.7$ was studied by H. Ohsato *et al.* [6] and the typical dielectric properties were shown by Ba₄Sm_{28/3}Ti₁₈O₅₄ (BST) as $\epsilon_r = 81$, $Q.f = 9600$ GHz and $\tau_f = -14$ ppm/^oC. The dielectric properties of BaO – Sm₂O₃ – 5TiO₂ were improved by replacing Sr for the Ba site. Good results were obtained for the composition (BaO)_{0.15}(Sm₂O₃)_{0.15}(TiO₂)_{0.7} with partial substitution of Ba by Sr by Nishigaki *et al.*

[19]. The $\text{BaO} - (\text{Sm}_{1-x}\text{La}_x)_2\text{O}_3 - 5\text{TiO}_2$ ceramic system was studied by N. Ichinose *et al.* [20]. The system showed the best dielectric properties for $x = 0.1$.

The effect of calcination and sintering on the microwave properties of $\text{Ba}_{6-3x}\text{Sm}_{8+2x}\text{Ti}_{18}\text{O}_{54}$ was studied by P. Laffez *et al.* [21]. Since the sintering temperature required for BST ceramics is very high and due to its commercial importance, methods to achieve low sintering temperature have been searched by researchers. Recently low melting point glasses are added to dielectric ceramics so as to reduce the sintering temperature. Some works are already conducted in this area and promising results are obtained. Results of the detailed study of the effects of glass addition on the microwave properties of $\text{BaO} - \text{La}_2\text{O}_3 - 4.7\text{TiO}_2$ are reported by C. C. Lee *et al.* [17]. Since $\text{BaO} - \text{La}_2\text{O}_3 - 4.7\text{TiO}_2$ has a positive temperature coefficient of resonant frequency, they used commercial glasses of negative τ_f like $\text{PbO} - \text{B}_2\text{O}_3 - \text{SiO}_2$, $\text{ZnO} - \text{B}_2\text{O}_3 - \text{SiO}_2$ and $\text{PbO} - \text{B}_2\text{O}_3$ etc as additives. The direct current field dependence of dielectric properties in $\text{B}_2\text{O}_3 - \text{SiO}_2$ glass doped $\text{Ba}_{0.6}\text{Sr}_{0.4}\text{TiO}_3$ ceramics has been investigated by Z. Jewei *et al.* [22]. Several authors reported [23-28] the effect of Bi_2O_3 addition on the microwave dielectric properties of $\text{BaR}_2\text{Ti}_4\text{O}_{12}$ and $\text{BaR}_2\text{Ti}_5\text{O}_{14}$ compounds. Recently, the low temperature sintering $\text{Ba}_{6-3x}\text{Sm}_{8+2x}\text{Ti}_{18}\text{O}_{54}$ ceramics by the addition of B_2O_3 and GeO_2 was reported by Y. Ota *et al.* [29]. More recently, the sintering temperature and microwave dielectric properties of ZnTiO_3 as a function of $\text{ZnO} - \text{B}_2\text{O}_3 - \text{SiO}_2$ were investigated by O. L. Zhang *et al.* [30]. All these studies show that the sintering temperature can be lowered by the glass addition without losing its microwave performance, provided the glass content is within a certain limit.

There are no reports regarding the systematic study of the effect of glass addition on the mechanical properties of the particular DR materials. N. Rodrigues *et al.* reported [31] the effect of lanthanide substitution on the elastic properties of $\text{BaLn}_2\text{Ti}_5\text{O}_{14}$. The elastic strength of DR materials is important due to both the commercial and structural stability aspects. In this chapter, the effect of glass addition on the elastic properties of BST ceramics is investigated and the results are presented.

4.2. Sample Preparation

The glass-added ceramics are prepared by the conventional solid-state reaction method as already described earlier. $\text{Ba}_4\text{Sm}_{28/3}\text{Ti}_{18}\text{O}_{54}$ ceramic powder is prepared from reagent grade BaCO_3 , Sm_2O_3 and TiO_2 , which are mixed in the stoichiometric ratios with distilled water. After ball-milling for about 24 hours, the dried powders are calcined at 1150°C for 4 hrs. The calcined powder is then added with a fixed wt % of glass and PVA (5%) and dry-pressed at 150 MPa to form cylindrical compacts. In present studies $\text{Al}_2\text{O}_3 - \text{SiO}_2$, $\text{B}_2\text{O}_3 - \text{SiO}_2$, $\text{La}_2\text{O}_3 - \text{B}_2\text{O}_3 - \text{TiO}_2$ and B_2O_3 glasses are used as the additives. The obtained pellets are then sintered at appropriate optimized temperatures.

4.3. Samples Studied

Different sets of samples are prepared to study the elastic properties. Each set consists of BST added with a particular glass in various proportions. The different sets are BST with (1) $\text{Al}_2\text{O}_3 - \text{SiO}_2$ (AS) (2) $\text{B}_2\text{O}_3 - \text{SiO}_2$ (BS) (3) B_2O_3 (B_1) and (4) $\text{La}_2\text{O}_3 - \text{B}_2\text{O}_3 - \text{TiO}_2$ glasses.

4.4. Structure by XRD

The microstructure of BST was supposed to be the tungsten bronze-type structure. This structure is made up of corners sharing $(\text{TiO}_6)^{-2}$ octahedra, which extend in the short axis (c) direction to form a network of rhombic and pentagonal channels [29, 30]. The structural formula is $[\text{Sm}_{8+2x}\text{Ba}_{2-3x}\text{V}_x]_{\text{A1}}[\text{Ba}_4]_{\text{A2}}\text{Ti}_{18}\text{O}_{54}$; A1 are the rhombic sites and A2 are the pentagonal sites. V stands for vacancy. In addition to the A1 and A2 sites, there is one more cation site, shown as the trigonal (C) sites, which are empty in our case.

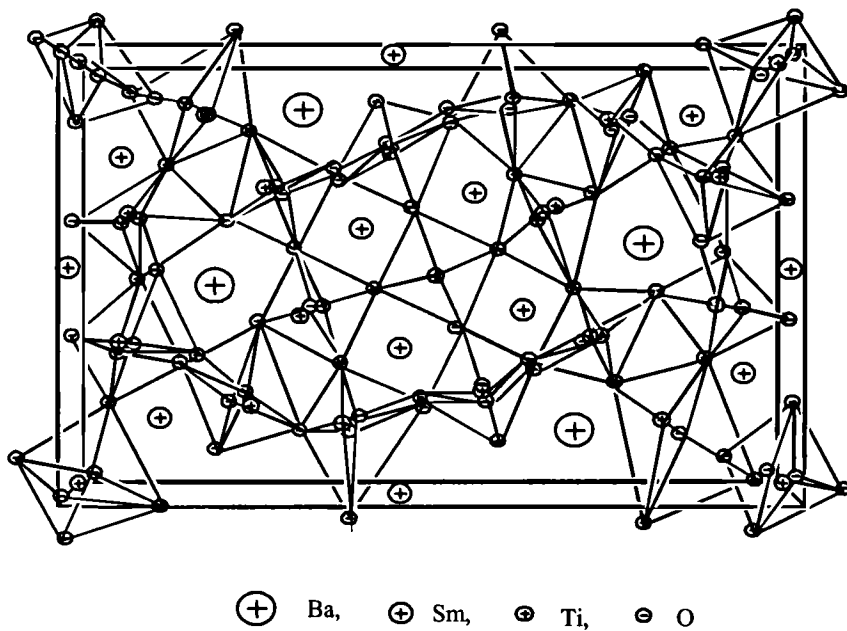


Fig.4.1: Projection of $\text{Ba}_4\text{Sm}_{9.33}\text{Ti}_{18}\text{O}_{54}$ in the (001) direction.

The X-ray powder diffraction patterns of the samples were recorded with a Bruker D8 Advance X-ray powder diffractometer. The patterns for the pure sample and the same added with different glasses are shown in Figures 4.2 – 4.5.

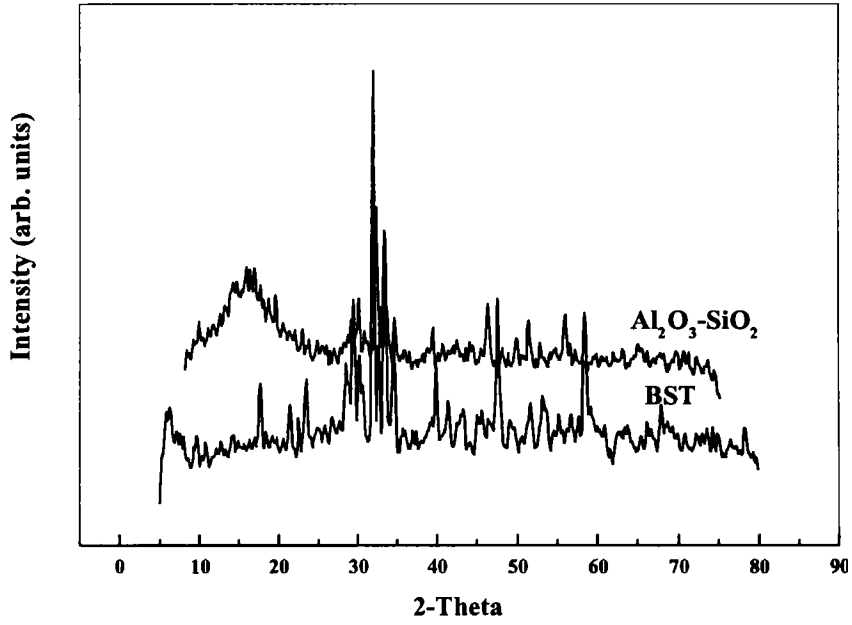


Fig. 4.2: XRD pattern of $\text{Al}_2\text{O}_3\text{-SiO}_2$ added BST

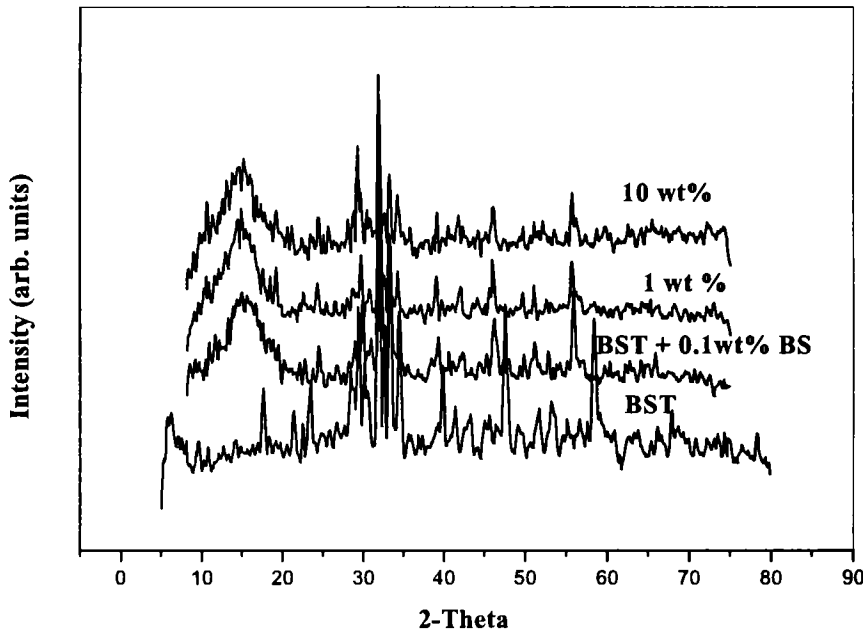


Fig. 4.3: XRD pattern of BST with $\text{B}_2\text{O}_3 - \text{SiO}_2$

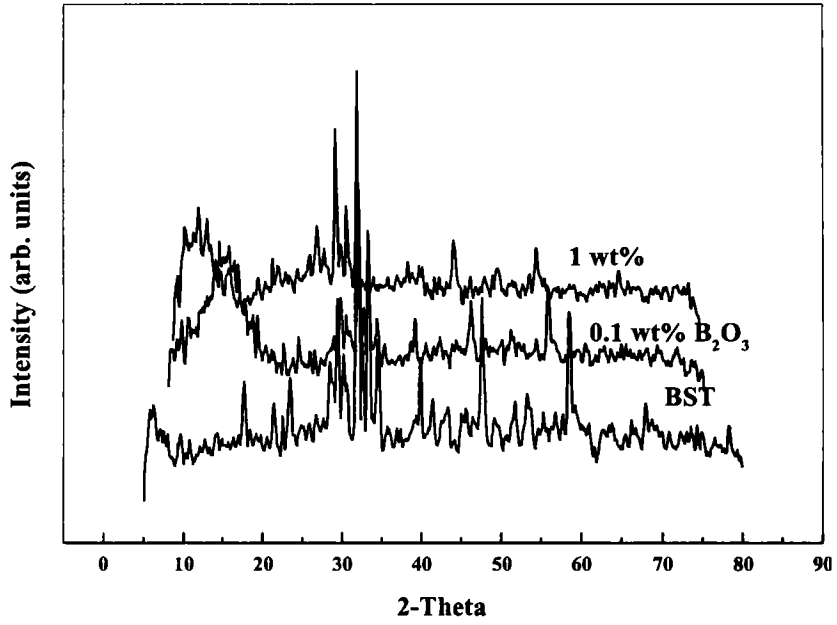


Fig. 4.4: XRD pattern of BST with B₂O₃ glass

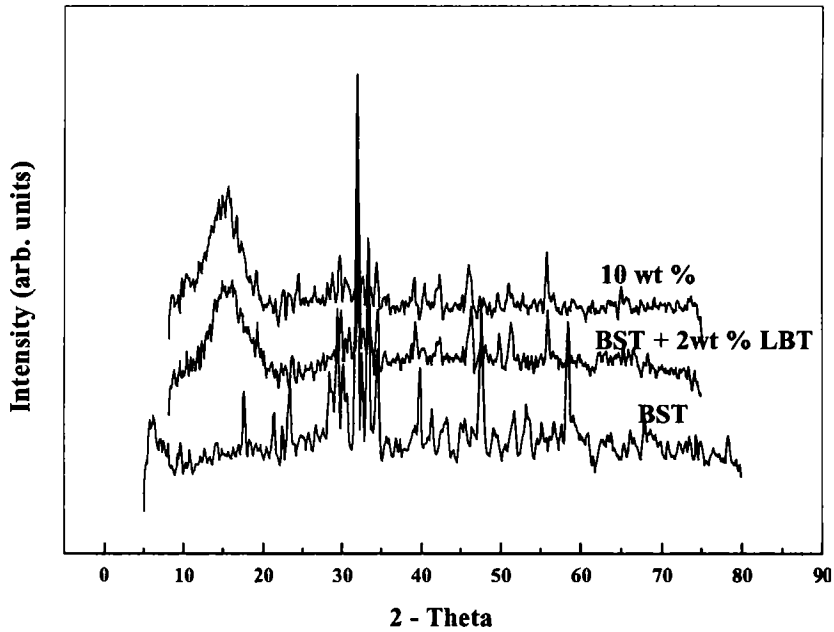


Fig. 4.5: XRD pattern of LBT added BST

4.5. Elastic Properties by Ultrasound Technique

The longitudinal (C_{11}) and transverse (C_{44}) elastic moduli of an isotropic sample can be determined using the relation $C_{ij} = \rho V^2$ where V is the velocity of the appropriate mode and ρ is the density of the sample. Knowing the longitudinal (V_l) and transverse (V_t) velocities and density, parameters like Young's modulus (Y), Bulk modulus (B), Poisson's ratio etc can also be determined.

Ultrasonic wave velocities in the ceramic samples have been measured by the Pulse echo overlap method using Matec 7700 pulse modulator and receiver system [32]. Pellets with exactly parallel and polished faces are used for the measurements. For longitudinal measurements X-cut quartz transducers of frequency 10 MHz is mounted on the sample using nonaq stopcock grease as the bond. Y-cut transducers are bonded with silicon grease for the transverse measurements. Two selected echoes are overlapped and time of transit of the ultrasonic wave for getting these echoes is measured. The McSkimin Δt criterion [33] has been applied to correct for the phase lag due to bonding medium on the rf echoes. The overall accuracy of elastic constant values is of the order of 0.1%. All details of ultrasonic measurements are already described in Chapter 2.

4.6. Results and Discussion

The elastic constants of various glass added BST ceramics are found to decrease with increasing % of glass addition. This is the true for all sets of BST with different glasses. The results are shown in Tables 4.1-4.4 and Figures 4.5-4.16.

The velocity of ultrasonic waves through a solid is very much dependent on the inhomogeneties present like grain boundaries, grain size, precipitates, presence of secondary phases etc. The densification of specimens is found to play an important role in the lowering of elastic strength in the glass-added samples. Due to the formation of glassy phase less dense samples are formed. The deviation may be due to factors inherent in the sintered specimen, such as (1) the presence of large heterogeneous interfaces, including air-glass, glass-ceramics and ceramics-air interfaces and (2) the modification of glass composition due to dissolution of trace amounts of ceramics in it.

In general, the results show that addition of glass results in a reduction in elastic moduli. The Poisson's ratio also decreases with glass addition. The decrease in elastic moduli is more or less proportional to the wt % of the glass added. This is a general result. The elastic moduli decrease irrespective of the added glass. So glass addition essentially results in a decrease in the mechanical strength and hardness of the specimen.

It may be noted that a small decrease in mechanical strength and hardness do not seriously affect the use of these materials as DR materials. Since addition of glass at low weight percentages significantly reduces sintering temperatures, one can afford to compromise for a small decrease in mechanical strength and hardness.

The results presented in this chapter are the first of this kind that throws light on the effect of glass addition on the mechanical properties of dielectric resonator materials.

G9098

Table 4.1: Elastic Properties of BST added with Al₂O₃ - SiO₂ glass

wt % of glass	V _l (m/s)	C ₁₁ (GPa)	V _t (m/s)	C ₄₄ (GPa)	Young's Modulus Y (GPa)	Bulk Modulus B (GPa)	Poisson's ratio
0.0	6607 ± 33	244 ± 6	3729 ± 18	77 ± 2	196 ± 5	140 ± 3	0.266
0.1	6477 ± 32	230 ± 6	3677 ± 18	74 ± 2	187 ± 5	131 ± 3	0.262
0.5	6419 ± 32	225 ± 6	3649 ± 18	73 ± 2	184 ± 5	130 ± 3	0.261
1	6378 ± 32	181 ± 5	3625 ± 18	59 ± 1	148 ± 4	103 ± 3	0.261
3	5737 ± 28	161 ± 4	3453 ± 17	58 ± 1	142 ± 4	83 ± 2	0.216



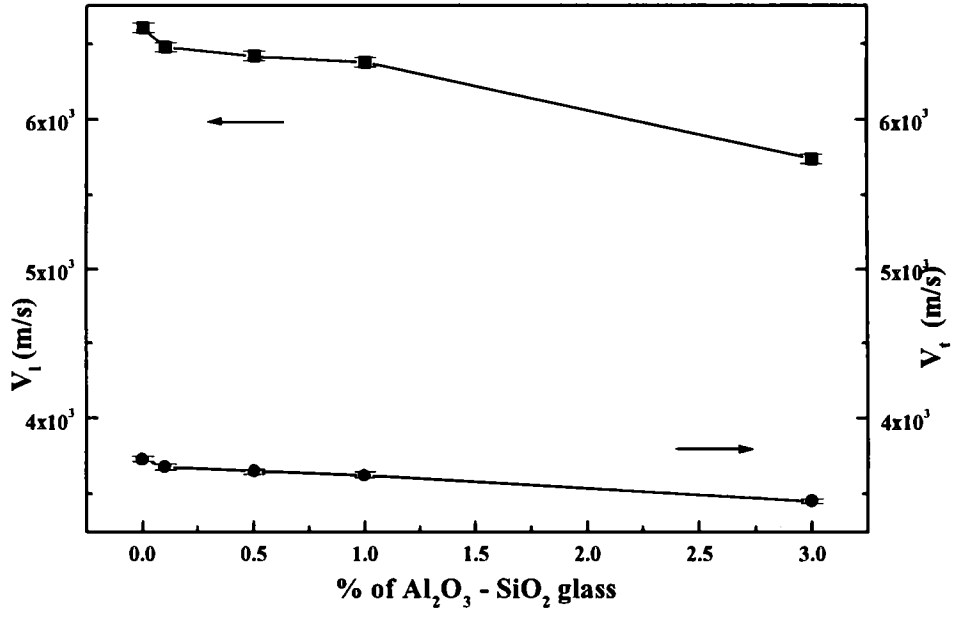


Fig.4.5: Variation of ultrasonic velocities with Al₂O₃ - SiO₂ addition

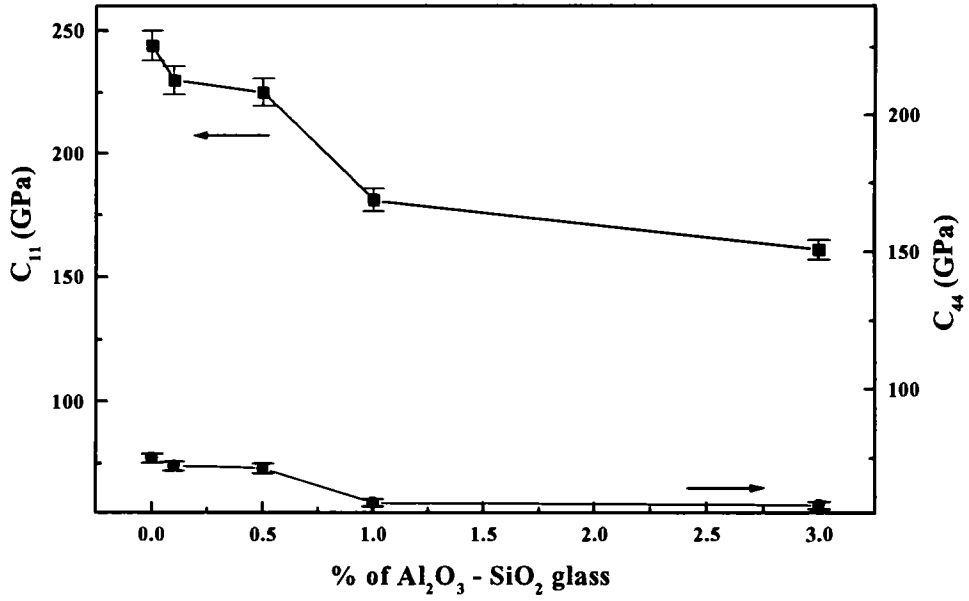


Fig. 4.6: Variation of C₁₁ and C₄₄ with Al₂O₃ - SiO₂ addition

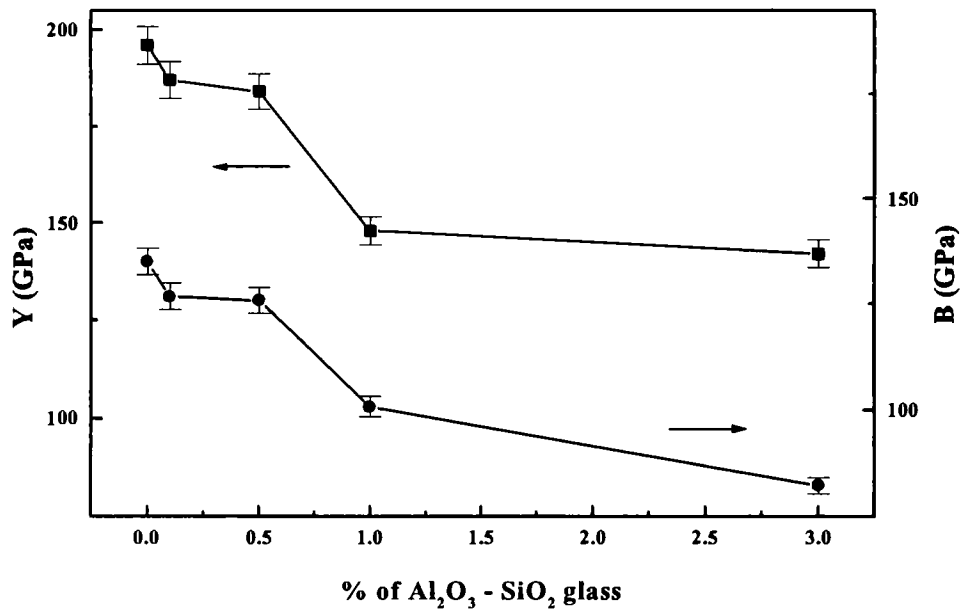


Fig. 4.7: Variation of Y and B with Al₂O₃ - SiO₂ addition

Table 4.2: Elastic Properties of BST added with B₂O₃ - SiO₂ glass

wt % of glass	V_l (m/s)	C₁₁ (GPa)	V_t (m/s)	C₄₄ (GPa)	Young's Modulus Y (GPa)	Bulk Modulus B (GPa)	Poisso -n's ratio
0.0	6607 ± 33	244 ± 6	3729 ± 18	77 ± 2	196 ± 5	140 ± 3	0.266
0.1	6622 ± 33	241 ± 6	3703 ± 18	75 ± 2	192 ± 5	141 ± 3	0.273
0.5	6504 ± 33	234 ± 6	3680 ± 18	75 ± 2	189 ± 5	134 ± 3	0.265
1	6104 ± 30	202 ± 5	3653 ± 18	72 ± 1	177 ± 4	106 ± 3	0.221
3	5843 ± 29	173 ± 4	3499 ± 17	62 ± 1	151 ± 4	90 ± 2	0.220
10	3690 ± 18	44 ± 1	2347 ± 12	18 ± 0.5	41 ± 1	20. ± 0.5	0.161

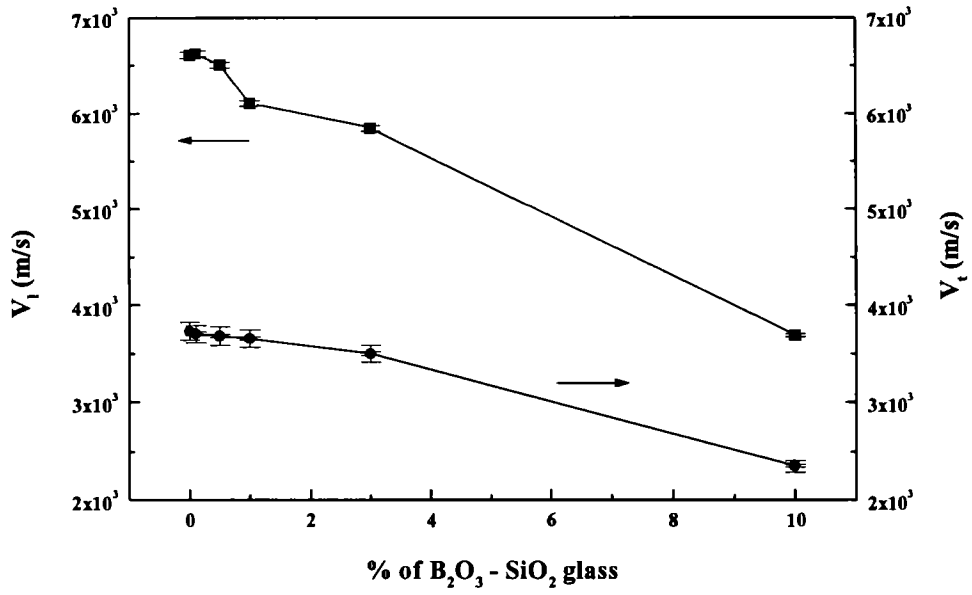


Fig. 4.8: Variation of ultrasonic velocities with B₂O₃ - SiO₂ addition

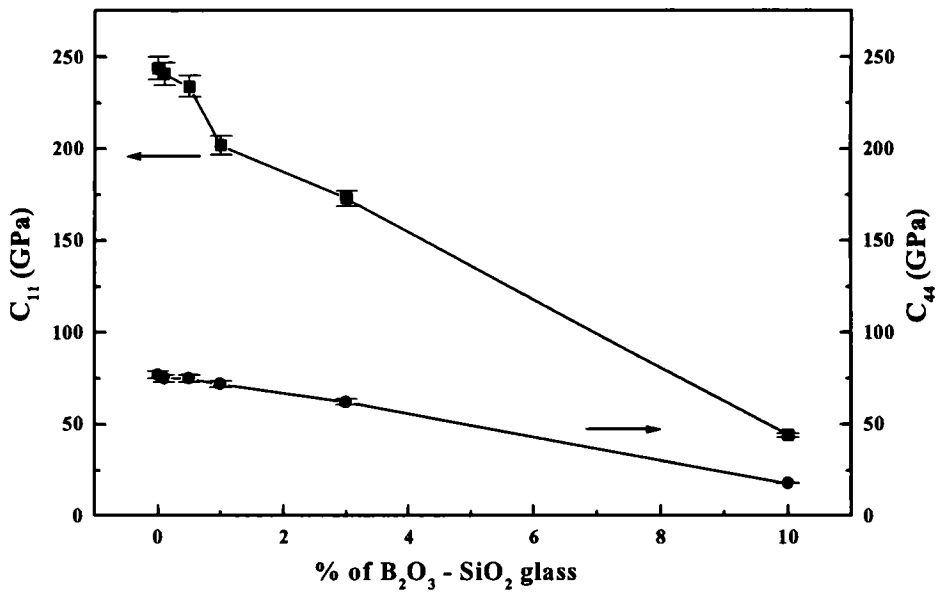


Fig. 4.9: Variation of C₁₁ and C₄₄ with B₂O₃ - SiO₂ addition

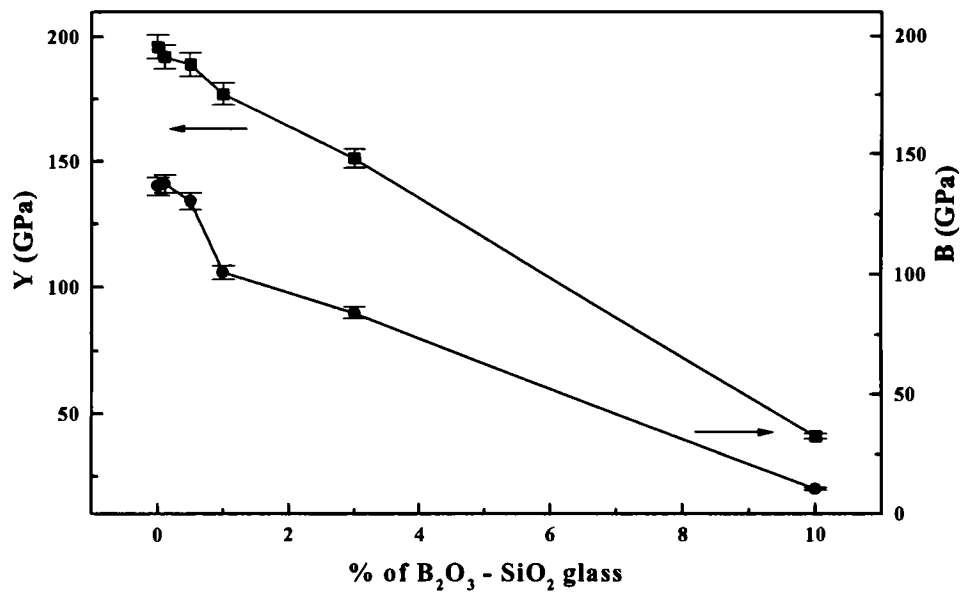


Fig. 4.10: Variation of Y and B with B₂O₃ - SiO₂ addition

Table 4.3: Elastic Properties of BST added with B₂O₃ glass

wt % of glass	V_l (m/s)	C₁₁ (GPa)	V_t (m/s)	C₄₄ (GPa)	Young's Modulus Y(GPa)	Bulk Modulus B (GPa)	Poisson's ratio
0.0	6607 ± 33	244 ± 6	3729 ± 18	77 ± 2	196 ± 5	140 ± 3	0.266
0.1	6614 ± 33	238 ± 6	3705 ± 19	75 ± 2	190 ± 5	138 ± 3	0.271
0.5	6210 ± 33	213 ± 5	3710 ± 19	76 ± 2	186 ± 5	112 ± 3	0.222
1	6195 ± 31	211 ± 5	3699 ± 18	75 ± 2	184 ± 5	111 ± 3	0.223
3	5980 ± 30	191 ± 5	3612 ± 18	70 ± 2	169 ± 4	98 ± 2	0.213

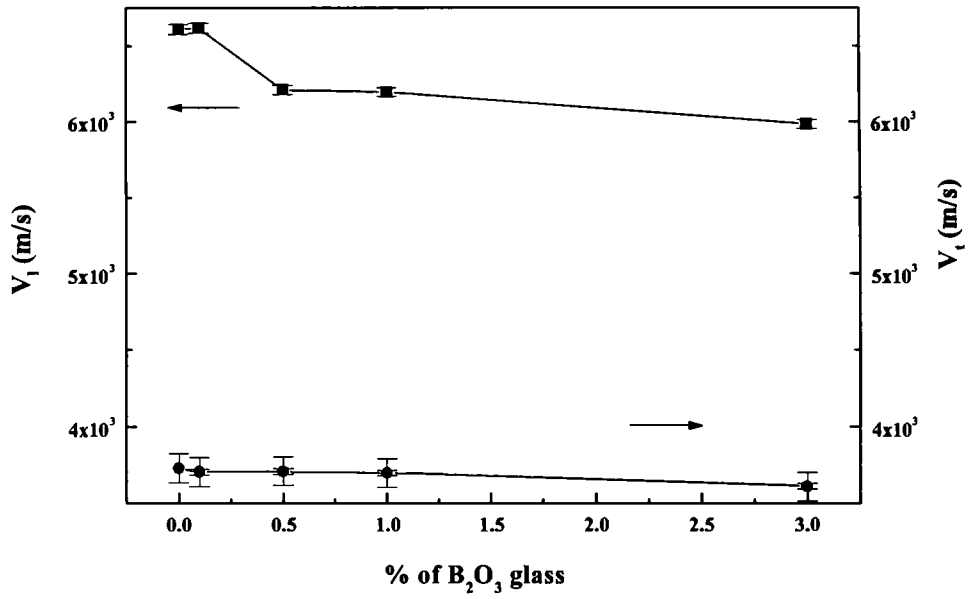


Fig.4.11: Variation of ultrasonic velocities with B₂O₃ addition

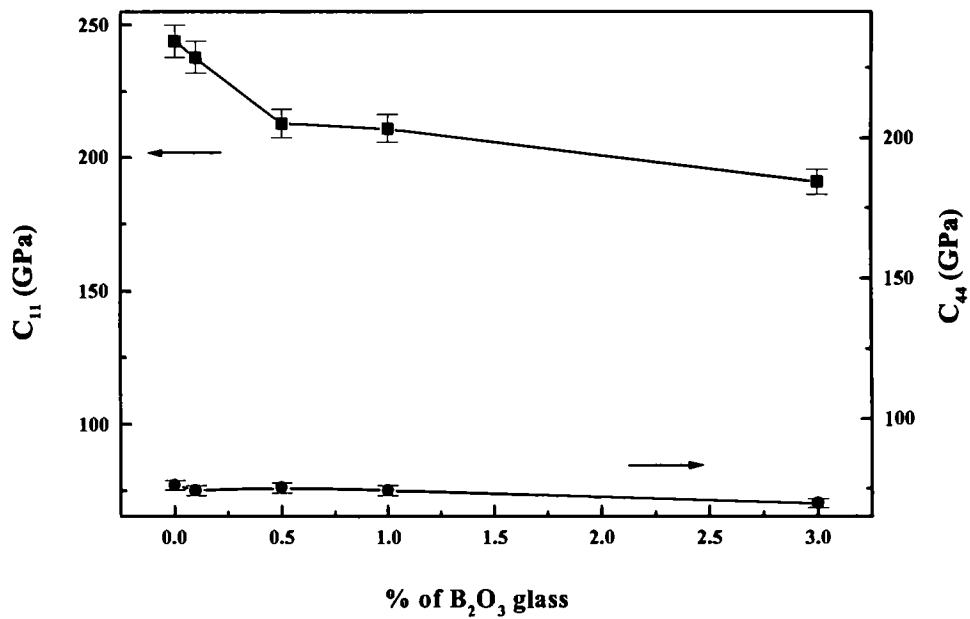


Fig 4.12: Variation of C₁₁ and C₄₄ with B₂O₃ addition

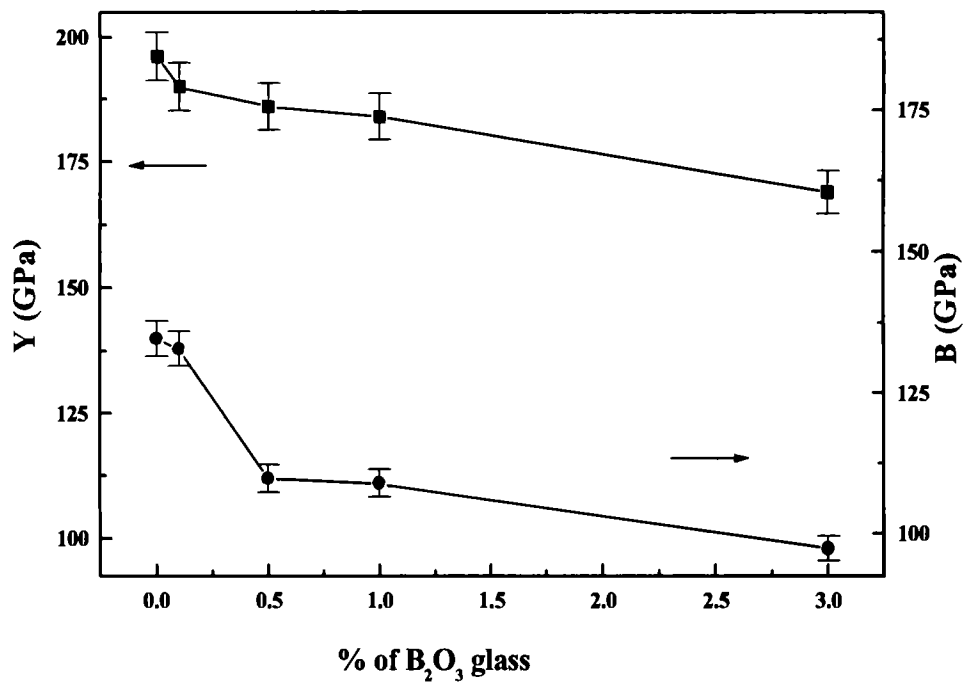


Fig. 4.13: Variation of Y and B with B₂O₃ addition

Table 4.4: Elastic Properties of BST added with LBT glass

wt % of glass	V_l (m/s)	C_{11} (GPa)	V_t (m/s)	C_{44} (GPa)	Young's Modulus Y (GPa)	Bulk Modulus B (GPa)	Poisson's ratio
0.0	6607 ± 33	244 ± 6	3729 ± 18	77 ± 2	196 ± 5	140 ± 3	0.266
2	5796 ± 19	157 ± 4	3522 ± 17	58 ± 1	140 ± 3	80 ± 2	0.207
10	6153 ± 30	198 ± 5	3658 ± 18	70 ± 2	171 ± 4	104 ± 3	0.226
20	6157 ± 30	177 ± 4	3682 ± 18	63 ± 2	155 ± 4	93 ± 2	0.222

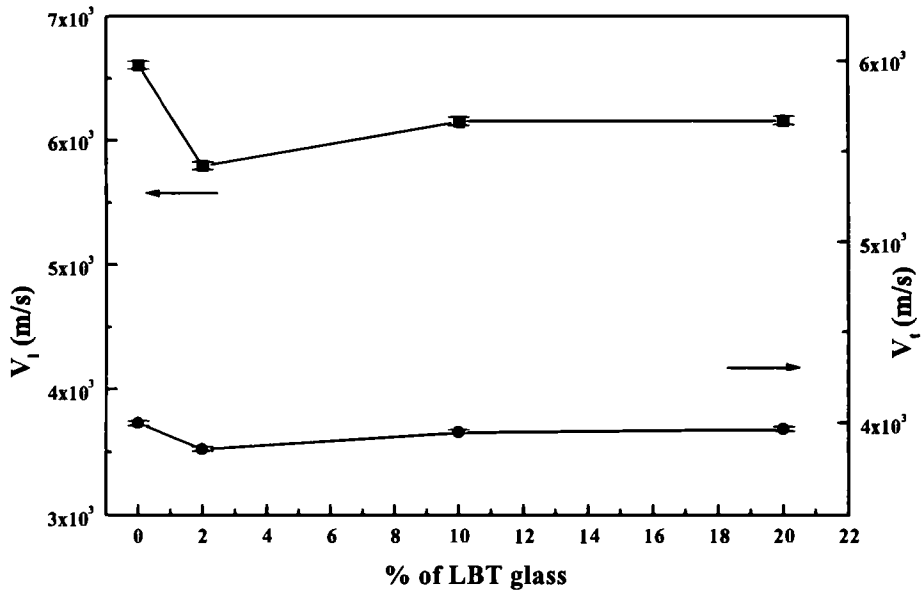


Fig.4.14: Variation of ultrasonic velocities with LBT addition

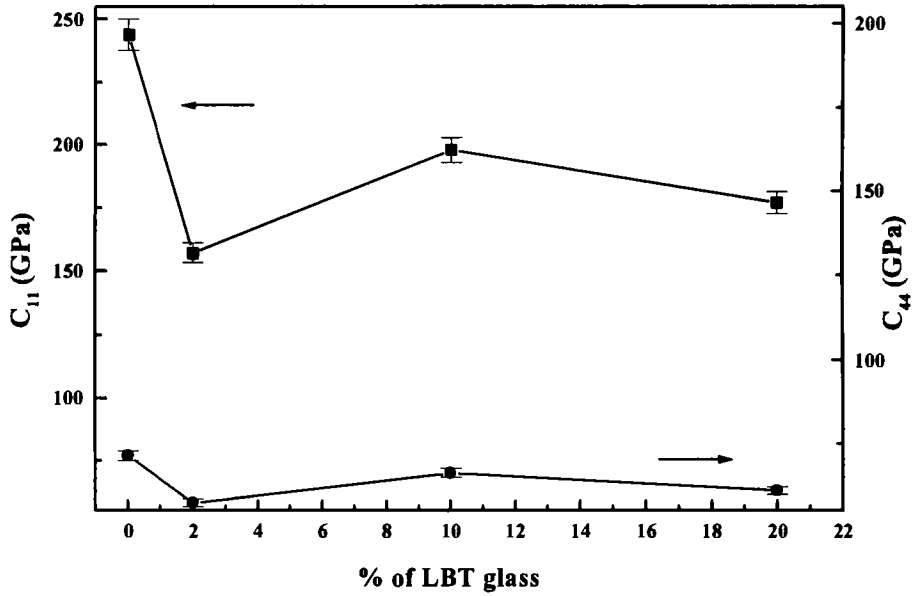


Fig. 4.15: Variation of C_{11} and C_{44} with LBT addition

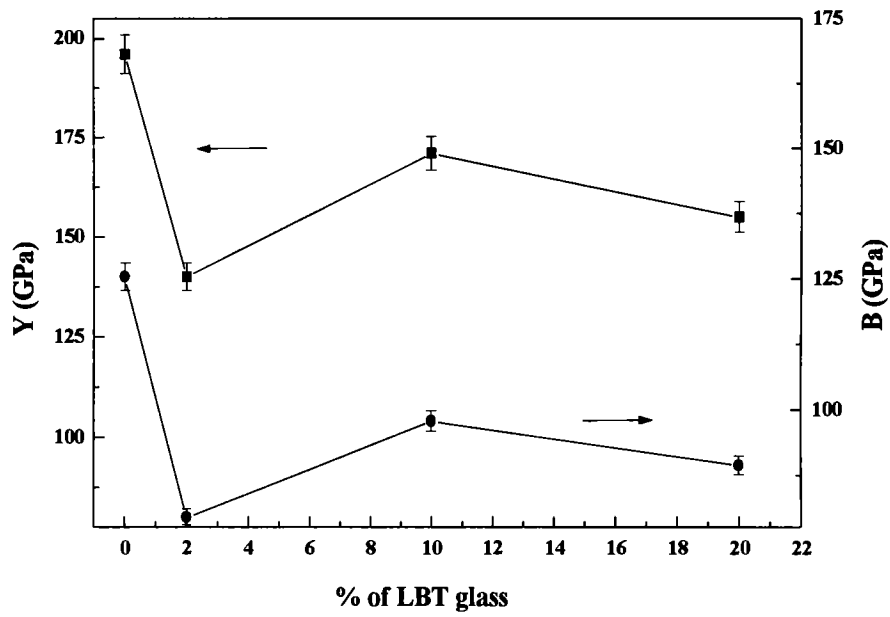


Fig. 4.16: Variation of Y and B with LBT addition

References

1. R. J. Cava, *J. Mater. Chem.* **11** (2001) 54
2. J. K. Plourde, C. L. Ren, *Applications of Dielectric Resonators in Microwave Components*, IEEE TMTT. (1968) 218
3. S. I. Hirano, T. Hayashi and A. Hattori, *J. Am. Ceram. Soc.* **77** (1991) 1320
4. S. B. Desu, H. M. O'Bryan, *ibid*, **68** (1985) 546
5. T. Takada, S. F. Wang, S. T. Syoshikawa, Jang, *ibid.* **77** (1994) 1909
6. H. Ohsato, T. Ohhashi, H. Kato, S. Nishigaki and T. Okuda, *Jpn. J. Appl. Phys.* **34** (1995) 187
7. J. Wakino, K. Minai, H. Tamura, *J. Am. Ceram. Soc.* **67** (1984) 278
8. H. Ohsato, H. Kato, M. Mizuta, S. Nishigaki and T. Okuda, *Jpn. J. Appl. Phys.* **32** (1995) 5413
9. D. Kolar, S. Gaberseek, B. Volavsek, H. S. Parker and R. S. Roth, *J. Solid State Chem.* **38** (1981) 158
10. M Valant, D. Suvorov and D. Kolar, *Jpn. J. Appl. Phys.* **35** (1995) 144
11. H. Ohsato, A. Komura, Y. Takagi, S. Nishigaki and T. Okuda, *ibid*, **37** (1998) 5357
12. J. M. Wu, M. C. Chang, P. C. Yao, *J. Am. Ceram. Soc.* **73(6)** (1990) 1599
13. M. Imaeda, K. Itoh, H. Ohsato, M. Mizuta, H. Kato, S. Nishigaki and T. Okuda, *Jpn. J. Appl. Phys.* **36** (1997) 6012
14. S. Nishigaki, H. Kato, S. Yano and R. Kamimura, *J. Am. Ceram. Soc. Bull.* **66(9)** (1987) 1405
15. C. J. Rawn, D. P. Birnie, M. Bruck, J.H. Enemark, R. S. Roth, *J. Mater. Res.* **13** (1998) 187

16. R. G. Matveeva, M. B. Varforomeev, L. S. Hyuschenko, *Russ. J. Inorg. Chem.* **29** (1984) 17
17. C. C. Lee and P. Lin, *Jpn. J. Appl. Phys.* **37** (1998) 6048
18. S. W. Jung, J. H. Lee, J. J. Kim, H. Y. Lee, S. H. Cho, *Mat. Chem. Phys.* **79** (2003) 282.
19. S. Nishigaki, H. Kato, S. Yano and R. Kamimura, *Ceram. Bull.* **66** (1987) 9
20. N. Ichinose and H. Amada, *J. Europ. Ceram. Soc.*, **21** (2001) 2751
21. P. Laffez, G. Desgardin and B. Raveau, *J. Mat. Sci.* **27** (1992) 5229.
22. Z. Jiwei, Y. Xi, C. Xiaogang, Z. L. Ying and H. Chen, *J. Mater. Sci.* **37** (2002) 3739
23. M. Valani, D. Kolar and D. Suvorov, *Proc. III Euroceramics*, edited by P. Duran and J. F. G. Fernandez (1993) 235
24. J. M. Durand and J. P. Boilot, *J. Mater. Sci. Lett.* **6** (1987) 134
25. F. Azough, P. Setaswan and R. Freer, *Materials and Processes for Wireless Communications* Eds: by T. Negas and H. Ling *Ceram. Trans* 53 (The American Ceramic Society) (1995) p.215
26. T. Negas and P. K. Davies, *ibid.* p.179.
27. D. Suvorov, M. Valant and D. Kolar, *ibid.* p.197.
28. M. Valant, D. Suvorov and D. Kolar, *J. Mater. Res.* **11** (1996) 928
29. Y. Ota, K. I. Kakimoto, H. Ohsato, T. Okawa, *J. Euroceram. Soc.* **24** (2004) 1755
30. Q. L. Zhang, H. Yang, J. L. Zou and H. P. Wang, *Mat. Lett.* **59** (2005) 880
31. N. Rodrigues and J. Philip, *J. Acoust. Soc. Ind.* **27** (1999) 235

32. E. P. Papadakis, *Physical Acoustics* (Eds: M. P. Mason, R. N. Thurston, Academic Press, New York) **12** (1976) 277
33. H. J. McSkimin, *J. Acoust. Soc. Am.* **33** (1961) 12

CHAPTER 5

Elastic properties of Borosilicate added BST ceramics

51. Introduction

Commercial wireless communication applications emerged in the late 1970s, evolved in the 1980s and have exploded through 1990s [1]. Numerous systems are rapidly filling the 400 MHz – 20GHz band. Cellular telephones (400 MHz – 1GHz), Television Receivers (TVRO, 2 – 5 GHz), Direct broadcasting (DBS, 11-13 GHz) and specialty satellite communications are now deployed worldwide. Wireless cables, high definition and interactive TV, collision avoidance, global positioning, cellular satellite and personal communications (PCS) of many types loom in the near future for consumers.

Among several factors, industrial growth has been spurred by the development of special ceramics and their commercialization as high volume, low cost products. These materials are easily integrated into rf/microwave circuits using glues, epoxies, screws or solder. They function as frequency filters, capacitors, inductors and signal distributing elements. Electrical requirements for the materials used are, low loss (high Q), high dielectric constant (ϵ_r) and very low temperature coefficient of resonant frequency (τ_f). High Q, not only minimizes circuit insertion

losses, but for some filter applications, also allows more channels, within a given frequency allocation. In addition, electrical noise is suppressed in oscillator devices.

Many systems have been investigated, for the research of new materials, but only a limited number led to interesting characteristics. Among them, the ternary systems $\text{BaO} - \text{R}_2\text{O}_3 - \text{TiO}_2$ with $\text{R} = \text{Sm}, \text{La}, \text{Nd}$ appear as potential candidates for microwave applications [2]. In this family best results are obtained for $\text{Ba}_{6-3x}\text{Sm}_{8+2x}\text{Ti}_{18}\text{O}_{54}$ (BST) with $x = 2/3$. Due to its commercial importance, lot of work has been done on the dielectric and structural properties of BST. The influences of calcination, sintering and composition upon microwave properties of BST have been studied. One major problem regarding BST ceramics is its high sintering temperature, due to which it cannot be processed along with the electrode material. Also, as an approach to obtain desired dielectric properties, mixing of two low loss materials having positive and negative temperature coefficients is well known as reported for the $\text{MgTi}_2\text{O}_5 - \text{TiO}_2$ system, $\text{BaTi}_4\text{O}_9 - \text{BaPr}_2\text{Ti}_4\text{O}_{12}$ system [3] etc. This approach should have wide applicability if a proper selection of two compounds is carried out. Sometimes, this aim is achieved by mixing glass to a DR material as reported by C. C. Lee *et al.* [4]. They found that by the addition of 20 wt% $\text{PbO} - \text{B}_2\text{O}_3 - \text{SiO}_2$ glass to $\text{BaO}.\text{La}_2\text{O}_3.4.7\text{TiO}_2$, the sintering temperature can be reduced to 900°C from 1300°C , resulting in a slight lowering of ϵ_r (64 from 92) and Q (1037 from 1653), but its temperature coefficient of resonance frequency is improved to $15.3 \text{ ppm} / ^\circ\text{C}$ from $40.3 \text{ ppm} / ^\circ\text{C}$ at 3 GHz. The densification of specimens was found to play an important role in improving the dielectric constant. Heterogeneous interfaces and dissolution of trace amounts of ceramics in glass

increased τ_f , whereas the latter decreased it. Glasses with a high Pb content like PbO – B₂O₃ – SiO₂, PbO – B₂O₃ etc have higher dielectric constant, presumably due to the high polarizability of Pb. While glasses containing SiO₂ like PbO – B₂O₃ – SiO₂, ZnO- B₂O₃ – SiO₂ etc have a relatively higher quality factor, which may be attributed to the low dielectric loss of silica glass. Z. Jiwei *et al.* [5] reported that the rigidity and intensity of Ba_{0.6}Sr_{0.4}TiO₃ samples added with 1 mol%, 5 mol%, 10 mol% and 20 mol% of B₂O₃ – SiO₂ glasses were as good as pure samples, keeping a decrease in sintering temperature as the glass content is increased. They also pointed out that the sintering temperature of the sample was not decreased when SiO₂ was used as the addend. It is inferred that, the dielectric tunability of Ba_{0.6}Sr_{0.4}TiO₃ is affected at a lower sintering temperature since the grain size is reduced.

Low temperature sintering of dielectric materials with glass addition has been successfully developed in several microwave dielectric systems, such as (Zr, Sn) TiO₄, BaO – TiO₂, ZnO – Nb₂O₅ – TiO₂, (Ca, Mg) TiO₃, BaO – Nd₂O₃ – TiO₂ etc [6-14]. However, the majority of the ceramic systems with glass and/or a mixture of additives offer relatively inferior dielectric performances relative to those of the high-temperature systems. Kim *et al.* demonstrated that the additions of 1-5 wt% B₂O₃ were effective in reducing the sintering temperature of the ZnTiO₃ ceramics from 1100 to 875 °C without degradation of microwave properties [5]. Q. L. Zhang *et al.* investigated the sintering behaviour and microwave properties as a function of ZnO – B₂O₃ – SiO₂ (ZBS) content [16]. It has been reported that addition of ZBS up to 2 wt% increased the density due to the formation of liquid phase whereas ZBS

addition above 2 wt% and high sintering temperature induced excess pores, due to the evaporation of the sintering aid, which in turn reduces the density of the ceramic sample. Low-temperature sintering of $Ba_{6-3x}Sm_{8+2x}Ti_{18}O_{54}$ (BST) ceramics by adding B_2O_3 and GeO_2 was studied by Y. Ota *et al.* [9]. In additive systems investigated, B_2O_3 ceramic powder was most effective in lowering the sintering temperature of BST (at $x = 2/3$). Takada *et al.* reported reduction of sintering temperature by $160^\circ C$ in $BaO - TiO_2 - WO_2$ systems using B_2O_3 glass [17]. Liu *et al.* [10] reported reduction in the sintering temperature of $Ca(Li_{1/3}Nb_{2/3})O_{3.8}$ ceramics from 1423 to 1263K by the addition of B_2O_3 ceramic powder.

In this chapter, the elastic properties of glass-added BST ceramics have been measured. The glasses used as additives are (i) $B_2O_3 - Bi_2O_3 - SiO_2 - ZnO$ (BBSZ), (ii) $BaO - B_2O_3 - SiO_2$ (BBS₁), (iii) $Ba_{30}B_{40}Si_{30}$ (BBS₂) and (iv) $Al_2O_3 - B_2O_3 - SiO_2$ (ABS). XRD pattern are taken to see whether there is any secondary phases in the glass-added samples, responsible for the particular elastic behaviour observed.

5.2. Sample Preparation

The glass-added ceramics are prepared by the conventional solid-state reaction method, as already described in earlier chapters. $Ba_4Sm_{28/3}Ti_{18}O_{54}$ ceramic powder was prepared from reagent grade $BaCO_3$, Sm_2O_3 and TiO_2 , which were mixed in the stoichiometric ratio with distilled water. After ball- milling for about 24 hrs, the dried powders were calcined at $1150^\circ C$ for 4 hrs. The calcined powder was then added with a fixed wt % of glass and PVA (5%) and dry-pressed at 150 MPa to form cylindrical compacts. In this study $B_2O_3 - Bi_2O_3 - SiO_2 - ZnO$, $BaO - B_2O_3 -$

SiO_2 , $\text{Ba}_{30}\text{B}_{40}\text{Si}_{30}$, $\text{Al}_2\text{O}_3 - \text{B}_2\text{O}_3 - \text{SiO}_2$ glasses are used as the additives. The obtained pellets were then sintered at appropriate optimized temperatures.

5.3. Samples Studied

Different sets of samples are prepared to study the elastic properties presented in this chapter. Each set consists of BST added with a particular glass in various proportions. The different sets are BST added with (i) $\text{B}_2\text{O}_3 - \text{Bi}_2\text{O}_3 - \text{SiO}_2 - \text{ZnO}$ (BBSZ), (ii) $\text{BaO} - \text{B}_2\text{O}_3 - \text{SiO}_2$ (BBS₁), (iii) $\text{Ba}_{30}\text{B}_{40}\text{Si}_{30}$ (BBS₂) and (iv) $\text{Al}_2\text{O}_3 - \text{B}_2\text{O}_3 - \text{SiO}_2$ (ABS).

5.4. Structural Characterization by XRD and SEM

The X-ray powder diffraction patterns of the samples were recorded with a Bruker D8 Advance X-ray powder diffractometer. The patterns for the pure sample and the same added with different glasses are shown in Figures 5.1 – 5.4.

The scanning electron micrographs of a few samples have been recorded using scanning electron microscopic (SEM, Model S – 2400, Hitachi, Japan) techniques. Samples for SEM were prepared by polishing and thermally etching for 30 minutes at a temperature $< 50 - 100$ °C of the sintering temperature and then cooling to room temperature. The SEMs of BST added with ABS are shown in Fig. 5(a)-5(d).

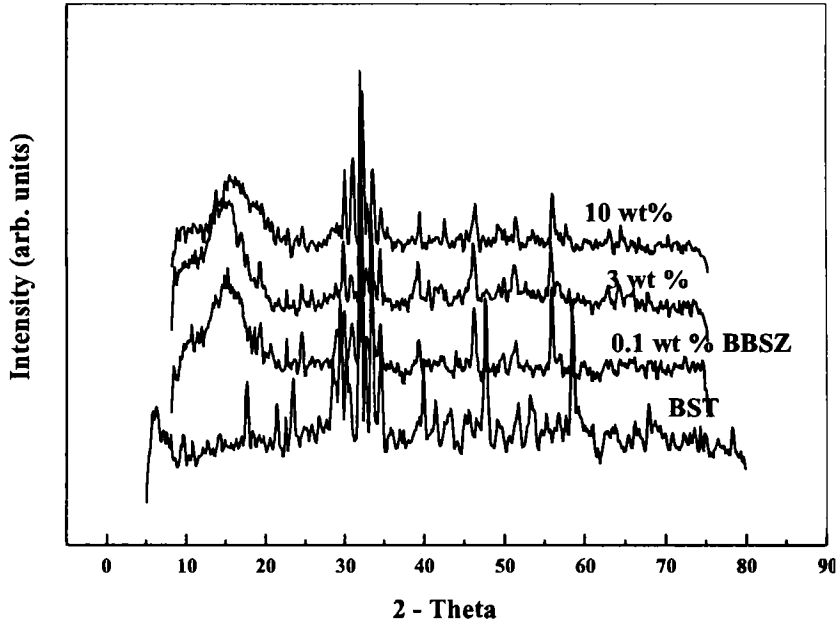


Fig. 5.1: XRD pattern of BST added with BBSZ glass

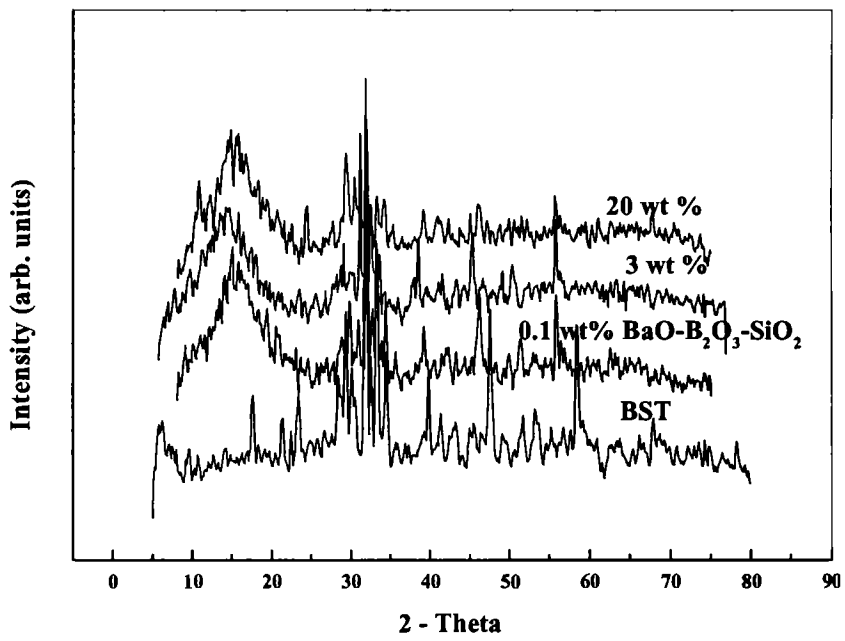


Fig.5.2: XRD pattern of BST added with BaO - B₂O₃ - SiO₂ glass

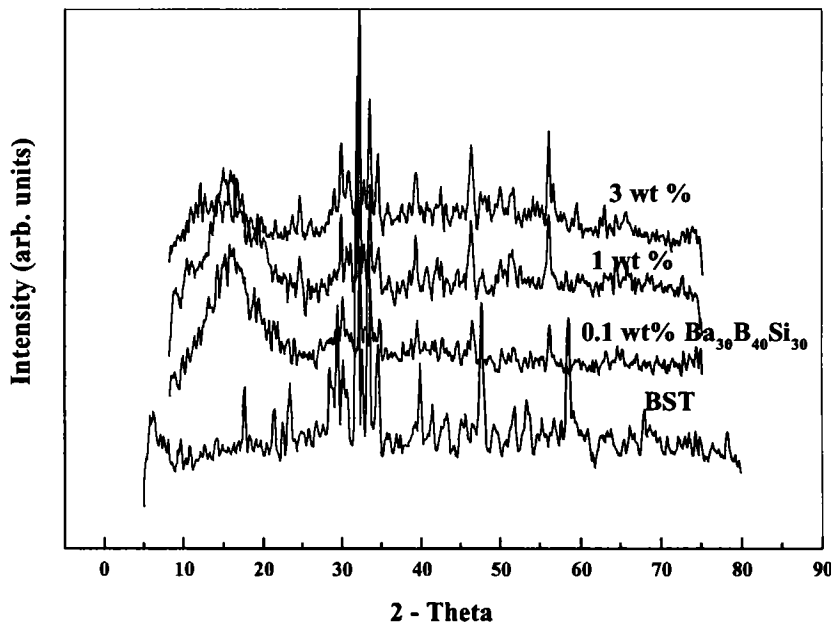


Fig.5.3: XRD pattern of BST added with $Ba_{30}B_{40}Si_{30}$ (BBS₂)

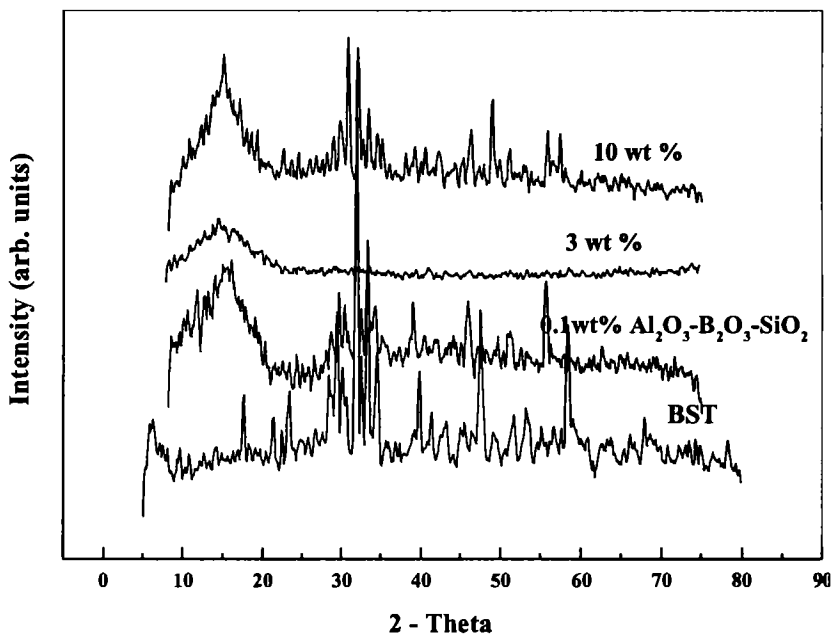


Fig. 5.4: XRD pattern of BST added with $Al_2O_3 - B_2O_3 - SiO_2$ (ABS).

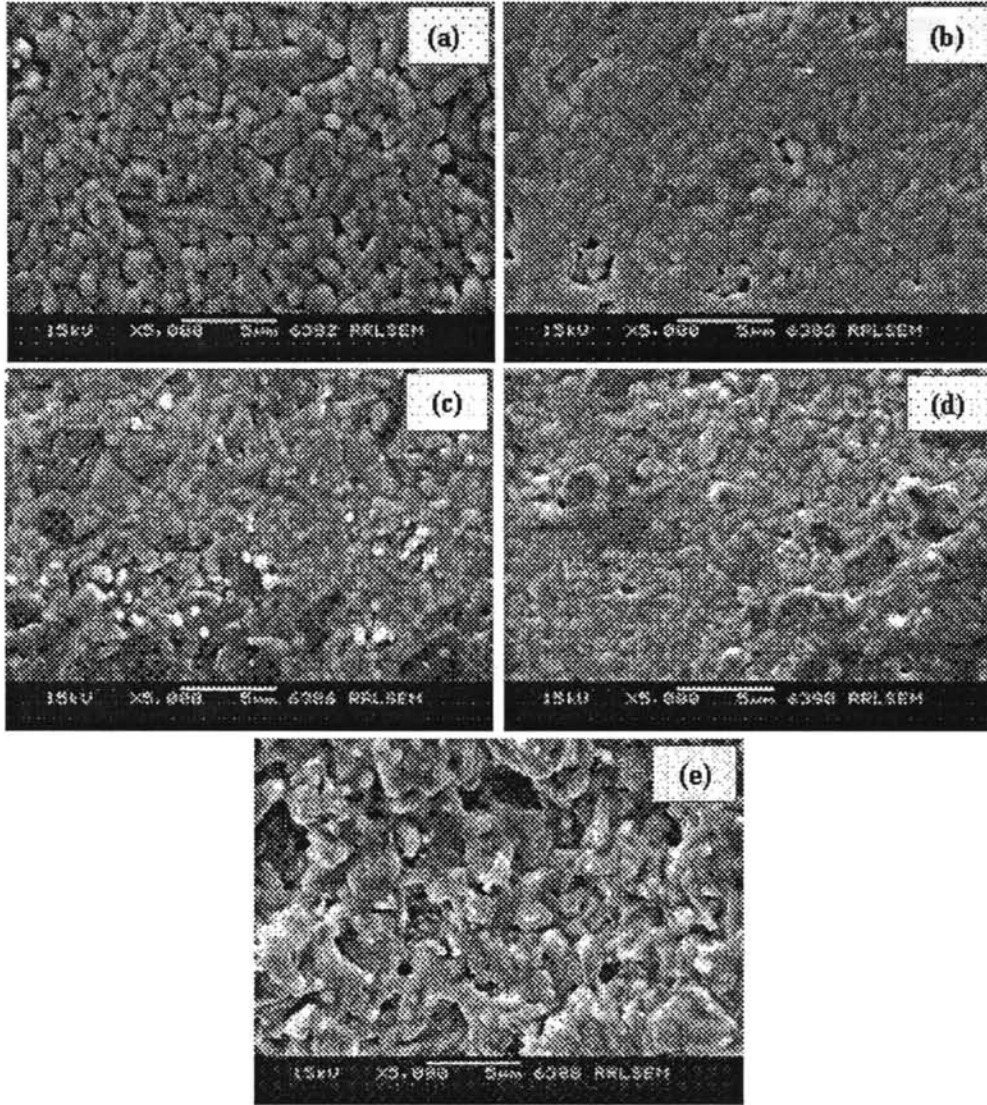


Fig. 5.5: SEM microstructure of $44\text{Al}_2\text{O}_3\text{-}30\text{B}_2\text{O}_3\text{-}26\text{SiO}_2$ glass added $\text{Ba}_4\text{Sm}_{9.33}\text{Ti}_{18}\text{O}_{54}$ (a) 0 wt %, (b) 1 wt %, (c) 2 wt %, (d) 3 wt % and (e) 4 wt %

5.5. Elastic properties by Ultrasonic Technique

Ultrasonic wave velocities in the ceramic samples have been measured by the Pulse echo overlap technique using Matec 7700 pulse modulator and receiver system [18]. Pelletised samples of thickness 5-6 mm have been used for the

measurements. The faces of the samples are well polished after making their faces parallel to each other. X-cut quartz transducer of resonant frequency 10 MHz is mounted on one end of the sample face using nonaq stopcock grease as the bond, which acts as the transmitter of ultrasonic waves in to the medium, as well as receiver of echoes from the medium. The time gap between two selected echoes is measured using the pulse echo overlap method. Knowing the thickness and density (ρ), the longitudinal velocity (V_l) and elastic modulus (C_{11}) can be calculated using relation $C_{11} = \rho V_l^2$. In order to get the transverse velocity (V_t) and modulus (C_{44}), Y-cut quartz transducer is bonded with silicon grease as the bonding medium. Using V_l and V_t elastic constants like Young's modulus, Bulk modulus, Poisson's ratio etc are calculated.

While measuring the time interval between selected echoes, the McSkimin Δt criterion [19] has been applied to correct the phase lag due to bonding medium on RF echoes. This technique helps to measure ultrasound transit in the sample to an accuracy of the order of few ppm.

5.6. Results and Discussion

Figures 5.1 – 5.4 shows the XRD patterns of BST added with different glasses. The peaks are of orthorhombic, tungsten–bronze type BST solid solution as reported by Okawa *et al* [20]. To understand how glass affects the microstructure of BST, scanning electron micrographs of BST added with ABS were taken (Fig.5.5). Secondary phases are observed in the Fig.5(b)-5(e). These can be due to the ABS

glass. As reactivity studies done up to 1350 °C show that ABS is non-reactive with BST.

The elastic properties of a glass-sintered ceramics may strongly depend on the densification, the microstructure and interaction between glass and ceramics at the molecular level. The reaction between the sintering aids and the ceramics may cause the formation of secondary phases, resulting in low elastic strength. In the high glass content samples, the density of pores may be high, which also will affect the density and hence the elastic strength. Another factor, which affects its mechanical strength, is the grain size of the material.

The longitudinal and transverse wave velocities, the corresponding elastic constants C_{11} and C_{44} , the Young's modulus, Bulk modulus and Poisson's ratios of the ceramics doped with different percentages of $B_2O_3 - Bi_2O_3 - SiO_2 - ZnO$, $BaO - B_2O_3 - SiO_2$, $Ba_{30}B_{40}Si_{30}$ (BBS₂) and $Al_2O_3 - B_2O_3 - SiO_2$ glasses are tabulated in Tables 5.1-5.4. The variations of these parameters with variation of glass concentration (in %) are plotted in Figures 5.6 – 5.18.

In general, the results show that addition of glass results in a reduction in elastic moduli. The Poisson's ratio also decreases with glass addition. The decrease in elastic moduli is more or less proportional to the wt % of the glass added. This is a general result. The elastic moduli decrease irrespective of the added glass. So glass addition essentially results in a decrease in the mechanical strength and hardness of the specimen.

It may be noted that a small decrease in mechanical strength and hardness do not seriously affect the use of these materials as DR materials. Since addition of

glass at low weight percentages significantly reduces sintering temperatures, one can afford to compromise for a small decrease in mechanical strength and hardness.

The results presented in this chapter are the first of this kind that throws light on the effect of glass addition on the mechanical properties of dielectric resonator materials.

Table 5.1: Elastic Properties of BST added with B₂O₃ - Bi₂O₃ - SiO₂ – ZnO glass

wt % of glass	V _l (m/s)	C ₁₁ (GPa)	V _t (m/s)	C ₄₄ (GPa)	Young's Modulus Y (GPa)	Bulk Modulus B (GPa)	Poisso- n's ratio
0.0	6607 ± 33	244 ± 6	3729 ± 18	77 ± 2	196 ± 5	140 ± 3	0.266
0.1	6616 ± 33	246 ± 6	3718 ± 18	78 ± 2	197 ± 5	142 ± 4	0.269
0.5	6512 ± 32	235 ± 6	3686 ± 18	75 ± 2	190 ± 5	135 ± 3	0.264
1	6180 ± 30	211 ± 5	3683 ± 18	74 ± 2	183 ± 4	111 ± 3	0.225
2	6097 ± 30	204 ± 5	3651 ± 18	73 ± 2	179 ± 4	106 ± 3	0.220
3	6009 ± 30	192 ± 5	3620 ± 18	70 ± 2	169 ± 4	99 ± 2	0.215
5	5848 ± 29	179 ± 4	3575 ± 18	67 ± 2	161 ± 4	90 ± 2	0.201
7	5405 ± 27	145 ± 3	3279 ± 16	53 ± 1	129 ± 3	74 ± 2	0.209
10	5543 ± 27	157 ± 4	3363 ± 17	58 ± 1	140 ± 3	80 ± 2	0.209

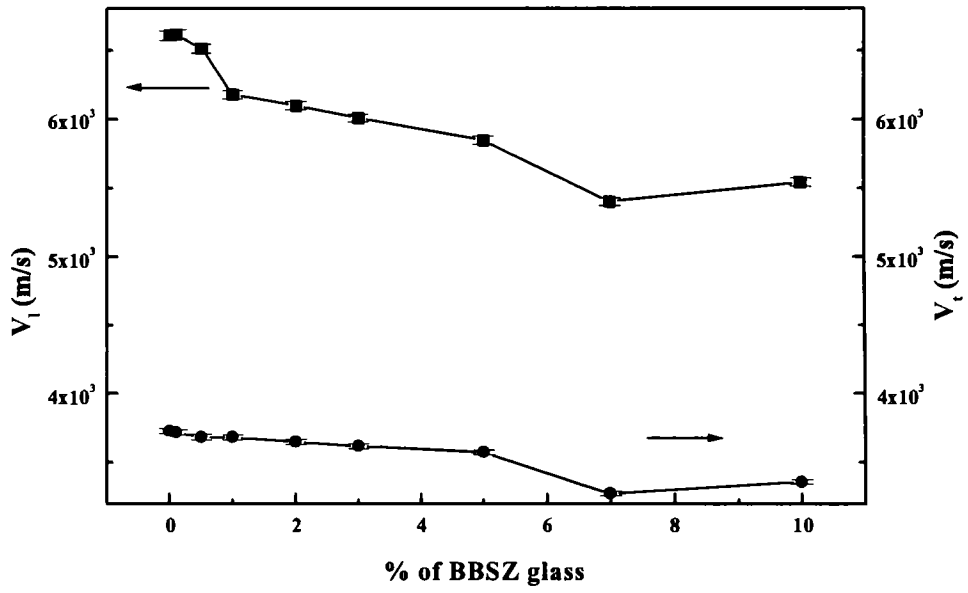


Fig.5.9: Variation of ultrasonic velocity of BST with BBSZ

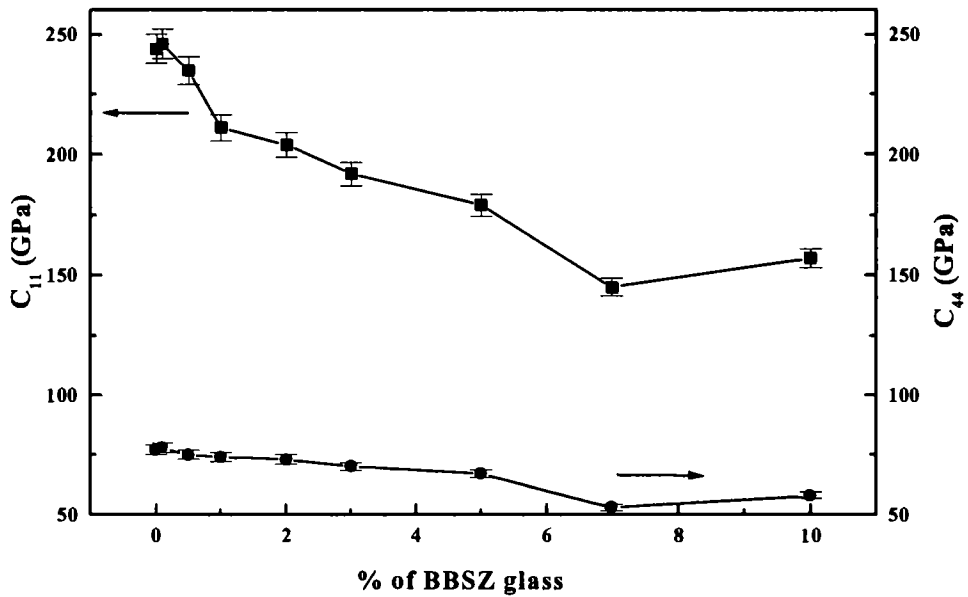


Fig.5.10: Variation of C_{11} and C_{44} with BBSZ addition

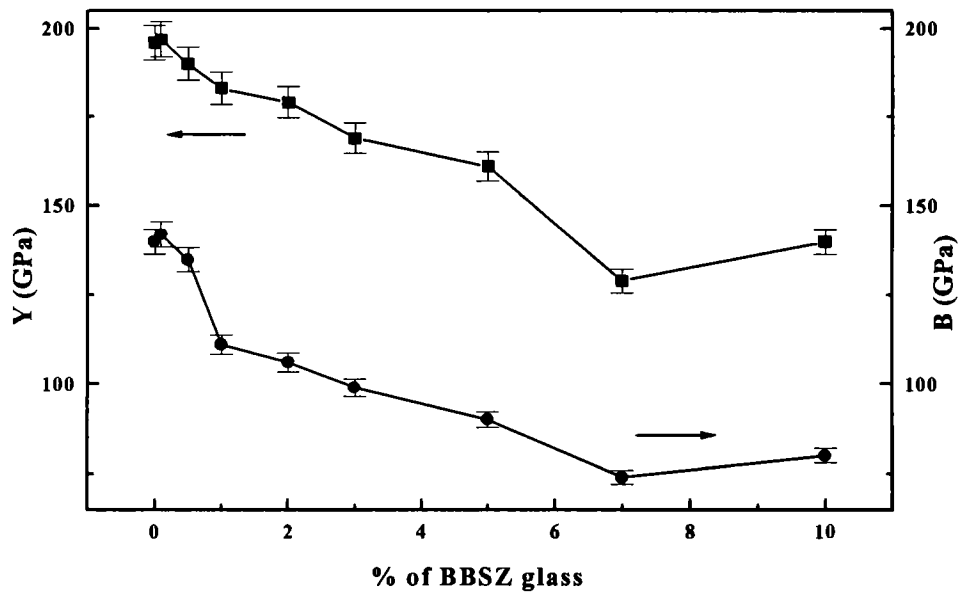


Fig. 5.11: Variation of Y and B with BBSZ addition

Table 5.2: Elastic Properties of BST added with BaO – B₂O₃ – SiO₂ glass

wt % of glass	V_l (m/s)	C₁₁ (GPa)	V_t (m/s)	C₄₄ (GPa)	Young's Modulus Y (GPa)	Bulk Modulus B (GPa)	Poisso- n's ratio
0.0	6607 ± 33	244 ± 6	3729 ± 18	77 ± 2	196 ± 5	140 ± 3	0.266
0.1	6523 ± 33	235 ± 6	3690 ± 18	75 ± 2	090 ± 5	135 ± 3	0.265
1	6245 ± 31	217 ± 5	3698 ± 18	76 ± 2	187 ± 5	115 ± 2	0.230
3	6159 ± 31	211 ± 5	3669 ± 18	75 ± 2	183 ± 5	111 ± 2	0.225
10	5440 ± 27	173 ± 4	3317 ± 16	64 ± 2	87 ± 2	87 ± 2	0.204
20	3625 ± 18	44 ± 1	2316 ± 12	18 ± 0.5	20 ± 0.5	20 ± 0.5	0.155

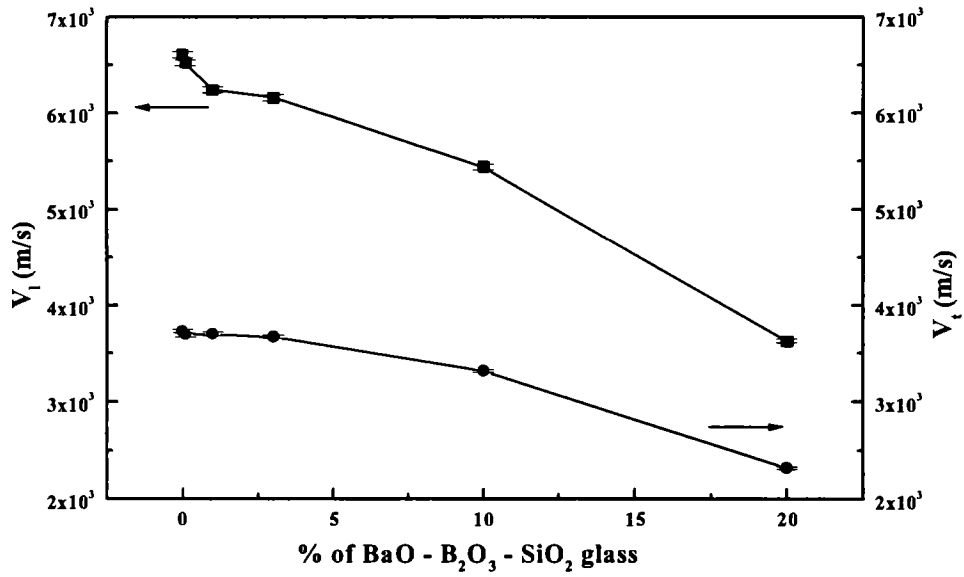


Fig.5.12: Variation of ultrasonic velocity with BaO – B₂O₃ – SiO₂ addition

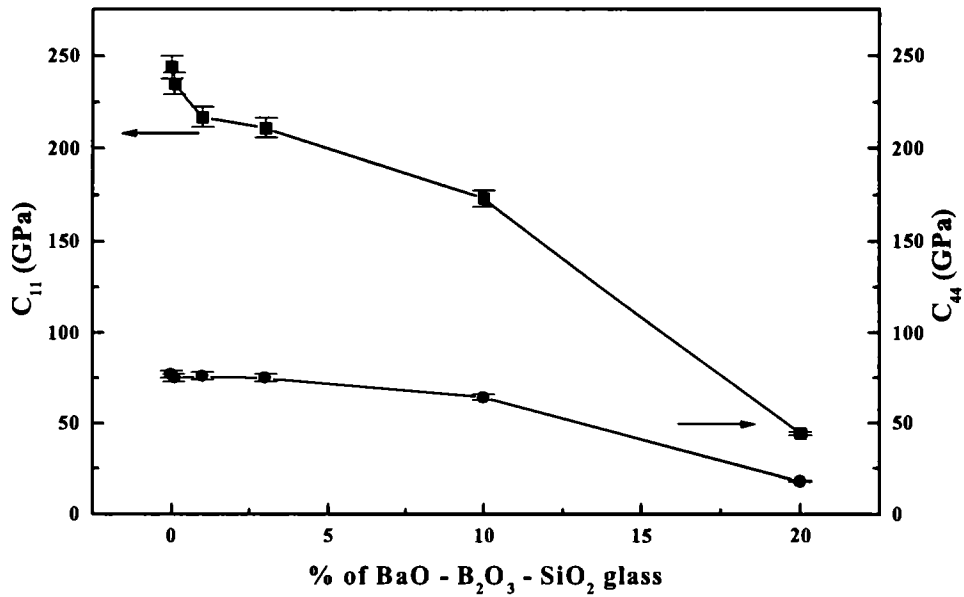


Fig.5.13: Variation of C₁₁ and C₄₄ with BaO – B₂O₃ – SiO₂ addition

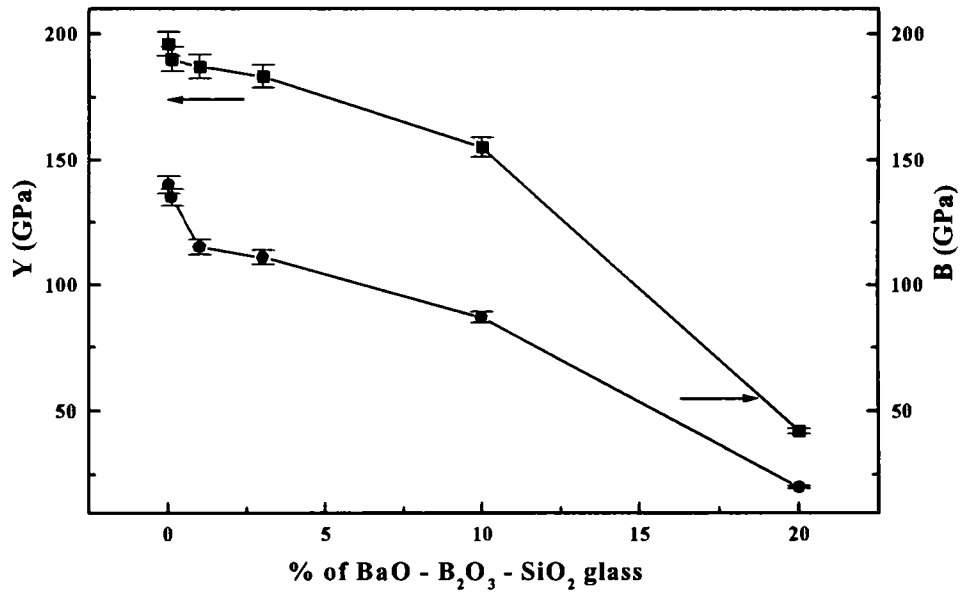


Fig.5.14: Variation of Y and B with BaO – B₂O₃ – SiO₂ addition

Table 5.3: Elastic properties of BST added with Ba₃₀B₄₀Si₃₀ glass

wt % of glass	V ₁ (m/s)	C ₁₁ (GPa)	V _t (m/s)	C ₄₄ (GPa)	Young's Modulus Y (GPa)	Bulk Modulus B (GPa)	Poisson's ratio
0.0	6607 ± 33	244 ± 6	3729 ± 18	77 ± 2	196 ± 5	140 ± 3	0.266
0.1	6663 ± 33	249 ± 6	3724 ± 19	78 ± 2	198 ± 5	145 ± 4	0.273
0.5	6643 ± 33	245 ± 6	3725 ± 18	77 ± 2	195 ± 5	142 ± 3	0.271
1	6196 ± 31	213 ± 5	3683 ± 8	75 ± 2	184 ± 5	112 ± 3	0.227
2	6100 ± 30	201 ± 5	3644 ± 18	72 ± 2	175 ± 4	105 ± 3	0.223
3	6087 ± 30	200 ± 5	3608 ± 18	70 ± 2	173 ± 4	106 ± 3	0.229

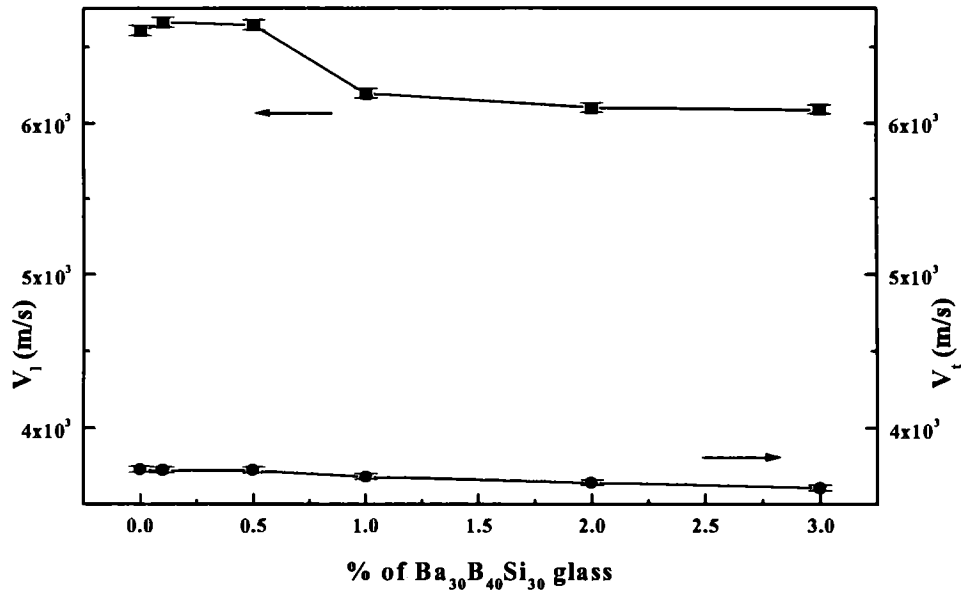


Fig.5.15: Variation of ultrasonic velocity with Ba₃₀B₄₀Si₃₀ addition

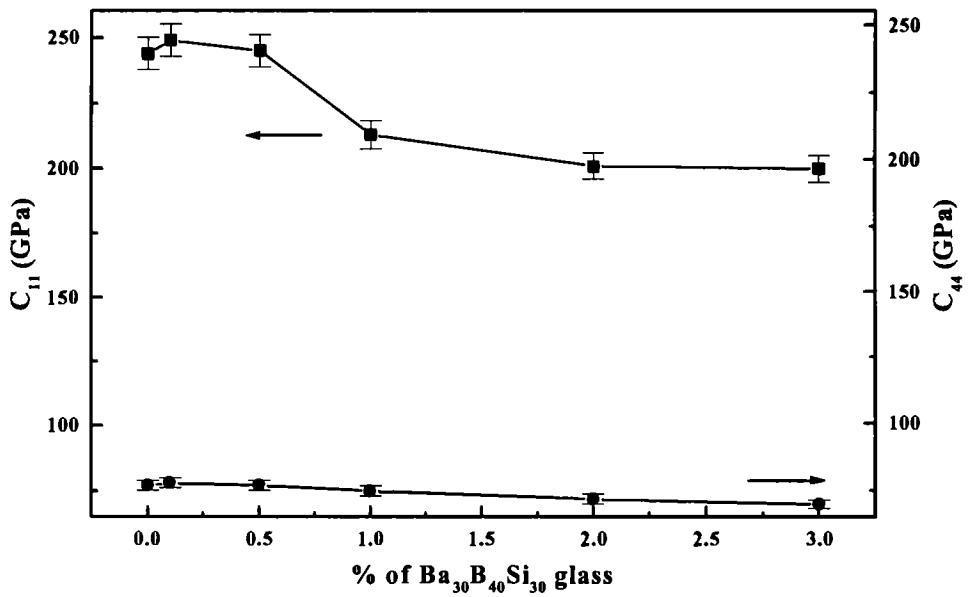


Fig.5.16: Variation of C₁₁ and C₄₄ with Ba₃₀B₄₀Si₃₀ addition

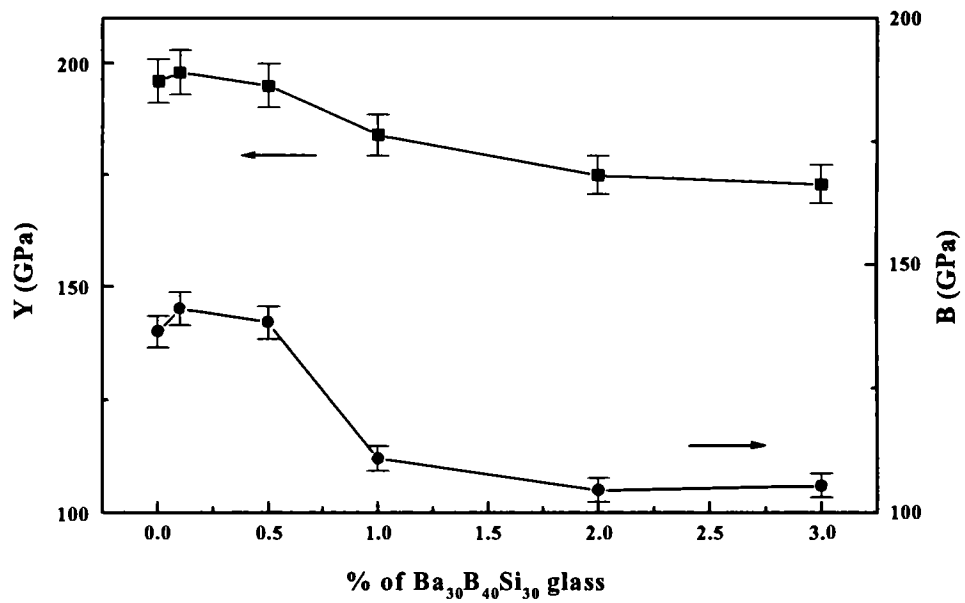


Fig.5.17: Variation of Y and B with $Ba_{30}B_{40}Si_{30}$ addition

Table 5.4: Elastic Properties of BST added with Al₂O₃ - B₂O₃ - SiO₂ glass

wt % of glass	V_l (m/s)	C₁₁ (GPa)	V_t (m/s)	C₄₄ (GPa)	Young's Modulus Y (GPa)	Bulk Modulus B (GPa)	Poisson's ratio
0.0	6607 ± 33	244 ± 6	3729 ± 18	77 ± 2	196 ± 5	140 ± 3	0.266
0.1	6578 ± 33	238 ± 6	3686 ± 18	75 ± 2	190 ± 5	139 ± 3	0.271
0.5	6445 ± 32	228 ± 6	3666 ± 18	74 ± 2	186 ± 5	130 ± 3	0.261
3	6242 ± 31	202 ± 5	3561 ± 18	66 ± 2	165 ± 4	114 ± 2	0.259
5	5962 ± 30	173 ± 4	3426 ± 17	57 ± 1	143 ± 3	97 ± 2	0.253
10	5598 ± 28	129 ± 3	3151 ± 16	41 ± 1	104 ± 3	74 ± 2	0.268

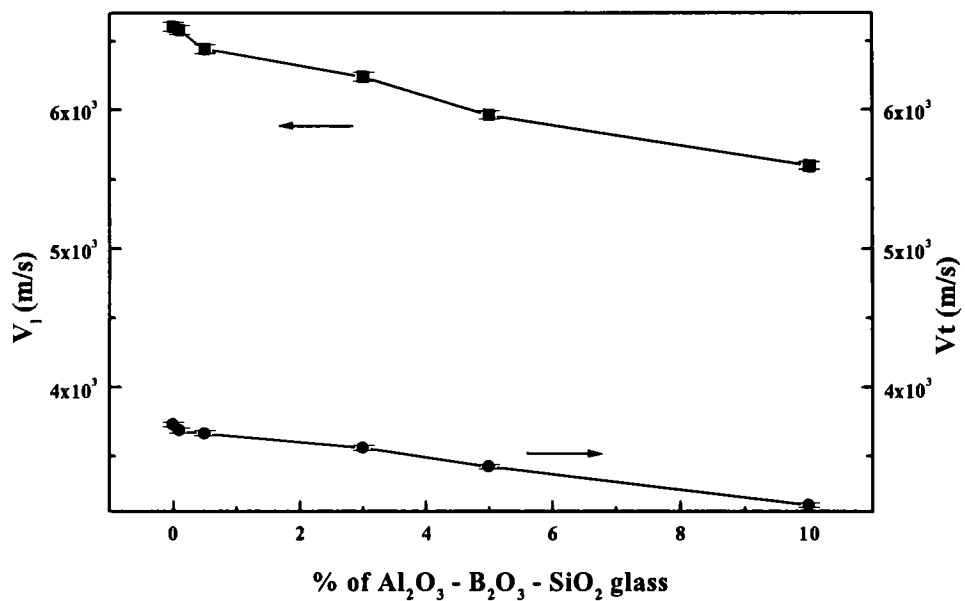


Fig.5.18: Variation of ultrasonic velocity with $\text{Al}_2\text{O}_3 - \text{B}_2\text{O}_3 - \text{SiO}_2$ addition

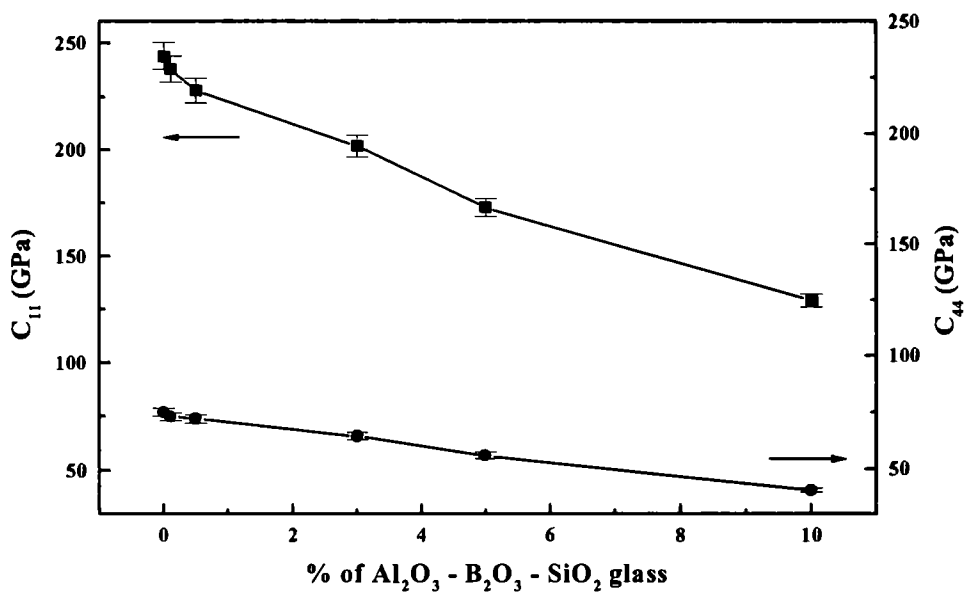


Fig.5.19: Variation of C_{11} and C_{44} with $\text{Al}_2\text{O}_3 - \text{B}_2\text{O}_3 - \text{SiO}_2$ addition

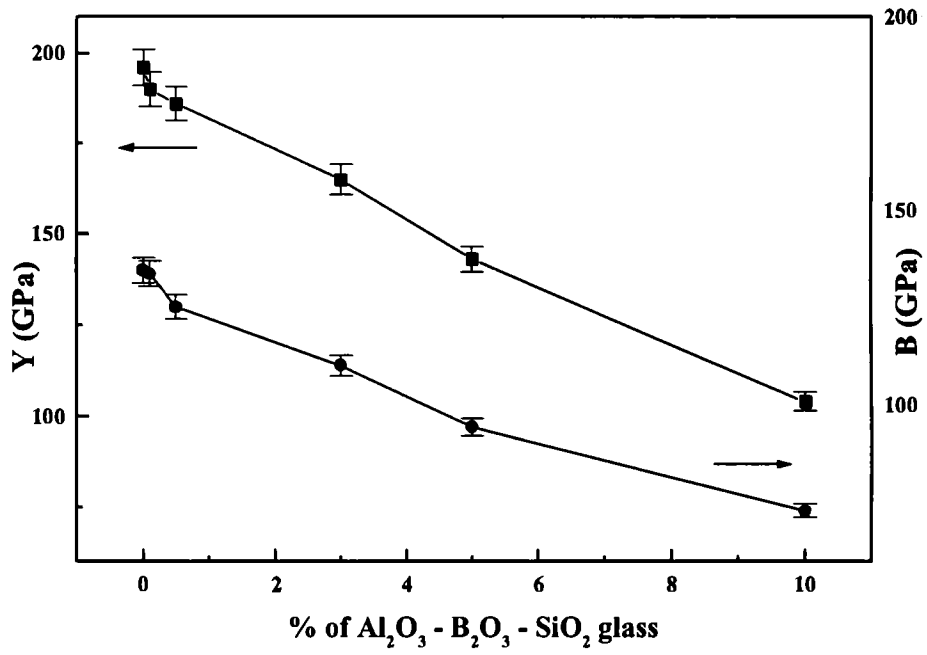


Fig.5.20: Variation of Y and B with $\text{Al}_2\text{O}_3 - \text{B}_2\text{O}_3 - \text{SiO}_2$ addition

References

- 1) T. Negas, G. Yeager, S. Bell and N. Coats, *Am. Ceram. Soc. Bull.* **72(I)** 1993
- 2) S. Nishigaki, H. Kato, S. Yang, R. Kamimura, *Am. Ceram. Soc. Bull.* **66** (1987) 1405
- 3) S. Fukuda, S. Shoda, A. Kunishige, R. Kitoh and I Awai, *J. Mat. Sci. Lett.* **13** (1994) 1290
- 4) C. C. Lee and P. Lin, *Jpn. J. Appl. Phys.* **37** (1998) 6048
- 5) Z. Jiwei, Y. Xi, C. Xiaogang, Z. L. Ying and H. Chen, *J. Mater. Sci.* **37** (2002) 3739
- 6) G.H. Huang, D.X. Zhou, J.M. Xu, X.P. Chen, D.L. Zhang, W.Z. Lu and B.Y. Li, *Mater. Sci. Eng., B, Solid-State Mater. Adv. Technol.* **99** (2003) 416
- 7) C.L. Huang, M.H. Weng, C.T. Lion and C.C. Wu, *Mater. Res. Bull.* **35** (2000) 2445
- 8) J.Y. Ha, J.W. Choi, S.J. Yoon, D.J. Choi, K.H. Yoon and H.J. Kim, *J. Eur. Ceram. Soc.* **23** (2003) 2413
- 9) Y. Ota, K.I. Kakimoto, H. Ohsato, T. Okawa, *J. Eur. Ceram. Soc.* **24** (2004) 1755
- 10) P. Liu, H. Ogawa, S.K. Kim and A. Kan, *J. Eur. Ceram. Soc.* **24** (2004) 1761
- 11) O. Demovsek, A. Naeini, G. Preu, W. Wersing, M. Eberstein and W.A. Schiller, *J. Eur. Ceram. Soc.* **21** (2001) 1693

- 12) D.S. Kim, H.B. Hong and K.S. Hong, *Jpn. J. Appl. Phys.* **41** (2002) 1465
- 13) D.W. Kim, K.S. Hong, C.S. Yoon and C.K. Kim, *J. Eur. Ceram. Soc.* **23** (2003) 2597
- 14) C.L. Huang, C.L. Pan and S.J. Shium, *Mater. Chem. Phys.* **78** (2002) 111
- 15) H.T. Kim, S.H. Kim and J.D. Byun, *J. Am. Ceram. Soc.* **82** (1999) 3043
- 16) Q. L. Zhang, H. Yang, J. L. Zhou and H. P. Wang, *Mat. Lett.* **59** (2005) 880
- 17) T. Takada, S. F. Wang, S. T. Syoshikawa and Jang, *ibid*, **77** (1994) 1909
- 18) E. P. Papadakis, *Physical Acoustics* (Eds: M. P. Mason, R. N. Thurston, Academic Press, New York) **12** (1976) 277
- 19) H. J. McSkimin, *J. Acoust. Soc. Am.* **33** (1961) 12
- 20) T. Okawa, M. Imaeda and H. Ohsato, *Jpn.J. Appl. Phys.* **39** (**9B**) (2000) 5645

CHAPTER 6

Elastic and structural properties of $\text{Ca}_{5-x}\text{A}_x\text{Nb}_2\text{TiO}_{12}$ (A = Mg, Zn) ceramics

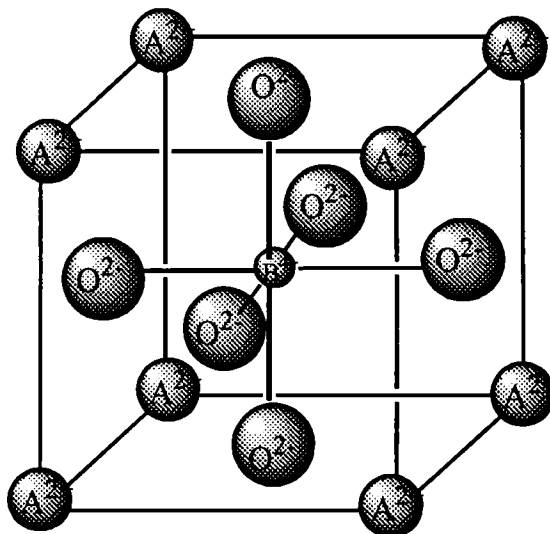
6.1. Introduction

Perovskites form an important class of mixed metal oxides with the general formula ABO_3 , possessing excellent properties that make them potentially useful for catalytic, electronic and ion-exchange applications [1]. The structural diagram of a typical perovskite is shown in Fig.6.1. The class of materials known as 'complex perovskites' is of considerable technological importance, particularly with regard to physical properties such as pyro- and piezoelectricity, linear and non-linear electro-optic effects and dielectric properties. An important difference between the complex perovskites and ideal perovskite structure ABO_3 is that complex perovskites have pairs of unlike valence cations in the B or A positions. Complex perovskites have revolutionized the microwave based wireless communication industry by reducing the size and cost of resonators, filters and oscillators in communication systems, ranging from cellular phones to global positioning systems. Complex perovskites can be of many types like $\text{A}(\text{B}_{1/2}'\text{B}_{1/2}'')\text{O}_3$, $\text{A}(\text{B}_{1/3}'\text{B}_{2/3}'')\text{O}_3$, $\text{A}(\text{B}_{2/3}'\text{B}_{1/3}'')\text{O}_3$, $(\text{A}_{1/2}'\text{A}_{1/2}'')\text{BO}_3$, $(\text{A}_{1/2}'\text{A}_{1/2}'')(\text{B}_{1/2}'\text{B}_{1/2}'')\text{O}_3$ etc. Many complex $\text{A}(\text{B}_x'\text{B}_y'')\text{O}_3$ type compounds, where B' and B'' are two different elements in different oxidation states and $x + y = 1$, were reported as early as in 1969 [3]. Many physical properties can be

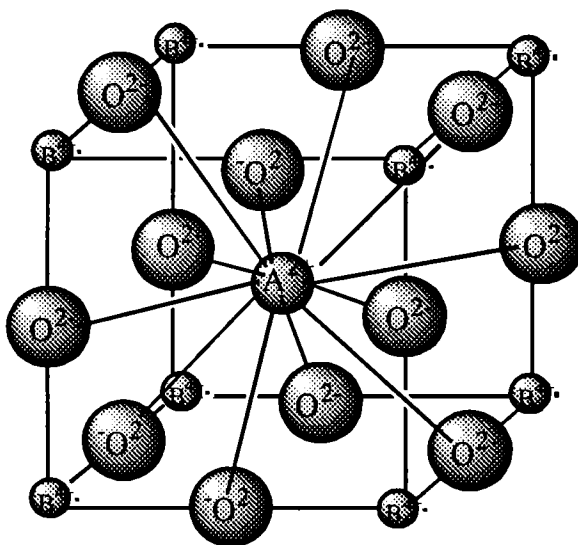
controlled by the cation combinations. The $A(B'B'')O_3$ materials have been extensively studied due to their excellent dielectric properties and unique order-disorder behaviour. In $A(B'B'')O_3$ perovskites, there are 1:2 and 1:1 ordering according to the arrangement of the B-site cations. The degree of ordering is usually known to depend on the size and charge difference of B-site cations. A larger difference must be favoured for a long-range ordering.

The crystal structure and dielectric properties of $Ca(B_{1/2}^{3+}B_{1/2}^{5+})O_3$ with $B' = Al, Cr, Mn, Fe$; $B'' = Nb, Ta$ and $Ca(B_{1/3}^{2+}B_{2/3}^{5+})O_3$ with $B' = Mg, Ca, Co, Ni, Cu, Zn$; $B'' = Nb, Ta$ perovskites were investigated by H.Kagata *et al.* [5]. They reported that all $Ca(B_{1/2}'B_{1/2}'')O_3$ had perovskites structures similar to $CaTiO_3$ with a unit cell including four simple perovskites cells. The size of the unit cell increases as the size of B-ion increases. M.Takata *et al.* [6] reported the microwave characteristics of $A(B_{1/2}^{3+}B_{1/2}^{5+})O_3$ ceramics with $A = Ba, Ca, Sr$; $B^{3+} = La, Nd, Sm, Yb$ and $B^{5+} = Nb, Ta$. H. Boysen *et al* [7]. studied the structure of dielectric resonators based on $Ba(B_{1/2}Nb_{1/2})O_3$ complex perovskites with $r_B = \frac{r_{B'} + r_{B''}}{2}$ $B = La, Pr, Nd, Sm, Eu, Gd, Tb, Dy, Er, Y$ and In . In these compounds, the dielectric properties are found to depend on the tolerance factor, $t = \frac{r_A + r_B}{\sqrt{2}(r_B + r_O)}$ where

$$r_B = \frac{r_{B'} + r_{B''}}{2}, r_A \text{ and } r_O \text{ are the ion radii of B-, A- and O-ions respectively.}$$



(a)



(b)

Fig.6.1: ABO_3 perovskite structure with (a) B^{4+} and (b) A^{2+} at the center of the unit cell

Microwave materials with high quality factor for frequency 2GHz and higher, such as $\text{Ba}(\text{Mg}_{1/3}\text{Ta}_{2/3})\text{O}_3$ and $\text{Ba}(\text{Zr}_{1/3}\text{Ta}_{2/3})\text{O}_3$ systems, are widely used for base station applications [9-10]. Ordered double perovskites oxides of the type $\text{A}_2\text{BB}'\text{O}_6$ showed improved dielectric properties and these oxides are being investigated as new substrate materials for microwave electronics applications [8]. Complex perovskite oxides of rare earths are reported to be good substrate materials for high temperature superconductors [11-13]. These materials have a fairly good lattice matching with YBCO and show promising substrate characteristics, like thermal and chemical stability and non-deteriorating effect on the superconducting transition temperatures of the YBCO superconductors, for the fabrication of high temperature superconducting films for microwave applications [13-16]. Several materials of class $\text{Ba}_2\text{RETaO}_6$ (RE = Gd, Pr, Nd, Dy, Eu) have been prepared and studied by different workers [17-19]. The binary niobate compounds with the general formula MNb_2O_6 (M = Mg, Zn, Co, Ni, Cu, Mn, Ca) were investigated and found to be promising candidates for fabrication of microwave devices [20-21]. The room temperature structures as well as the temperature dependent conductivity and dielectric properties of the $\text{A}_3\text{CoNb}_2\text{O}_9$ (A = Ca^{2+} , Sr^{2+} , and Ba^{2+}) triple perovskite have been investigated by V. Ting *et al.* [22].

Following the observation by Harmer, Setter, Cross and others [23-25] of B-site superlattice ordered structure in both $\text{Pb}(\text{Sc,Ta})\text{O}_3$ and $\text{Pb}(\text{Mg,Nb})\text{O}_3$ perovskites, A – site superlattice ordered structures have also been observed in A-site complex perovskites [26-27]. The structural change of $\text{Ca}_{1-x}\text{Sr}_x\text{TiO}_3$ perovskites is studied by T. Yamanaka *et al.* [28]. They observed a sequential structural change orthorhombic \rightarrow tetragonal \rightarrow cubic, with increasing Sr substitution. E. S. Kim *et al.*

reported [29] the dependence of porosity on the microwave dielectric properties of complex perovskite $(\text{Pb}_{1/2}\text{Ca}_{1/2})(\text{Fe}_{1/2}\text{Ta}_{1/2})\text{O}_3$ ceramics. The microwave dielectric properties of the $(1-x)\text{Na}_{1/2}\text{Nd}_{1/2}\text{TiO}_3-x\text{La}(\text{Mg}_{1/2}\text{T}_{1/2})$ system in relation to ordering was investigated by J. B. Kim *et al.* [30]. Previous workers have reported crystal structures and dielectric properties of A-site substituted solid solutions of $(\text{Sr},\text{Ba},\text{Ca})(\text{Ga}_{1/2}\text{Ta}_{1/2})\text{O}_3$ [31], $(\text{Sr},\text{Ba},\text{Ca})(\text{Y}_{1/2}\text{Ta}_{1/2})\text{O}_3$ [32] and $(\text{Sr},\text{Ba},\text{Ca})(\text{N}_{1/2}\text{W}_{1/2})\text{O}_3$ [33]. They found that the temperature coefficient of dielectric constant (τ_{ϵ_r}) is correlated with the linkage of BO_6 octahedra in the perovskite structure. Preparation and properties of $\text{Ba}_{2-x}\text{Sr}_x\text{SmTaO}_6$ ($x = 0 - 2$) was reported by James *et al.* [34]. The dielectric constant, dielectric loss and conductivity values at 10 MHz were found to decrease with Sr content. Also there is variation in lattice constant for the different compounds, due to the preferential occupation of smaller Sr^{2+} ions at larger Ba^{2+} sites, resulting in a decrease of lattice parameter. Recently, Thirumal *et al.*, Kim *et al.* and Desu *et al.* have investigated the substitution of the Zn site with Mg of various dielectric ceramics [35-37] to form solid solution and improve dielectric properties of microwave materials. Chang *et al.* [38] reported the effect of Mg^{2+} substitution on the microstructure and microwave dielectric properties of $(\text{Zn}_{1-x}\text{Mg}_x)\text{Nb}_2\text{O}_6$ ceramics. They found that the sintering temperature increased while the dielectric constant decreased with increasing Mg content. The quality factors of $(\text{Zn}_{1-x}\text{Mg}_x)\text{Nb}_2\text{O}_6$ ceramics were found to be lower than those of ZnNb_2O_6 and MgNb_2O_6 and the τ_f value is minimum at $x = 0.5$.

Cava *et al.* reported a low τ_f bulk dielectric in the $\text{Ca}_2\text{Ta}_2\text{O}_7 - \text{Ca}_2\text{Nb}_2\text{O}_7$ binary system [39]. Cava *et al.* also reported the low τ_f low loss materials,

$\text{Ca}_5\text{Nb}_2\text{TiO}_{12}$ and $\text{Ca}_5\text{Ta}_2\text{TiO}_{12}$ [40]. The effect of Zr doping in $\text{Ca}_5\text{Nb}_2\text{Ti}_{1-x}\text{Zr}_x\text{O}_{12}$ have also been studied [41]. The microwave properties of $\text{Ca}_5\text{A}_2\text{TiO}_{12}$ ($\text{A} = \text{Nb}, \text{Ta}$) and $\text{Ca}_5\text{Nb}_{2-x}\text{Ta}_x\text{TiO}_{12}$ are studied by Bijumon *et al.* [42-43]. Bijumon *et al.* also reported the low loss, temperature stable $\text{Ca}_x\text{Zn}_{(5-x)}\text{Nb}_2\text{TiO}_{12}$ ($x = 0 - 1$) dielectrics. More recently, this material is reported to be suited for wide band resonator antennas. $\text{Ca}_{5-x}\text{A}_x\text{Nb}_2\text{TiO}_{12}$ ($\text{A} = \text{Mg}, \text{Zn}$ and $x = 0 - 5$) is another set of novel materials reported by Bijumon *et al.* [43].

In this Chapter, the elastic properties of these materials are studied using the ultrasonic pulse echo overlap method. Since the dielectric properties are very much related to the local structure, the study of the structure related elastic properties is of much significant importance from the application point of view.

6.2. Sample Preparation

The $\text{Ca}_{5-x}\text{A}_x\text{Nb}_2\text{TiO}_{12}$ ($\text{A} = \text{Mg}, \text{Zn}$ and $x = 0 - 5$) ceramic samples are prepared following the conventional solid-state reaction method. Stoichiometric amounts of high purity CaCO_3 , $\text{MgCO}_3/\text{ZnCO}_3$, Nb_2O_5 and TiO_2 were weighed and ball milled in distilled water for 24 hrs. The mixture was dried and calcined at temperatures in the range 1200-1400°C for 4 hours each. The calcined powders were again well ground for 1h in an agate mortar and then mixed with PVA (5wt%). The powders were then dry-pressed at 200 MPa to form cylindrical compacts of about 12mm diameter and 6 mm height. The obtained pellets were then preheated at 600°C and then sintered in the temperature range 1550-1600°C.

6.3. Samples Studied

Ultrasonic studies have been carried out on the following samples, (i) $\text{Nb}_2\text{TiO}_{12}$, (ii) $\text{Ca}_{5-x}\text{Mg}_x\text{Nb}_2\text{TiO}_{12}$ and (iii) $\text{Ca}_{5-x}\text{Zn}_x\text{Nb}_2\text{TiO}_{12}$ with $x = 0$ to 5.

6.4. Structure of $\text{Ca}_{5-x}\text{A}_x\text{Nb}_2\text{TiO}_{12}$

$\text{Ca}_5\text{Nb}_2\text{TiO}_{12}$ belongs to the complex perovskite family [40-41, 44-45] $\text{A}_4(\text{BB}'\text{B}'')\text{O}_3$, and can conveniently be written as $\text{Ca}(\text{Ca}_{1/4}\text{Nb}_{2/4}\text{Ti}_{1/4})\text{O}_3$. The B – ions ($\text{BB}'\text{B}''$) occur on the (111) planes in 1:2:1 ratio. Each (111) plane contains one type of small ion-oxygen octahedron, and the planes are ordered in 1:2:1 stoichiometric proportion, in the sequence Ca-Nb-Nb-Ti-Ca-Nb-Nb-Ti-.... The resulting symmetry, due to the (111) type plane stacking and accompanying small oxygen displacement, is trigonal. Partial disorder, which mixes the different B-site ions within single (111) planes, is very common under normal synthetic conditions. The unit cell has orthorhombic symmetry with a cell volume involving multiple simple perovskite subcells [45]. The unusual double zero crossing of τ_f is explained by Cava *et al.* as due to some order/disorder transition in the B-site at high temperature [39-41]. Again, the conventional powder X-ray diffraction patterns revealed that the material remains single-phase perovskite through the range of temperature. However, Bendersky *et al.* [44] have reported that according to back-scattered SEM, slight compositional variations were also detected, especially for lower sintering temperatures. $\text{Ca}_{5-x}\text{A}_x\text{Nb}_2\text{TiO}_{12}$ may be written as, $\text{Ca}_4(\text{CaNb}_2\text{Ti})\text{O}_{12}$ for $x = 0$ and $\text{A}_4(\text{ANb}_2\text{Ti})\text{O}_{12}$ for $x = 5$. For $1 \leq x \leq 4$ the material may not be a single phase of $(\text{Ca}_{5-x}\text{A}_{x-1})(\text{ANb}_2\text{Ti})\text{O}_{12}$, since Ca^{2+} site is too big for A^{2+} ions to get

substituted. Therefore $(Ca_{5-x}A_{x-1})(ANb_2Ti)O_{12}$ may be a mixture of different chemical phases for $1 \leq x \leq 4$.

The structure and phase purity of the samples was examined by powder X-Ray Diffraction (XRD) methods using CuK_{α} radiation (Philips X-Ray Diffractometer). Microstructural analysis of the sintered and thermally etched surfaces of the ceramic samples were held using scanning electron microscopic (SEM, Model S – 2400, Hitachi, Japan) techniques. The X-ray diffraction patterns of the samples are shown in Fig. 6.2 and the SEM photographs are shown in Fig. 6.3.

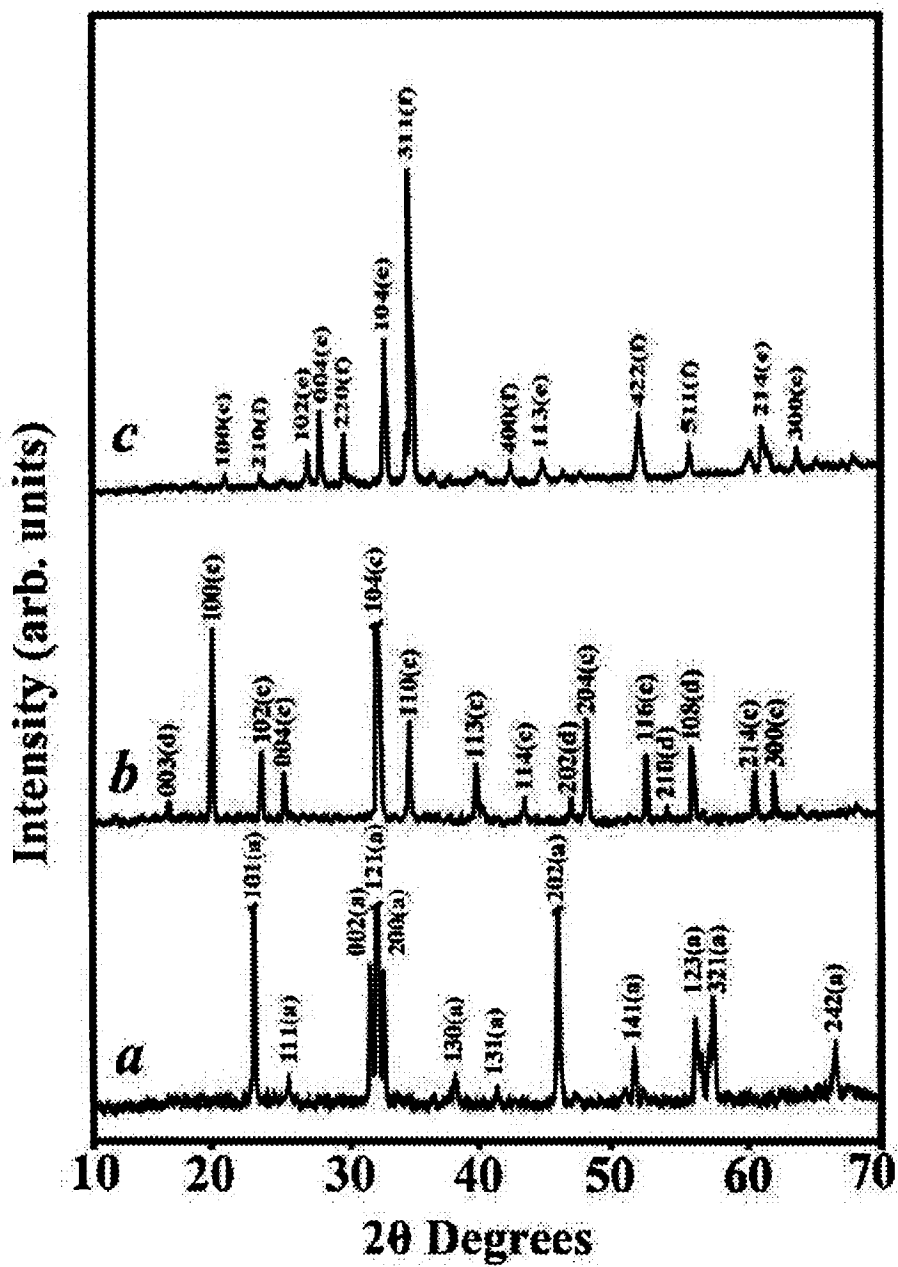


Fig.6.2: X-Ray diffraction patterns of (a) $\text{Ca}_5\text{Nb}_2\text{TiO}_{12}$
 (b) $5\text{MgO-Nb}_2\text{O}_5\text{-TiO}_2$ and (c) $5\text{ZnO-Nb}_2\text{O}_5\text{-TiO}_2$ ceramics

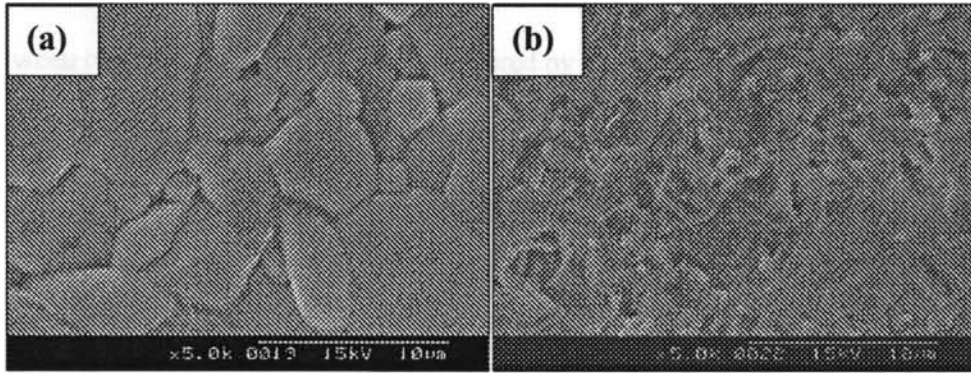


Fig. 6.3: Typical SEM pictures of (a) $5\text{MgO-Nb}_2\text{O}_5\text{-TiO}_2$ and
(b) $5\text{ZnO-Nb}_2\text{O}_5\text{-TiO}_2$ ceramics

6. 5. Elastic Properties by ultrasound technique

Ultrasonic wave velocities in the ceramic samples have been measured by the pulse echo overlap technique using Matec 7700 pulse modulator and receiver system [46]. Pelletised samples of thickness 5-6 mm with perfectly parallel and polished faces have been used for the measurements. To transmit the longitudinal and transverse elastic waves and to receive their echoes, 10 MHz X-cut and Y-cut quartz transducers respectively are used. To measure the velocities, the time gap between two neighbouring echoes is measured by the pulse echo overlap method. To correct the phase shift due to the bonding medium (used between the sample and transducer), McSkimin Δt criterion [47] is used. Measurement technique followed was similar to that described in the previous chapters.

Knowing the sample thickness and density, the elastic moduli can be obtained from the expression $C_{ij} = \rho V^2$, where V is the velocity of the appropriate mode. Elastic parameters like, Young's modulus, Bulk modulus, Poisson's ratio etc can also be found out from the measured longitudinal and transverse velocities. The overall accuracy of elastic constant values of the order of 0.1%.

6.6. Results and Discussion

The structural transformation of $\text{Ca}_{5-x}\text{Mg}_x\text{Nb}_2\text{TiO}_{12}$ and $\text{Ca}_{5-x}\text{Zn}_x\text{Nb}_2\text{TiO}_{12}$ ceramics with compositional variations have been described elsewhere [48]. It is established that, the solid solutions based on $\text{Ca}_{5-x}\text{A}_x\text{Nb}_2\text{TiO}_{12}$ (A = Mg, Zn) was formed only for x up to 1. However, for $x > 1$, the XRD patterns exist as a mixture of two or more phases. Fig. (6.2) shows the XRD spectra of $\text{Ca}_5\text{Nb}_2\text{TiO}_{12}$, and

$\text{Ca}_{5-x}\text{Mg}_x\text{Nb}_2\text{TiO}_{12}$ & $\text{Ca}_{5-x}\text{Zn}_x\text{Nb}_2\text{TiO}_{12}$ ceramics for $x = 5$. XRD reflections of $\text{Ca}_5\text{Nb}_2\text{TiO}_{12}$ ceramics [See Fig. 6.2(a)] are indexed based on perovskite orthorhombic symmetry [42]. $\text{Ca}_{5-x}\text{Mg}_x\text{Nb}_2\text{TiO}_{12}$ for $x = 5$, was identified [Fig. 6.2(b)] as a mixture of $\text{Mg}_4\text{Nb}_2\text{O}_9 - \text{MgTiO}_3$ phases and are indexed accordingly. The intermediate compositions ($2 \leq x \leq 4$) are not shown in figure, but they were found [48] to be formed as a mixture of $\text{Mg}_4\text{Nb}_2\text{O}_9 - \text{CaTiO}_3$ phases. The XRD pattern recorded from the powdered specimens of $\text{Ca}_{5-x}\text{Zn}_x\text{Nb}_2\text{TiO}_{12}$ ceramics for $x = 5$ are depicted in Fig. 6.2 (c). As in the case of magnesium substitution, in this case also with $x = 5$, $\text{Ca}_{5-x}\text{Zn}_x\text{Nb}_2\text{TiO}_{12}$ was identified as a mixture of $\text{Zn}_4\text{Nb}_2\text{O}_9 - \text{ZnTiO}_3$ phases. However, Zn^{2+} substitution for $2 \leq x \leq 4$ has resulted in the formation of materials comprising mixture phases like $\text{Ca}_3\text{Nb}_2\text{O}_8$, Zn_2TiO_4 , CaTiO_3 , $\text{Zn}_4\text{Nb}_2\text{O}_9$ and ZnTiO_3 [20].

Microstructure of $\text{Ca}_5\text{Nb}_2\text{TiO}_{12}$ has been reported [43] earlier with uniform distribution of large grains of about 10 μm size. Fig. 6.3 shows few typical SEM photographs recorded from the surface of sintered and thermally etched $\text{Ca}_{5-x}\text{A}_x\text{Nb}_2\text{TiO}_{12}$ ($\text{A} = \text{Mg}, \text{Zn}$) specimens for $x = 5$. The surface morphology of $5\text{MgO}-\text{Nb}_2\text{O}_5-\text{TiO}_2$ is depicted in Fig. 6.3(a), which shows pore eliminated grains with two distinct shapes indicating the formation of $\text{Mg}_4\text{Nb}_2\text{O}_9$ and MgTiO_3 phases in the sample. The microstructure of $5\text{ZnO}-\text{Nb}_2\text{O}_5-\text{TiO}_2$ ceramics is depicted in Fig. 6.3(b). Indication of the occurrence of liquid phase sintering can be found in the grain boundaries of the specimen and the presence of the same may be responsible for grain growth. The formation of liquid phase may be due to the evaporation of ZnO similar to the same reported in the case of $\text{Ba}(\text{Zn}_{1/3}\text{Ta}_{2/3})\text{O}_3$ ceramics [24].

Non-uniformity in the size and shape of grains indicates the formation of mixture phases as confirmed from XRD analysis.

The measured longitudinal and transverse velocities of ultrasonic waves in $\text{Ca}_{5-x}\text{Mg}_x\text{Nb}_2\text{TiO}_{12}$ and $\text{Ca}_{5-x}\text{Zn}_x\text{Nb}_2\text{TiO}_{12}$ ceramics are shown in Tables 6.1 – 6.2. It can be seen from the tables that, in both the systems the wave velocities show an initial increase for $x = 0$ to 1 and then an abrupt decrease for $1 < x < 2$. The values again increases for $x > 2$ and thereafter almost remains unaffected within experimental errors. It should be remembered that, the ceramics form phase pure compositions up to $x = 1$ and thereafter mixture phases were formed [20]. The drastic change in ultrasonic wave velocity at the transition point could be related to the structural transformation. The Poisson's ratio of the samples vary between 0.31 to 0.16 (within experimental error), which also follows the same trend as shown by the wave velocity inside the ceramic specimens. The elastic properties of $\text{Ca}_{5-x}\text{Mg}_x\text{Nb}_2\text{TiO}_{12}$ and $\text{Ca}_{5-x}\text{Zn}_x\text{Nb}_2\text{TiO}_{12}$ ceramics are depicted in Figures 6.4-6.9 respectively. In both the systems the properties like longitudinal/transverse elastic moduli C_{11}/C_{44} , Young's modulus (Y) and Bulk modulus (B) are observed to be higher for compositions with $x = 0$ and 1. It is evident from the figures that, all the elastic properties are higher for Mg^{2+} -based compounds compared with their zinc analogue. Beyond $x = 1$, the elastic properties of $\text{Ca}_{5-x}\text{Mg}_x\text{Nb}_2\text{TiO}_{12}$ and $\text{Ca}_{5-x}\text{Zn}_x\text{Nb}_2\text{TiO}_{12}$ decrease abruptly to reach their lowest values within all compositions and again increases for $x > 2$. It is known that the local structure, mechanical strength and hence elastic properties of ceramics are highly controlled by their phase purity. Hence in the present case the decreased elastic properties of $\text{Ca}_{5-x}\text{Mg}_x\text{Nb}_2\text{TiO}_{12}$ and $\text{Ca}_{5-x}\text{Zn}_x\text{Nb}_2\text{TiO}_{12}$ ceramics can be attributed to their mixture

phases beyond $x = 1$. Moreover, the abrupt change in elastic properties observed for $x > 1$ can also be correlated to the structural transformation of the materials from their phase pure form to mixture phases for higher extent of substitution of the concerned material. However, it can be seen from Tables 6.1 – 6.2 and Figures. 6.4 - 6.9 that, $\text{Ca}_4(\text{ANb}_2\text{Ti})\text{O}_{12}$ ($A = \text{Mg, Zn}$) is the strongest compound with the maximum values for elastic properties. This could be due to the possible substitution of Mg/Zn ions with lesser radius [25] than Ca^{2+} in perovskite B-site of $\text{Ca}(\text{Ca}_{1/4}\text{Nb}_{2/4}\text{Ti}_{1/4})\text{O}_3$ material to contribute more ordering and symmetry to the system [20]. All other compositions ($x > 1$) contain mixed-phases and for such mixed-phase samples, the mechanical properties are difficult to explain.

Table 6.1: Elastic properties of $\text{Ca}_{5-x}\text{Mg}_x\text{Nb}_2\text{TiO}_{12}$

x	V_l (m/s)	C_{11} (GPa)	V_t (m/s)	C_{44} (GPa)	Young's Modulus Y (GPa)	Bulk Modulus B (GPa)	Poisson's ratio
$\text{Nb}_2\text{TiO}_{12}$	6433 ± 32	166 ± 4	3609 ± 18	52 ± 1	133 ± 3	96 ± 2	0.270
0	5530 ± 27	123 ± 3	3550 ± 17	51 ± 1	116 ± 3	55 ± 1	0.155
1	8452 ± 42	302 ± 8	4508 ± 27	86 ± 2	224 ± 6	188 ± 5	0.301
2	7028 ± 35	210 ± 5	4186 ± 21	74 ± 2	182 ± 5	111 ± 2	0.225
3	8289 ± 41	289 ± 7	4453 ± 22	84 ± 2	216 ± 5	178 ± 4	0.297
4	7855 ± 39	260 ± 6	4429 ± 22	82 ± 2	209 ± 5	150 ± 4	0.267
5	7742 ± 38	250 ± 6	4320 ± 21	78 ± 1	198 ± 5	146 ± 4	0.273

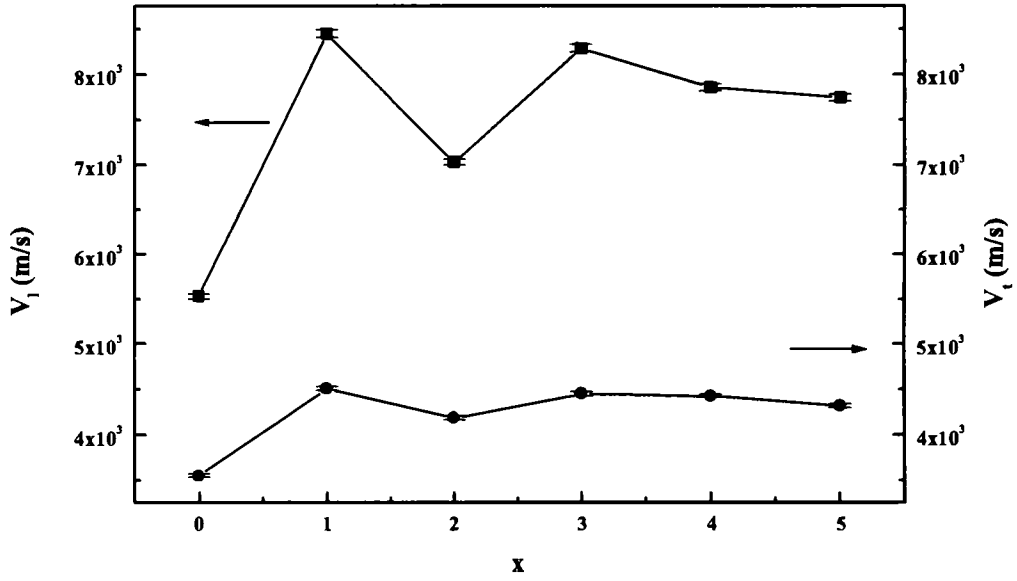


Fig. 6.4: Variation of ultrasonic velocity in $\text{Ca}_{5-x}\text{Mg}_x\text{Nb}_2\text{TiO}_{12}$

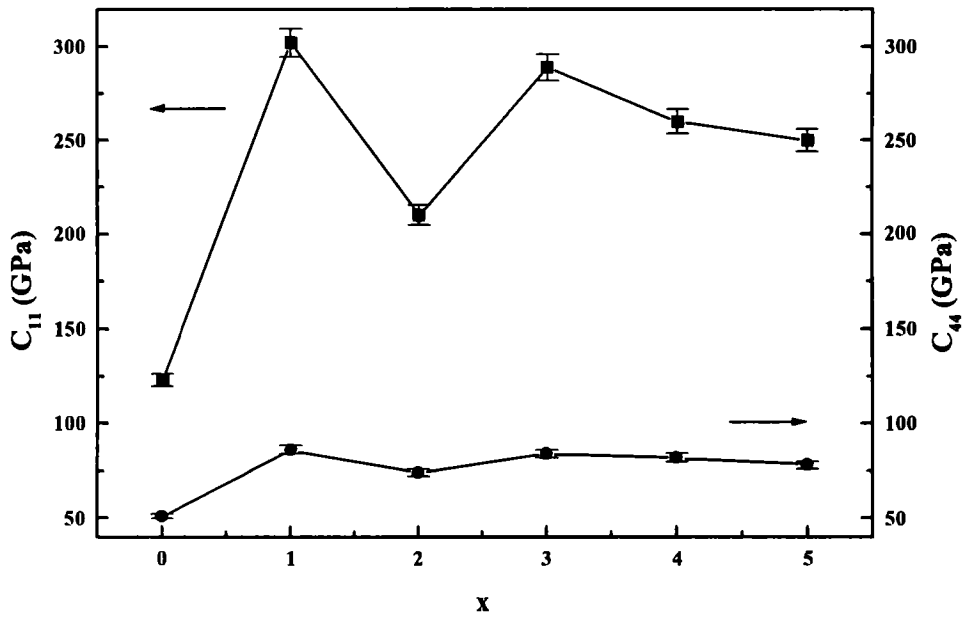


Fig.6.5: Variation of C_{11} and C_{44} in $\text{Ca}_{5-x}\text{Mg}_x\text{Nb}_2\text{TiO}_{12}$

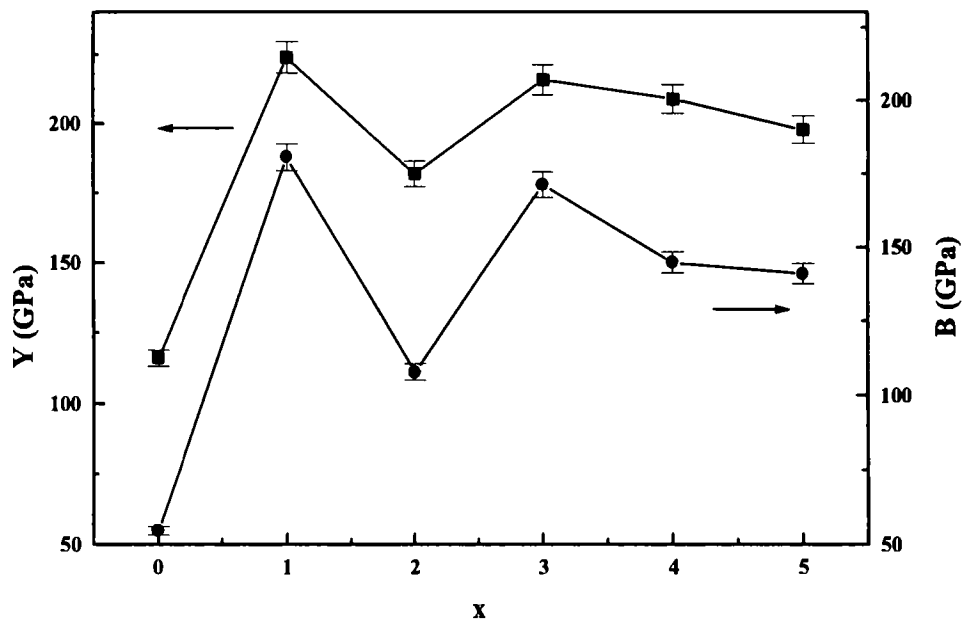


Fig.6.6: Variation of Y and B in $\text{Ca}_{5-x}\text{Mg}_x\text{Nb}_2\text{TiO}_{12}$

Table 6.2. Elastic Properties of $\text{Ca}_{5-x}\text{Zn}_x\text{Nb}_2\text{TiO}_{12}$

x	V_l (m/s)	C_{11} (GPa)	V_t (m/s)	C_{44} (GPa)	Young's Modulus Y (GPa)	Bulk Modulus B (GPa)	Poisson's ratio
0	5530±27	123±3	3550±17	51±1	116±3	55±1	0.155
1	7683±38	267±7	3911±19	66±1	175±4	167±4	0.325
2	5820 ± 29	147 ± 4	3179 ± 16	44 ± 1	113 ± 3	89 ± 2	0.287
3	7016 ± 35	233 ± 6	3639 ± 18	63 ± 1	165 ± 4	149 ± 4	0.316
4	6368 ± 32	205 ± 5	3343 ± 17	57 ± 1	148 ± 4	130 ± 3	0.309
5	6007 ± 30	199 ± 5	3161 ± 16	55 ± 1	144 ± 4	126 ± 3	0.308

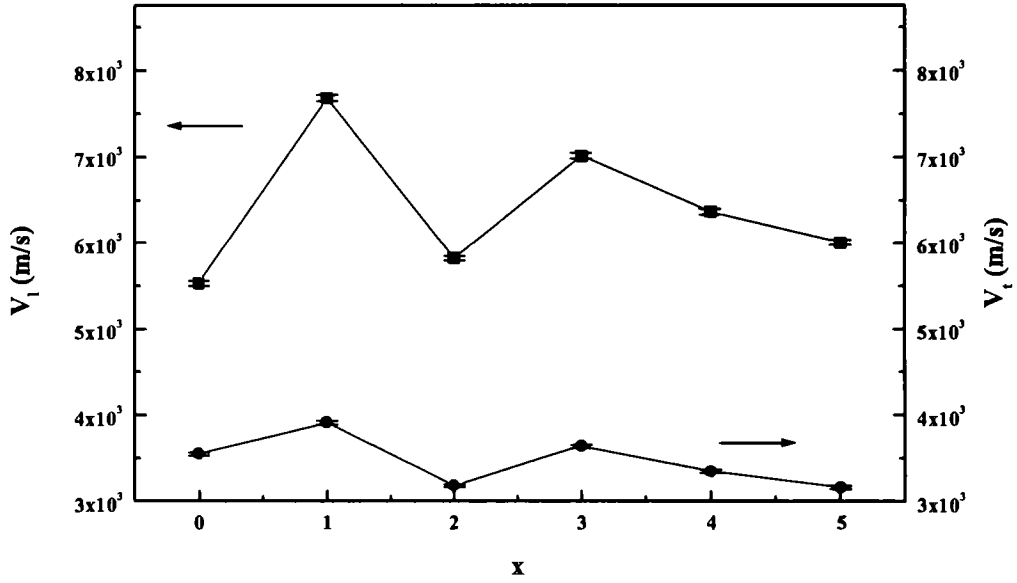


Fig.6.7: Variation of ultrasonic velocity in $\text{Ca}_{5-x}\text{Zn}_x\text{Nb}_2\text{TiO}_{12}$

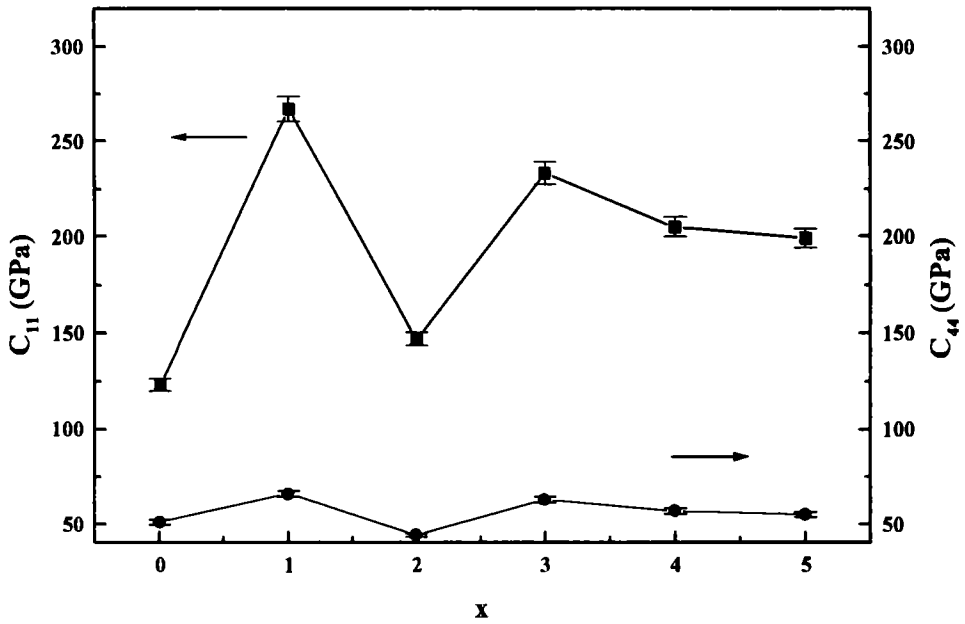


Fig.6.8: Variation of C_{11} and C_{44} in $\text{Ca}_{5-x}\text{Zn}_x\text{Nb}_2\text{TiO}_{12}$

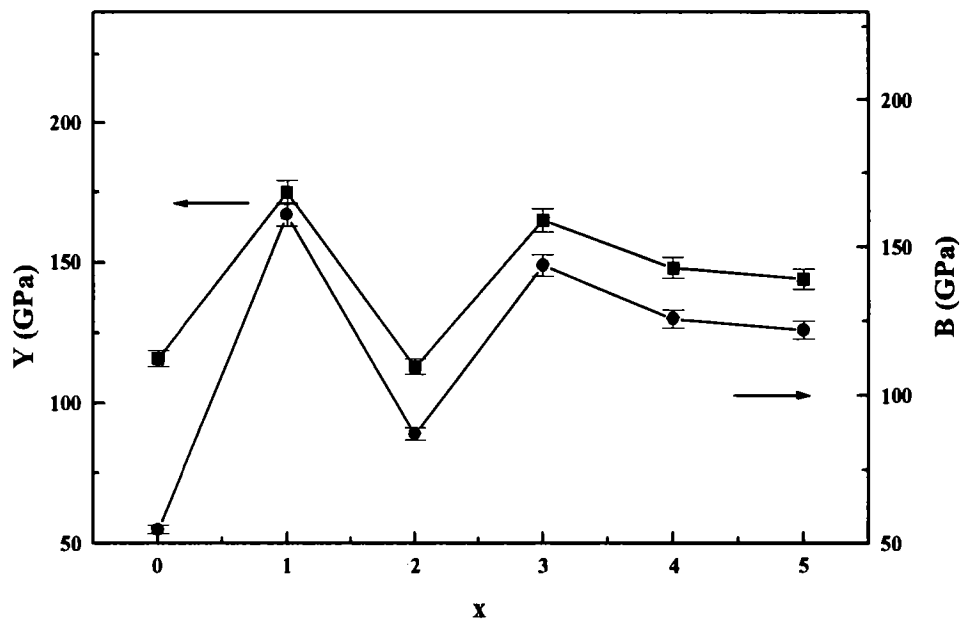


Fig.6.9 Variation of Y and B in $\text{Ca}_{5-x}\text{Zn}_x\text{Nb}_2\text{TiO}_{12}$

References

1. G. T. Stanford and R. A. Condrate Sr, *J. Mat. Sci. Lett.* **3** (1984) 303
2. G. Blasse and A. F. Corsmit, *J. Solid State Chem.* **6** (1973) 513
3. F. S. Galasso, *Structure, Properties and Preparation of perovskite Type Compounds*, Pergamon Press, Oxford (1969)
4. Jac Beom Kim, Ki Hyun Yoon and Yong S. Cho, *J. Am. Ceram. Soc.* **88**[3] (2005) 612
5. H. Kagata and J. Kato, *Jpn. J. Appl. Phys.* **33** (1994) 5463
6. M. Takata and K. Kageyama, *J. Am. Ceram. Soc.* **72**[10] (1989) 1955
7. http://wwwhasylab.desy.de/science/annual_reports/2000_report/part1/contrib/46/2662.pdf
8. A. Tauber, S. C. Tidow, R. D. Finnegan and W. D. Wilber, *Physica C.* **256** (1996) 340
9. K. Kakegwa, T. Wakabayashi and Y. Sasaki, *J. Am. Ceram. Soc.* **69** (1986) c-82
10. D. A. Sagada and S. Nambu, *J. Am. Ceram. Soc.* **759** (1992) 2573
11. C. D. Brandle and V. J. Fratello. *J. Mat. Res.* **5**(10) (1990) 2160
12. J. Koshy, K.S. Kumar, Y. P. Yadava and A. D. Damodaran, *J. Mat. Sci. Lett.* **13** (1994) 670
13. J. James, O. B. S. Kumar, S. Senthil Kumar, P. Prabhakar Rao and K. V. O. Nair, *Mat. Lett.* **57** (2003) 3641
14. J. Kurian, S. P. Pai, J. James and J. Koshy, *J. Mat. Sci.* **12** (2001) 173

15. R. Jose, J. James, A. M. John, R. Divakar and J. Koshy, *J. Mater. Res.* **15** (2000) 2125
16. P. K. Davies, J. Tong and T. Negas, *J. Am. Ceram. Soc.* **80** (1997) 1727
17. T. G. N. Babu, J. Koshy, Y. Sudershan and S. V. Bhat, *J. Supercond.* **10** (3) (1997) 193
18. T. G. N. Babu and J. Koshy, *Mat. Lett.* **33** (1997) 7
19. T. G. N. Babu and J. Koshy, *J. Solid State Chem.* **133** (1997) 522
20. M. Maeda, Y. Yamamura and T. Ikeda, *Jpn. J. Appl. Phys. Suppl.* **26**(2) (1987) 76
21. H. J. Lee, I. T. Kim and K. S. Hong, *Jpn. J. Appl. Phys.* **36**, (Part 2, 10A) (1997) 1318
22. V. Ting, Y. Liu, L. Noren, R. L. Withers, D. J. Goossens, M. James and C. Ferraris, *J. Solid State Chem.* **177** (2004) 4428
23. M. P. Harmer, A. Bhalla and L. E. Cross, *Mat. Lett.* **2** (1984) 278
24. N. Setter and L. E. Cross, *J. Appl. Phys.* **51** (1980) 4536
25. J. Chen, H. M. Chan and M. P. Harmer, *J. Am. Ceram. Soc.* **72** (1989) 593
26. K. Grace, *J. Am. Ceram. Soc.* **71** (1988) 454
27. C. Randall, *Ferroelectrics* **76** (1987) 277
28. T. Yamanaka, N. Hirai and Y. Komatsu, *Am. Mineralogist.* **87** (2002) 1183
29. E. S. Kim, H. S. Park, K. H. Yoon, *Mat. Chem. Phys.* **79** (2003) 213
30. J. B. Kim, K. H. Yoon and Y. S. Cho, *J. Am. Ceram. Soc.* **88**[3] (2005) 612
31. M. Takata, K. Kageyama, *J. Am. Ceram. Soc.* **72** (1989) 1955
32. T. Fuji, T. Takahushi, S. Shimada and K. Kageyama, *J. Electrocerm.* **3** (4) (1999) 387

33. T. Fuji, H. Sato, S. Ito and G. L. Messing, *Solid state Ionics* **172** (2004) 485
34. J. James, M. Sankar, S. Senthilkumar and K. V. O. Nair, *Mat. Chem. Phys.* **83** (2004) 328
35. M. Thirumal, I. N. Jawahar, K. P. Surendran, *Mat. Res. Bull.* **37** (2002) 185
36. H. T. Kim, S. Nahu and J. D. Byun, *J. Am. Ceram. Soc.* **82** (1999) 3476
37. S. B. Desu and H. M. O'Bryan, *J. Am. Ceram. Soc.* **68** (1985) 546
38. Y. C. Chang, J. Wang, Z. X. Yue, Z. Gui and L. Li, *Ceram. Internat.* **30** (2004) 87
39. R. J. Cava, J. J. Krajewski and R. S. Roth, *Mat. Res. Bull.* **33**, No. 4 (1998) 527
40. R. J. Cava, J. J. Krajewski and R. S. Roth, *Mat. Res. Bull.* **34**, No. 3 (1999) 355
41. R. J. Cava, J. J. Krajewski and R. S. Roth, *Mat. Res. Bull.* **34**, Nos. 12/13 (1999) 1817
42. P. V. Bijumon, P. Mohanan and M. T. Sebastian, *Jpn. J. Appl. Phys.* **41** (2002) 3834
43. P. V. Bijumon, P. Mohanan and M. T. Sebastian, *Mat. Lett.* **57** (2003) 1380
44. L. A. Bendersky, J. J. Krajewski and R. J. Cava, *J. Euro. Ceram. Soc.* **21** (2001) 2653
45. R. J. Cava, *J. Mater. Chem.* **11** (2001) 54
46. E. P. Papadakis, *Physical Acoustics* (Eds: M. P. Mason, R. N. Thurston, Academic Press, New York) **12** (1976) 277
47. H. J. McSkimin, *J. Acoust. Soc. Am.* **33** (1961) 12

48. P. V. Bijumon, P. Mohanan and M. T. Sebastian, *J. Appl. Phys.*

(communicated)

49. W. Ahn, H. J. Jang, S. Nahm, H. M. Park and H. J. Lee, *J. Eur. Ceram. Soc*

23 (2003) 2473

CHAPTER 7

Summary and Conclusions

The present work is an attempt to probe the elastic properties in some dielectric ceramics, by using ultrasonic pulse echo overlap technique. The base materials selected for study – $\text{Ba}_{6-x}\text{Sm}_{8+2x}\text{Ti}_{18}\text{O}_{54}$ and $\text{Ca}_5\text{Nb}_2\text{TiO}_{12}$ – are very important dielectric ceramics used for microwave communications as well as for substrate materials. Even though microwave dielectric properties of these ceramics have been studied extensively, not much work has been done on their elastic properties, which in turn determines the mechanical strength and stability of these materials. Since the elastic properties are closely linked with the structure of the materials, we tried to explain the structure also, with the help of XRDs and SEMs of selected test samples.

We have prepared various dielectric ceramics following the conventional solid state reaction route in collaboration with the ceramics research group at Regional Research Laboratory, Thiruvananthapuram. Since the commercially used BST ceramics have very high sintering temperature, considerable efforts have been made to prepare BST ceramics having reduced sintering temperatures, by adding different additives, such as glasses. About a dozen different glasses are added with their percentage varying from 0.1 to more than 10 %. The ultrasonic measurements are performed in all the sets of samples. It is found that the elastic moduli continuously decrease with the addition of glasses. The result is the same in almost all cases irrespective of the glasses added, with the exception of a few. This can be

99098

explained as due to the glassy phase formation, since no formation of any important peaks are observed in the XRD patterns of glass added samples. Also the increasing grain size has been found in the scanning electro micrographs of ABS doped BST samples points to the lowering of elastic strength and hardness of the samples.

$\text{Ca}_5\text{Nb}_2\text{TiO}_{12}$ are low loss low τ_f materials. We have reported the elastic properties of these materials for the first time. $\text{Ca}_{5-x}\text{A}_x\text{Nb}_2\text{TiO}_{12}$ (A = Mg, Zn) is another set of novel materials used in wide band resonator antennas. Elastic and structural properties of these have also been measured and reported. The variation in the mechanical strength of the different samples are linked to the structural stability of the perovskite materials.

Only very limited data is available on the elastic properties of dielectric resonator ceramics. In all the samples investigated in this thesis, the information provided would be very useful while selecting these materials for specific applications. Since the data would be valuable from the application point of view, measurement of the elastic properties of other known ceramics need to be done. Preparation of newer and better materials is another challenging work.

Now, ceramic substrate materials have been prepared which exhibit high values of thermal conductivity. Such materials are now extensively being used as substrate materials for microwave integrated circuits. When it comes to such applications, it is important to know the mechanical properties of such materials. Mechanical stability and hardness are important parameters in this respect. These parameters are determined by the elastic modulus of the material. Ultrasonics is the best method to measure the elastic properties of such materials. So there is plenty of scope for doing very practically useful work in this area.

